

**MODE II INTERLAMINAR FRACTURE TOUGHNESS OF FLAX AND GLASS
EPOXY HYBRID COMPOSITES**

by

Wilfred Stephen Ekeoseye
Master of Science (MSc) Mechanical Engineering
Coventry University, United Kingdom, 2013

A thesis
presented to Ryerson University
in partial fulfillment of the requirements
for the degree of

Master of Applied Science
in the program of
Mechanical and Industrial Engineering

Toronto, Ontario, Canada, 2020

©Wilfred Stephen Ekeoseye 2020

AUTHOR'S DECLARATION FOR ELECTRONIC SUBMISSION OF A THESIS

I hereby declare that I am the sole author of this thesis. This is a true copy of the thesis, including any required final revisions, as accepted by my examiners.

I authorize Ryerson University to lend this thesis to other institutions or individuals for the purpose of scholarly research

I further authorize Ryerson University to reproduce this thesis by photocopying or by other means, in total or in part, at the request of other institutions or individuals for the purpose of scholarly research.

I understand that my thesis may be made electronically available to the public.

Mode II Interlaminar fracture toughness of flax and glass epoxy hybrid composites

Wilfred Stephen Ekeoseye

Master of Applied Science (MASc)

Mechanical and Industrial Engineering

Ryerson University

2020

Abstract

Delamination is a significant mode of failure in composite materials during service; It prevents the adequate dissemination of load between plies lowering the strength of the material, which could consequently lead to a cascading effect of failure. Providing more data on the delamination properties of composite material during loading will increase the adoption of composite materials in more industries. This study aims to characterize the mode II interlaminar fracture toughness of hybrid composites – hybrid one $[0_G/0_F]_{8S}$, hybrid two $[0_{4G}/0_{4F}]_S$ and hybrid three $[0_{4G}/(90/0)_{2F}]_S$. Furthermore, this study explores the application of Finite Element Analysis as a tool to assess the damage in a composite material during delamination. In this study, mode II fracture toughness of three hybrids of flax and glass epoxy is characterized according to the ASTM standard D7905 standard. Finite Element Analysis is applied to assess the failure in the flax plies of the respective hybrid.

Acknowledgements

First, I would like to thank my thesis supervisor Dr. Habiba Bougherara. Your expertise, patience, guidance and support throughout this research helped me advance my knowledge in composite materials, finite element analysis and it made this thesis possible.

I would also like to also extend my gratitude to the members of the review committee: for reviewing my thesis and their generous helpful suggestions.

My sincere thanks to Dr. Zainab Al-Hajaj and Ahmed Sarwar for teaching me the compression manufacturing process of composite materials. Also, I would like to thank Mr. Alan Machin of the department of mechanical and industrial engineering who taught me how to use the 3-point testing machine which was invaluable for this research.

Finally, I would like to thank my wife, Akpevwe Onoyovwi-Ekeoseye for her patience and who had to take on a lot more so that I could complete my research and thesis.

Dedication

I dedicate this thesis to my late Father, Chief Stephen Ekeoseye, who throughout his lifetime etched in my consciousness the importance of knowledge and education.

Table of Contents

Abstract	iii
Acknowledgements.....	iv
Dedication.....	v
List of Tables	viii
List of Figures.....	x
List of Appendices	xii
1 Introduction	1
1.1 Background	1
1.2 Objectives and Research Motivation.....	3
2 Literature Review.....	5
2.1 Hybrid Materials	9
2.2 Flax Fibre.....	10
2.3 An overview of Glass fibre	13
2.4 An Overview of Epoxy.	14
2.5 Finite Element Analysis and Delamination.....	16
2.5.1 Virtual Crack Closure Technique (VCCCT).....	18
2.6 Hashin Criterion.....	21
2.7 Laminate properties in ANSYS simulation software	24
2.7.1 Laminate Engineering Constants.....	26
2.8 Representative Volume Element (RVE).....	27
3 Mode II Interlaminar Fracture Toughness	30
3.1 An overview of Mode II interlaminar fracture toughness	30
3.2 Data Reduction.....	32
3.3 Candidate fracture toughness	34
3.4 Flexural modulus	35
4 End Notch Flexural Specimen configuration and Experimental Test Set-Up.....	36
4.1 Composite Specimen Manufacturing	37
4.2 ENF Specimen Dimension.....	41
4.3 Experimental End Notch Flexural Test Procedure.	43
4.4 Procedure for obtaining the Flexural Properties applying ANSYS simulation software.	45
4.5 Laminate Flexural Modulus	47
5 Experimental Results and Discussion.	48
5.1 Mode II interlaminar fracture toughness of hybrid one.....	50

5.2	Mode II interlaminar fracture toughness of hybrid two.....	57
5.3	Mode II interlaminar fracture toughness of hybrid three	60
5.4	Damage observed in the hybrid specimens.....	62
5.5	Discussion.....	65
6	Finite Element Analysis.....	72
6.1	Geometry.....	72
6.2	End Notch flexural sample modelling (Preprocessing).....	74
6.3	ENF Simulation Boundary Conditions and simulation setup.....	76
6.3.1	Boundary Conditions	76
6.3.2	Simulation setup in ANSYS	77
6.4	Mesh Convergence Analysis.....	78
6.5	Results and Discussion of Finite Element Simulation Result	81
6.5.1	Hybrid one.....	82
6.5.2	Hybrid two.....	87
6.5.3	Hybrid three.....	92
7	Conclusion and Future Work	99
	Appendix.....	104
	References.....	107

List of Tables

Table 2-1: Summary of initiation and propagation mode I fracture toughness (G_{Ic}) of flax epoxy values of flax epoxy composites from literature.....	8
Table 2-2: Glass fibre (E-glass) Mechanical properties [11]	14
Table 2-3: Typical properties of Epoxy Matrix [48]	15
Table 2-4: typical properties of Fibre reinforced epoxy composite materials [11].....	15
Table 4-1: The layup code and layup sequence of the three specimens tested.....	36
Table 4-2: Dimensions of samples of Hybrid 1 ([0G/0F] 8S) tested.....	42
Table 4-3: Dimensions of samples of Hybrid 2 [04G/04F] S tested.	42
Table 4-4: Dimensions of samples of Hybrid 3 [04G/ (90/0)2F] S tested.....	42
Table 4-5: Material Properties of E glass [74].....	45
Table 4-6: Material Properties of Epoxy [22]	46
Table 4-7: RVE generated material property of glass epoxy composite using ANSYS MD.....	47
Table 4-8: Material and their approximated flexural modulus.	47
Table 5-1: Applied forces F1 and F2 for the exploratory study.....	49
Table 5-2: The compliances of the exploratory study of the hybrid one	52
Table 5-3: Compliances of tested samples of the hybrid one material	54
Table 5-4: Candidate fracture toughness of hybrid one material [0 _G /0 _F] _{8S}	55
Table 5-5: Flexural modulus of hybrid one material [0 _G /0 _F] _{8S}	55
Table 5-6: Percentage of candidate fracture toughness for Hybrid 1 [0G/0F]8S.....	56
Table 5-7: Mode II fracture toughness and flexural modulus of hybrid One.....	57
Table 5-8: Compliances of tested samples of the hybrid two material	57
Table 5-9: Candidate fracture toughness of hybrid two material [0 _{4G} /0 _{4F}] _S	58
Table 5-10: Flexural modulus of hybrid two material [0 _{4G} /0 _{4F}] _S	58
Table 5-11: Percentage of candidate fracture toughness for Hybrid 2 [04G/04F] S	59
Table 5-12: Mode II fracture toughness and flexural modulus of hybrid two	59
Table 5-13: Compliances of tested samples of the hybrid three material.....	60
Table 5-14: Candidate fracture toughness of hybrid three material [0 _{4G} / (90/0) _{2F}] _S	61
Table 5-15: Flexural modulus of hybrid three material [0 _{4G} / (90/0) _{2F}] _S	61
Table 5-16: Percentage of candidate fracture toughness for Hybrid three [0 _{4G} / (90/0) _{2F}] _S	62
Table 5-17: Mode II fracture toughness and flexural modulus of hybrid three	62
Table 5-18: Flexural Modulus of hybrid one,two and three material.....	70
Table 5-19: Mode II fracture toughness of the hybrid, flax and glass epoxy composite material	71

Table 6-1: Remote Displacement settings.....	77
Table 6-2: Longitudinal failure analysis of the flax epoxy plies in Hybrid one.....	84
Table 6-3: Transverse failure analysis of the flax epoxy plies in hybrid one.....	86
Table 6-4: Longitudinal failure analysis of the flax epoxy plies in Hybrid two.....	90
Table 6-5: Transverse failure analyses of the flax epoxy plies in Hybrid two.....	91
Table 6-6: Longitudinal failure analyses of the flax epoxy plies in Hybrid three.....	95
Table 6-7: Transverse failure analyses of the flax epoxy plies in Hybrid three.....	96

List of Figures

Figure 1-1: The basic modes of delamination (1a: Mode I, 1b: Mode II, 1c: Mode III, 1c) [11].....	3
Figure 2-1: The composition of a flax fibre plant. [47]	13
Figure 2-2: A diglycidyl ether of bisphenol molecule [48]	14
Figure 2-3: A molecule of diethylene triamine [48].....	15
Figure 2-4: The 3D VCCT crack geometry [58].....	20
Figure 2-5: ABD matrix and the coupling between laminate forces and deformations [10].....	25
Figure 2-6: Shape of Representative Volume Element in ANSYS [10].....	29
Figure 3-1: The ENF specimen and ENF fixtures [13]	30
Figure 3-2: The ENF specimen and roller arrangement [13]	31
Figure 3-3: Plot of force vs displacement and the highlighted maximum load [13].	33
Figure 4-1: A Carver compression moulding machine.....	37
Figure 4-2: Specimen Layout.....	41
Figure 4-3: ENF specimen, Fixture and Dimensions [13].....	43
Figure 4-4: The ENF mode II test set-up	44
Figure 4-5: Diamond Representative Volume Element [74]	46
Figure 5-1: The plot of displacement vs force (F1) of Hybrid 1 exploratory study. (The red data points are excluded from the analysis).....	51
Figure 5-2: The plot of displacement vs force (F2) Hybrid 1 exploratory study (The red data points are excluded from the analysis).....	51
Figure 5-3: The plot of force (after fracture) vs displacement of Hybrid 1 exploratory study. (The red data points are excluded from the analysis; excluded data was according to the rule in ASTM D7905 [13])	52
Figure 5-4: Crack length cubed (a^3) vs Compliance (C)	53
Figure 5-5: Delamination observed in hybrid one	63
Figure 5-6: Delamination and secondary delamination in observed in the hybrid two material.....	64
Figure 5-7: Delamination and secondary interbundle delamination in the hybrid three material.....	64
Figure 5-8: Force vs Displacement during compliance calibration test of Hybrid 1,2 and 3	65
Figure 5-9: Failure modes in hybrids of glass and carbon laminates with different ply thickness. [75]	66
Figure 5-10: Mode II Interlaminar Fracture Toughness G_{IIc} of hybrid 1, 2 and 3.....	67
Figure 5-11: Mode II fractural toughness of different architecture of flax epoxy composite [6]	68
Figure 6-1: Geometry of laminate for the FEA analysis.....	73
Figure 6-2: Geometry of loading rollers used in the simulation.	73

Figure 6-3: Model setup of the mode II ENF simulation.	75
Figure 6-4: ENF geometry with boundary conditions	76
Figure 6-5: Project Schematic of the ANSYS ENF simulation.	77
Figure 6-6: Number of mesh element vs Force reaction	80
Figure 6-7: Plot of Displacement (mm) vs Force (N) of the experimental and FEA results after fracture test of the hybrid one material.	82
Figure 6-8: Mode II fracture toughness distribution at the crack front.....	83
Figure 6-9: Mode II fracture toughness across the width of the hybrid one specimen.	83
Figure 6-10: Plot of Displacement (mm) vs Force (N) of the experimental and FEA results after fracture of hybrid two	88
Figure 6-11: Mode II fracture toughness across the width of the hybrid two specimen	89
Figure 6-12: Plot of Displacement (mm) vs Force (N) of the experimental and FEA results after fracture of hybrid three	93
Figure 6-13: Mode II fracture toughness across the width of the hybrid three specimen.....	94

List of Appendices

Appendix 1: Complete Dimensions of Hybrid 1 ([0G/0F] 8S), Hybrid 2 [04G/04F] S and Hybrid 3 [04G/ (90/0)2F] S	104
Appendix 2: Material property of flax epoxy composite [22].....	105
Appendix 3: Material property of glass epoxy composite (obtained from RVE analysis using ANSYS [74]).....	106

1 Introduction

1.1 Background

Composite materials are susceptible to delamination during their service life, significantly reducing the performance of the material. Delamination is defined as the separation of two laminae in a laminate between their interface. The detection of these damage mode requires sophisticated and expensive non-destructive methods. Delamination in composite materials can reduce the stiffness of the material by up to 60% [1], and it is a major limiting factor that has hindered the wider application of composite materials [2]. Therefore it is important to improve the understanding of the delamination resistance of composite materials so as to reduce the over design of composite parts [3, 4] in order to realize the full weight saving opportunities that lie in the application of composite material achievable [5].

The ability of a material to resist the initiation and propagation of delamination is referred to as the fracture toughness of the material. The interlaminar fracture toughness of composite material is measured as the critical strain energy release rate G_c or the critical value of the stress intensity factor K_c [6, 7]. If the value of K and G_I is below the K_c and G_{Ic} of the material respectively, the material will be able to resist crack initiation.

Interlaminar fracture or delamination between plies in a composite material is among the most common damage mechanism of reinforced polymer laminates because these material generally have weak interlaminar strength. The interlaminar fracture toughness property is important because it provides a measure of the structural integrity of the composite structure, more so since delamination is difficult to detect during visual inspection [8].

There are three major causes of delamination in service. (1) low-velocity impact – this does not leave any trace of damage on the surface of the composite but usually leads to internal

delamination; (2) Shear stresses, this occurs at the interfaces between two laminae, usually near the edges of the composite material, and this type of stresses ultimately leads to debonding of the ply surfaces; (3) Tensile stresses over the interface between two plies [9].

Some other causes of delamination may include the entrapment of moisture during the manufacturing of the composite material, engineering property mismatch between interfacial layers, improper curing, and inclusions. Also, after a low-velocity impact, the possibility of delamination increases. The tensile, flexural and compressive strength of composite materials can be severely affected by the initiation and growth of delamination, which results in the reduction of the stiffness of the material [7].

A composite material can be sufficiently weakened by the presence of longitudinal cracks and delamination cracks, which propagates and results in a final fracture [10]. The effect of the presence of delamination cracks is very severe; they prevent the distribution of loads between plies in the laminate which is essential to the strength of the material. Without the proper distribution of load between the plies in a composite material, the separated plies acts in parallel to support the applied load. The plies with the lowest strength fail, resulting in a cascading effect of failure on the remaining plies [11].

The interlaminar fracture toughness of a material can be determined for three modes of loading: (i) Tension, referred to as Mode I, the opening mode and it is represented as G_{Ic} ; (ii) in-plane shear, referred to as Mode II, the sliding mode, and it is represented as G_{IIc} ; and (iii) Out of plane shear referred to as Mode III, the tearing mode, denoted by G_{IIIc} . The fracture toughness for the different modes can be measured for crack initiation and crack growth in the composite laminate [6, 12]. Figure 1-1 a, b and c shows the modes in which Interlaminar fracture occurs (a) Tension – mode I (b) shear – mode II and (c) out-of-plane shear – mode III.

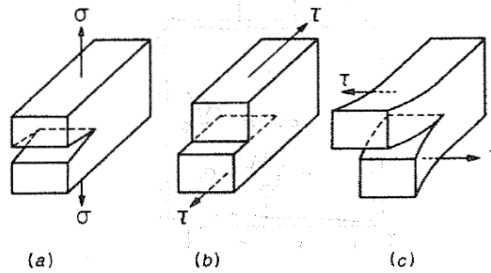


Figure 1-1: The basic modes of delamination (1a: Mode I, 1b: Mode II, 1c: Mode III, 1c) [11]

Understanding fracture the fracture toughness property of composite material is important. This property will help designers to explore the potential of composite materials in structural applications, predicting in-service failure, lifetime and behaviour of the composite material in service.

This thesis hopes to increase the knowledge and understanding of the fracture toughness of hybrids of flax and glass epoxy composite. The main goal of this thesis is to characterize the mode II interlaminar fracture toughness of hybrids of flax and glass fibre in an epoxy matrix.

The Virtual Crack Closure Technique (VCCT) method is used to model the crack initiation and to analyze the stress distribution in the plies of the hybrid laminate.

1.2 Objectives and Research Motivation

The main objective of this research is to increase the knowledge and understanding of the mode II fracture toughness of a hybrid composite material made up of flax fibre and glass fibre in an epoxy thermoset matrix with the goal of characterizing the mode II fracture toughness of the hybrid material.

This study will apply ASTM, D7905 standard [13] to investigate the mode II fracture toughness and the 3D Virtual Crack Closure Technique (VCCT) to model the end notch flexural experiment. The Hashin-criteria will be applied in the Finite Element Analysis simulation to determine which ply is likely to fail during mode II delamination.

An end-notch flexural test will be performed on three hybrids of flax and glass fibre to determine their mode II interlaminar fracture toughness. A total of 15 specimens is tested with – five specimens per hybrid material. The end-notch flexural tests require that two compliance calibration test and a fracture test to be performed on each specimen. Thus, a total of 3 experiments per sample is required to successfully characterize the mode II fracture toughness of each hybrid material.

For this research, at least 3 X 15 experiments are performed. A least square linear regression analysis is done to obtain the compliance calibration coefficients from each experiment which are then applied to evaluate the fracture toughness of the respective hybrid.

Another focus of this research is the application of finite element analyses (FEA) using ANSYS commercial simulation software to model the end notch flexural test and to validate the simulation results by comparing them to those obtained from the experiment. The goal of carrying out this simulation of the mode II fracture toughness is to determine if FEA simulation tools like ANSYS can be practical as an assessment tool, in other to evaluate the performance of each ply and analyze the distribution of stress in each layer of the different hybrid laminate without carrying out additional experiments. Furthermore, the parameters required to model the mode II fracture toughness experiment successfully can be established.

To the author's knowledge, no existing research has investigated the effects of the layup sequence of hybrids of flax and glass epoxy on the mode II fracture toughness, and no other research has applied a finite element analysis tool to analyze the ply response to loading during mode II delamination. This research aims to fill this knowledge gap.

2 Literature Review

Interlaminar failure in the interface of two plies in laminated composite material, also referred to as delamination, is one of the major failure mechanisms of composite materials.

Delamination can be defined as the separation of two laminae in a laminate across their interface. There are different causes of delamination: (1) low-velocity Impact, which leads to internal delamination. (2) Shear stresses, this occurs at the interfaces between two laminae, near the edges of the composite material (3) Tensile stresses in the interface between 2 plies [9].

The flexural, tensile, and compressive strength of composite material is severely affected by the presence of delamination, which results in the decrease of the stiffness of the material; this is a general concern in the application of composite materials [18].

Kim et al. [14], in their research on the influence of fibre direction and mixed-mode ratio on delamination fracture toughness of carbon/epoxy laminates, observed that while other failure mechanisms impact the mechanical properties of composites, interlaminar delamination is one of the major damage mechanisms. Improving the understanding of this mechanism will increase the adoption and development of composite materials [19].

In the last decade, delamination has been recognized as a limiting factor in the application of composite material. Different methods have been proposed to investigate the interlaminar fracture toughness of materials [7]. To understand the cause of failure in service, due to the presence of interface debonding, the Linear-Elastic Fracture Mechanics (LEFM) was developed to aid in material selection and designing of engineering components to reduce the possibility of failure of engineering components [12].

The ability of a material to resist the propagation of delamination is referred to as the fracture toughness of the material. The interlaminar fracture toughness of composite materials is measured by

the critical Strain Energy Release Rate (SERR) G_c or the critical value of the stress intensity factor K_c [6, 7]. If the value of the stress intensity factor K and the Strain Energy Release Rate G_I is below the critical values K_c and G_{Ic} , respectively of the material, the material will be able to resist delamination propagation, but if the inverse is the case, delamination will occur.

The critical energy release rate G_c of a laminate composite material is defined as the amount of energy required for a delamination crack to initiate or propagate through a unit area of the material. The unit for the G_c , are joules per square (J/m^2) or Newtons per metre (N/m) [15].

The ASTM, D5528 Standard [16], D7905 Standard [17], and D6671 Standard [18] describe in detail standards for investigating mode I, mode II and mixed-mode I/mode II interlaminar fracture toughness of composite materials. The ASTM, D5528 Standard [16], describes the standard tests for determining the mode I interlaminar fracture toughness G_{Ic} of the composite material by using a double cantilever beam (DCB) sample. The ASTM, D7905 Standard [17], describes the tests for determining G_{IIc} the mode II interlaminar fracture toughness using the end-notched flexural (ENF) specimen. The ASTM D6671 Standard [18] describes the tests to determine the fracture toughness G_c at various mode I and mode II loading ratio using the Mixed-mode Bending (MMB) Specimen.

For each of these tests, a load vs displacement curve is produced, which provides data to determine the onset and the growth or propagation of delamination. These data are used for obtaining the fracture toughness of the composite material.

There has been a significant number of researches that have evaluated the delamination properties of composite materials; some of these researches evaluated different phenomena that can influence crack initiation and crack growth in a composite material. The research by Argüelles et al. [19] studied the effect of high temperatures from 20 to 200°C and moisture on the mode I and mode II interlaminar fracture toughness of Carbon PEEK composite material, and in their work noted that

other researchers have evaluated the effect of the speed of loading, volume fraction, fibre treatments, the type of matrix and the manufacturing method on the interlaminar fracture toughness of composite materials.

Additionally, there have been numerous works done on the characterization of the mechanical properties of flax fibre during static and fatigue loading [20-23]. Despite the increased interest and number of researches on flax fibre composites, there is still low availability of information on flax fibre interfacial properties; thus, more data and more information on the properties of flax fibre is still needed. This data is needed to help designers understand how flax composites will respond to loading and are essential to the design of structures made of natural composite materials [24].

As earlier stated, the interlaminar fracture toughness properties of composite materials are essential for the design of structures with composite materials, thus, to further improve the application of natural fibres like flax fibre, more understanding of the fracture toughness is needed. There are a few studies on the fracture toughness properties of flax fibre composites. Some authors have researched the mode I and mode II interlaminar fracture toughness of flax fibre composite materials [6, 24-28]. For example, Bensadoun et al. [6] sought to understand how the architecture of flax fibres affects its fracture toughness. They performed mode I and mode II fracture toughness experiments on unidirectional, quasi unidirectional, plain weave and twill fibre architectures of flax fibres and compared their interlaminar fracture properties. The results showed that the twill architecture has a higher fracture toughness, compared to the other flax architectures and further showed how the lay-up sequence of the flax composite materials could affect the interlaminar fracture toughness of the material.

Another study by Saidane et al. [24] evaluated the mode I interlaminar fracture toughness of flax fibre and the effects of hybridization on the fracture toughness of unidirectional flax/glass a

hybrid of flax. The results showed that the fracture toughness of the hybrid at initiation was close to the glass fibre crack initiation, and the fracture toughness of the crack propagation was higher for the hybrid flax reinforced epoxy than the glass-reinforced epoxy and the flax fibre reinforced epoxy.

Table 2-1 summarises the research on mode I interlaminar fracture toughness for crack initiation and propagation of flax epoxy composite from literature. So far, these are the only research that has investigated the fracture toughness of flax epoxy composites. Thus, these data are not enough to improve designer confidence in the application of flax epoxy reinforced polymer materials, and more information is required.

From the research done so far on flax epoxy composite [6, 24-28], no two composite materials have the same configuration and fracture toughness. Thus, it is difficult to find a trend because the data available is limited. Hence, more research, experiment and engineering simulation are required to increase the knowledge of the fracture toughness initiation and propagation of flax epoxy composites.

Table 2-1: Summary of initiation and propagation mode I fracture toughness (G_{Ic}) of flax epoxy values of flax epoxy composites from literature.

Material Name	Layup Code	Fracture toughness G_{Ic} (J/m^2)		References
		Initiation	Propagation	
UD Flax Epoxy	$[0]_{16}$	771	1250	[26]
FFRE	$[0]_{10}$	1079.20	1560	[24]
HFRE	$[(0_{GF}/0_F)_6]_s$	944.8	2080	
Weave 2/2	$[0]_{10}$	363	962	[27, 28]
Plain Weave	$[0]_4$	457	1158	[6]
Twill low twist	$[0]_4$	754	1597	
Twill High twist	$[0]_8$	607	1151	
Quasi-UD [0,90]	$[0,90]_s$	662	1341	
Quasi-UD [90,0]	$[90,0]_s$	777	995	
UD2 [0,90]	$[0,90]_{2s}$	655	1086	
UD2 [90,0]	$[90,0]_{2s}$	496	663	

*where UD represents unidirectional, FFRE represents Flax Fibre Reinforced Epoxy and HFRE represents Hybrid Flax Reinforced Epoxy.

2.1 Hybrid Materials

Hybrid composites are one of the fast developing class of materials in polymer composites. There has been significant research on various properties of hybrid composites [29-34]. In the past few years, hybrid composite materials with thermoset or thermoplastic matrices reinforced with natural fibres and synthetic fibres have gotten a lot of attention [29].

Hybrid composite materials are obtained from the combination of more than one type of fibre reinforcement material in the same matrix. Some researchers have suggested that cellulosic natural fibres with synthetic will reduce the environmental impact of synthetic composite material while improving the performance of the material. They noted that this is a favourable compromise between environmental sustainability and performance [29]. This proposal was further validated by Jawaid et al. [30] in their work, where an extensive review of cellulosic/synthetic fibre hybrid composites was carried out. They further stated that hybrid materials have one significant advantage over non-hybrid materials; one type of fibre in the hybrid material could complement the property the other fibre(s) in the hybrid is lacking. Thus, any composite material consisting of cellulosic and synthetic reinforcement fibre will display the advantageous properties of the different constituent fibres.

In a study of the of flax/carbon fibre hybrids by Dhakal et al. [29], where their mechanical properties, water absorption and thermal stability were investigated, they concluded that the new hybrid was cost-effective, had better mechanical and thermal stability than the pure carbon fibre material.

In a research by Sarasini et al. [34], that investigated the resistance of carbon and flax hybrid to low-velocity impact, concluded that the hybrid material had better mechanical and impact properties.

This research hopes to answer the following question. Can hybridizing glass fibre with flax fibre improve its mode II delamination fracture toughness? Experiments will be applied to evaluate the mode II fracture toughness and Finite Element Analysis analyze the flax epoxy plies for failure at delamination. Other tools applied in this research are the Representative Volume Element, Virtual Crack Control Technique and the Hashin Criteria. The following sections provide an overview of the key elements used in the research.

2.2 Flax Fibre.

Flax fibre is a natural fibre whose specific mechanical properties are comparable to those of glass fibres. This reason has resulted in increased interest by researchers who have led to a significant number of researches over the last decade. Flax fibre is also one of the strongest plant fibre [35], [36]. In the last two decades, the application of composite materials with natural fibre reinforcements has continually grown in the maritime, aerospace, construction, sports and automotive sectors of industry. For example, Yan et al. [37], investigated the crashworthiness of flax epoxy composite material in automobile applications in their research, they measured the crush force efficiency, the specific absorbed energy and the total energy absorbed. They concluded that due to the high strength to weight ratio, energy absorption capability and corrosion-resistant properties, composites with flax fibre reinforcements have a high potential to be used as energy absorber devices in automotive.

In another work by Yan et al. [38], the application of flax fibre reinforced composite as a sustainable construction material was investigated, a composite column made of flax reinforcement fibre and concrete was tested to characterize its uniaxial compression and flexural properties. It was concluded in this research that the flax fibre improved the flexural and compressive properties of the concrete structure.

Research by Shah et al. [39], sort to answer the question can E-glass be replaced by flax fibres? A comparative study of the mechanical properties was performed between two identical wind turbine blades, one made of E-glass and the other of flax fibre. The researchers concluded that E-glass could be suitably replaced by flax fibre as a structural reinforcement fibre.

Other research has shown that the flax fibre has a very high potential for use in most industries and has been adopted and is also being widely applied in the sports industries in surfing boards, bicycle frames, paddles and other sporting equipment. It has also has been applied in small boats and paddles manufacturing [40].

A review by Pickering et al. [41] highlights several advantages of natural composites like flax fibres over synthetic fibres. These advantages include high specific stiffness, high specific strength, low density, low production cost and low emissions of toxic fumes during manufacturing.

Another important advantage of natural fibres over synthetic fibres is, in the end life cycle of a natural fibre reinforced composite which was subjected to a combustion process, the released amount of CO₂ of the fibres is neutral relating to the amount absorbed during there growth. Hence, natural fibre is termed a CO₂ neutral reinforcement fibre [36]. Also, natural fibres composites possess better economic, ecological and technical advantages compared to other composites made from synthetic fibres [42].

Shah et al. [42], in their research on developing plant fibre composites for structural applications reported that flax fibres are proposed as a prospective substitute to the E-glass fibres in composite materials. They elaborated by stating that 87% of the 8.7 million tonnes of fibre reinforcement polymer used in the world are based on E-glass and plant fibre has a big potential for significant market capture.

Flax composites possess good acoustic, thermal, insulation, damping and enhanced vibration absorption properties, which are desirable properties that have resulted in an increase of its application [43].

Canada produces the highest amount of flaxseed in the world. Flax fibres are obtained from the straw of oilseed flax stalk [44]. The amount of energy required to manufacture flax fibres is less intensive than that required for mineral fibres [45].

Flax elementary fibre has elongated single cell thick walls that surround a luminal cavity. These cell walls are responsible for the properties of flax fibres. Flax elementary fibres have variable cross-sectional areas. These elementary fibres are usually in bundles referred to as technical fibres with a middle lamella, which is a pectin layer that cements the connecting cells together. Hence, flax fibres can be referred to as a composite because they comprise of semi-crystalline cellulose microfibrils that are oriented 10° and embedded in a two-phase amorphous matrix. The contents of the plant composite are cellulose, hemicellulose and lignin [42], [46], [47].

Furthermore, the elementary fibres, which are single plant cells, consist of a primary cell wall, a secondary cell wall and a lumen. The lumen is an open channel in the fibres centre, which can be up to 1.5% of its cross-sectional area. The primary cell wall is about $0.2 \mu\text{m}$ thin and consists of pectin, lignin and cellulose. Most of the fibre diameter is made of the secondary cell wall. The flax fibre plant composition is shown in Figure 2-1. The secondary cell wall consists of highly crystalline cellulose microfibrils oriented spirally at an approximate angle of $+10^\circ$ to the fibre's axis and amorphous hemicellulose. This oriented crystalline cellulose structure makes flax fibre stiff and strong when loaded in tension [48].

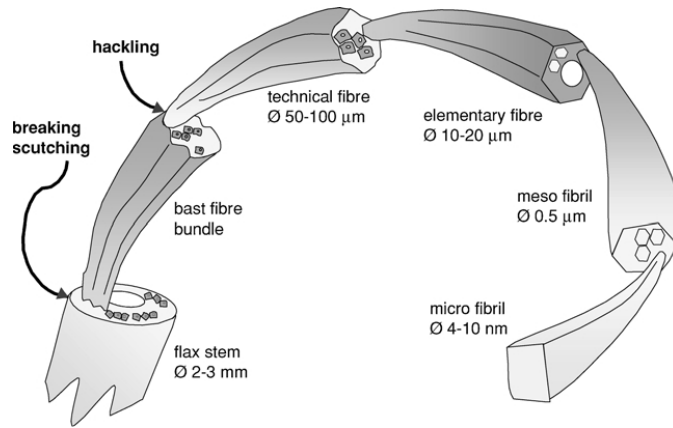


Figure 2-1: The composition of a flax fibre plant. [47]

2.3 An overview of Glass fibre

The most common and well know polymer reinforcement material used in composite manufacturing of fibre-reinforced polymer composite is glass fibre. Its high tensile strength and low cost make it a very desirable material. Commercially, glass fibres are available as fibreglass roving, woven roving, chopped strand mats and continuous strand mats. These various forms are because of the vast application of glass fibre [11]. Glass fibre also have excellent chemical resistance, exceptional insulation properties [49], they are also non-flammable and heat resistant [50]. The most common and well know polymer reinforcement material used in composite manufacturing of fibre-reinforced polymer composite is glass fibre.

There are two types of glass fibre widely used in fibre reinforced polymer composites; they are the electrical grade glass or E-glass and S-glass fibres (“S” for strength). E-glass is the cheaper of the two fibres and is more commonly used compared to S-glass. S-glass has higher tensile strength and was developed for use in the aerospace industry [49]. The difference in the mechanical properties between E-glass and S-glass is due to their chemical composition. The chemical composition of E-glass is 54.5wt% SiO₂, 17wt% CaO, 14.5wt% Al₂O₃, 8.5wt % B₂O₃, 4.5wt% MgO and 0.5wt% Na₂O, while S-Glass has 64wt % SiO₂, 26wt% Al₂O₃ and 10wt% MgO [49].

In 2015, more than five million tons of glass fibre was used in reinforced polymer composite. This makes up 90% of all fibre reinforcement used in that year. Various research has studied the strength of glass fibre [51]. The mechanical property of E-Glass fibre is shown in Table 2-2 below.

Table 2-2: Glass fibre (E-glass) Mechanical properties [11]

Mechanical properties	
Tensile Strength	3.1 – 3.8 GPa
Tensile Modulus	76 – 81 GPa
Density (ρ)	2.54 – 2.62 g/cm ²
Poisson's ratio	0.18

2.4 An Overview of Epoxy.

One of the most common thermoset matrices in composite manufacturing is the epoxy matrix.

Epoxy is an organic liquid with low molecular weight made up of epoxide groups that contain two carbon atoms and one oxygen atom. To obtain the epoxy matrix, a starting material containing two epoxide groups with the molecule having one epoxide group at each end, shown in Figure 2-2, commonly referred to as diglycidyl ether of bisphenol. Then other materials are mixed in, and these ingredients – diluents are added to decrease the viscosity of the epoxy compound. Also, flexibilizers may be added to improve the impact toughness of the epoxy matrix after it has cured [49].

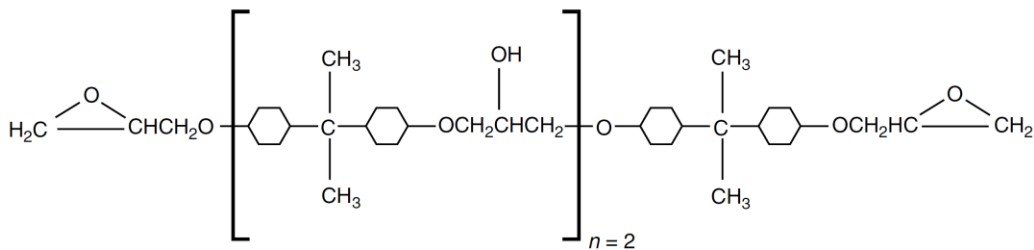


Figure 2-2: A diglycidyl ether of bisphenol molecule [48]

The curing process of the epoxy referred to as polymerization is initiated by adding a small amount of a curing agent. A common curing agent is diethylene triamine. A molecule of diethylene triamine is shown in Figure 2-3. The polymerization process transforms the liquid epoxy into a solid-state when the hydrogen atom of the curing agents reacts with the starting material's molecules which

form a cross-link causing the formation of a three-dimensional network structure. The polymerization process is initiated at room temperature but elevated temperatures ranging up to 250°C are usually applied in a duration of time to complete the curing process. In general, most epoxy matrixes used in the manufacture of composite materials are cured at 150°C or less [49].

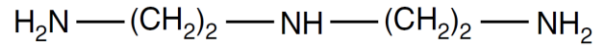


Figure 2-3: A molecule of diethylene triamine [48]

The typical properties of epoxy resin are shown in Table 2-3. This table shows the density, tensile strength, tensile modulus and other important properties of the epoxy matrix.

Table 2-3: Typical properties of Epoxy Matrix [48]

Density (g/cm ³)	1.2-1.3
Tensile strength, MPa	55-130
Tensile Modulus, GPa	2.75-4.10
Poisson's ratio	0.2-0.33
Coefficient of thermal expansion, 10 ⁻⁶ m/m per °C	50-80
Cure shrinkage, %	1.0 - 5.0

The typical mechanical properties of some carbon fibre and glass fibre reinforced in epoxy composite materials are shown in Table 2-4.

Table 2-4: typical properties of Fibre reinforced epoxy composite materials [11]

Material Description	Fiber Volume fraction V_f	Density (g/cm ³)	E_L (GPa)	E_T (GPa)	G_{LT} (GPa)	σ_{LU} (MPa)
Carbon Epoxy. T300/N5208	0.70	1.6	181.0	10.30	7.17	1500
Carbon Epoxy. AS/H3501	0.66	1.6	138.0	8.91	7.10	1447
Carbon Epoxy. IM6/epoxy	0.66	1.6	203.0	11.20	8.40	1540
E-glass Epoxy. T300/N5208	0.45	1.80	38.6	8.27	4.14	1062

2.5 Finite Element Analysis and Delamination

Advancement in Finite Element Analysis (FEA) has made it possible to predict and assess the crack growth and propagation property in composite materials. One way this can be achieved is by applying the Virtual Crack Closure Technique (VCCT). The VCCT operates on the assumption that the amount of energy released during the crack initiation or propagation is equal to the energy required for the crack to close and return to its original position. The VCCT method is implemented in engineering simulation software by computing the energy release rates components for the nodal relative displacements and the nodal forces [8].

With the growth of computer modelling and simulation software capabilities that provide highly detailed structural Finite Element Analysis, and the growth of the computing capacity of CPU's, commercially available FEA software are capable of effectively analyzing the behaviour of composite materials during delamination.

This section in the literature review aims to review FEA and how it has been applied to assess delamination in composite materials. The delamination models that are available in commercially FEA software are also reviewed. Finally, the FEA evaluated to determine if it is a suitable tool to assess the behaviour of composite materials during delamination.

One of the first failure mode to occur at the onset of damage in a composite material is delamination [52]. This failure mode has received an enormous attention from researchers which has led to the development of standardized techniques for evaluating the mode I, mode II and the mixed-mode I and II by the American Society of Testing and Materials (ASTM). Furthermore, there has been growth in the development of numerical models, which predicts the onset and propagation of delamination and some of these models have been implemented in different commercially available FE software [53].

Researchers have extensively investigated the interlaminar fracture toughness of composite materials over the last decade. These studies have focused on different aspects such as fracture initiation, fracture propagation, critical damage zone, composite material sensitivity to notch and failure modes applying several theoretical, numerical and experimental methods [11].

Agarwal et al.[11] highlighted that there are several reasons why several theoretical, numerical and experimental techniques have been applied to study the interlaminar fracture toughness of composite materials. Firstly, the complex nature of delamination. The damage mechanisms and failure modes are not the same for different composite materials, and to properly investigate these modes and mechanisms of failure, different tools and techniques may have to be applied. Secondly, it was further stated that there is no consensus on the best failure criteria for composite materials. There have been several numerical and semi-empirical methods developed to evaluate the different failure modes and the complex damage mechanisms in composite laminates.

Although this situation of having several techniques to evaluate the fracture toughness of composite material is undesirable because it further creates a divide in the development of a unified design procedure for predicting the failure of composite laminate, it cannot be avoided because of the large number of variables that may influence the interlaminar fracture toughness of composite materials. Furthermore, there is a large number of experimental data on the fracture toughness of different composite materials and these data may not be useful in the design of other laminates because of the numerous variables that may affect the delamination properties of a composite material as was previously stated [11].

2.5.1 Virtual Crack Closure Technique (VCCT)

There are a variety of techniques that can be used to compute the Strain Energy Release Rates (SERR) in assessing the onset and growth of delamination in finite element analysis. Some of these techniques are the finite crack extension method, the virtual crack extension method, cohesive zone model (CZM), the J-integral method and the equivalent domain integral method. However, the Virtual Crack Closure Technique is the most widely [54].

The virtual crack closure technique (VCCT) was first proposed for 2D crack configurations by Rybicki et al. [55] and Tan et al. [56] extended this research to the 3D application by proposing a method to obtain the energy release rate G or the value of stress intensity factor K using nodal forces and displacements in FE analysis, this method was referred to as the 3D Virtual Crack Closure Technique (3D VCCT). This technique used the fundamental assumption that a finite number of straight-line segments can estimate any continuous function.

An 8-node and 20-node element was employed for several cracked bodies. The method was validated when sample plates with surface cracks with notches and other samples without notches were analyzed. The results obtained using the force and the crack opening displacement (COD) method were compared. The method demonstrated that the 3D VCCT method is easy to implement, accurate and requires multiple elements [56].

Additionally, a study by Krueger et al. [57] that compared the experimental results obtained from tests on a graphite/epoxy composite material with layup sequence $[\pm 45/0/\mp 45/0/\pm 45]$ to the 2D and 3D Virtual crack closure technique, noted in their report that the interlaminar fracture changes across the width of the laminate and concluded that this width effect could only be accounted for in a 3D VCCT finite element analysis, thus stating that the 3-Dimensional VCCT will produce more accurate results compared to 2D dimensional VCCT.

Delamination is one of the common modes of failure of composite materials, to characterize the onset and propagation of this mode of failure, the VCCT has gained an increased interest in the last two decades because of the growth in the application of fracture mechanics models to assess the delamination damage of composite materials during the design and certification of composite materials. The total strain energy release rate G_T , Mode I (G_I), Mode II (G_{II}) and Mode III (G_{III}) components due to interlaminar tension, shear and scissoring shear can be assessed with the VCCT technique [54, 58].

In a commercial simulation software like ANSYS, the Virtual Crack Closure Techniques (VCCT) is computed based on results from the 2D and 3D finite element analyses. This is achieved by implementing the modified crack closure method, which is based on the assumption that the energy required to open a surface is the same energy that is required to close that surface but goes further to analyze the stress around a crack tip. The energy release rate G is obtained in the analysis phase of the simulation, and the results are saved for postprocessing [59].

Also, in ANSYS, the 3D VCCT energy-release rate is defined as [59] :

$$G_I = -\frac{1}{2\Delta A} \cdot R_y \cdot \Delta v \quad (2.1)$$

$$G_{II} = -\frac{1}{2\Delta A} \cdot R_x \cdot \Delta u \quad (2.2)$$

$$G_{III} = -\frac{1}{2\Delta A} \cdot R_z \cdot \Delta w \quad (2.3)$$

Where; ΔA = crack-extension area. (as shown in Figure 2-4)

G_I, G_{II}, G_{III} = Mode I, II and III are the respective energy release rate

$\Delta u, \Delta v, \Delta w$ = relative displacement between the top and bottom nodes of the crack face in the local x, y and z coordinates respectively.

R_x, R_y, R_z = reaction forces at the crack-tip node

A 3D schematic of a crack geometry is shown in figure 2-4.

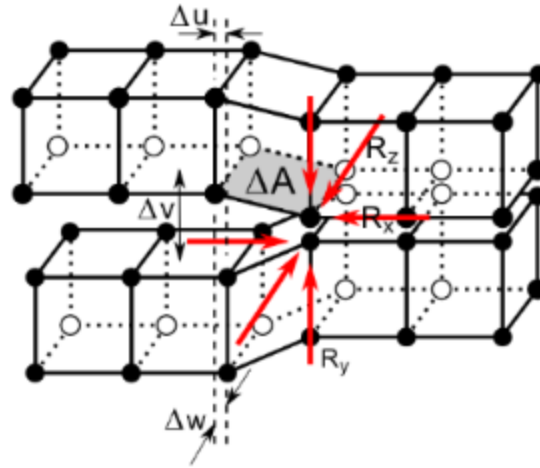


Figure 2-4: The 3D VCCT crack geometry [58]

The 3 Dimensional Virtual Crack closure technique has been applied by Khatir et al. [60], Shokrieh et al. [61], Xie et al. [62], Xie et al. [63], Krueger et al.[57] and by the Society of Automotive and National Institute for Aviation [58] in their research to assess the delamination properties of different composite laminates and they have concluded that applying the 3D VCCT to analyze delamination onset and propagation in Finite Element Analysis produces highly accurate results that are comparable to other numerical techniques and also to experimental results. Thus, for this thesis research, the Virtual Crack Closure Technique is employed in investigating the mode II interlaminar fracture toughness of the hybrid material in this study.

2.6 Hashin Criterion

Failure criteria predict failure under different loads or stresses based on curve fits of data obtained from laboratory experiments. The failure criteria described in this chapter predicts the initiation of failure under uniaxial load in the laminas. Although this criterion is limited, it can only determine when a failure occurs and not able to track the failure propagation through the composite material or damage evolution until complete laminate failure [64], it is sufficient to analyze the failure of the composite materials investigated in this study.

In ANSYS, failure criteria are defined in terms of a failure index; this is defined by equation 2.4 shown here [64];

$$I_F = \frac{\textit{stress}}{\textit{strength}} \quad (2.4)$$

Failure is predicted to have occurred if $I_F \geq 1$.

Another ratio used in FEA is the strength ratio, it is defined as shown in equation 6.5

$$R = \frac{1}{I_F} = \frac{\textit{strength}}{\textit{stress}} \quad (2.5)$$

Failure is said to have occurred when $R \leq 1$.

In this research, the Hashin criterion is selected as the criterion to investigate the failure of the flax ply in the hybrid laminate to determine how the ply behaves during delamination.

Hashin proposed a quadratic polynomial solution to predict the mechanical properties of unidirectional fibre composite materials. In the proposal, isotropy is assumed in the cross-sectional plane of the composite material. He recognized that there was a problem in the prediction of failure of fibre reinforced composite due to the present state of stress of the material. He went on to propose

a failure criterion whose polynomial coefficients are based on the tensile, compression and shear tests results obtained from the laboratory.

Research by Hashin [65] on the failure criteria for unidirectional composite, he stated that a composite material could fail in two primary mode: (i) The fibre mode, in this mode, the composite could fail as a result of fibre rupture due to tensile load or fail due to fibre buckling as a result of compression load. Furthermore, this fibre modes also refers to tensile or compressive failure in the fibre direction; (ii) A matrix mode, in this mode, failure is as a result of plane crack parallel to the fibre which could occur because of tension or compression load on the composite material. He also stated that when a failure in a composite occurs, if the plane of failure can be identified, it will be possible to identify the normal stresses and shear stresses on the plane as the cause of failure. Therefore, stresses responsible for failure in a composite material are the σ_1 , σ_2 , and σ_6 which are the applied stresses in the longitudinal (the fibre direction), transverse (perpendicular to the fibre direction) and the shear direction of the material respectively.

The Hashin plane stress Failure Criteria for the different failure modes are stated in equation 2.6 to 2.9 [64] and [65].

Fibre Mode:

Tensile Fibre Mode: if $\sigma_1 \geq 0$

$$I_{Fft}^2 = \left(\frac{\sigma_1}{F_{1t}}\right)^2 + \left(\frac{\sigma_6}{F_6}\right)^2 \quad (2.6)$$

Fibre Compressive Mode: $\sigma_1 < 0$

$$I_{Ffc}^2 = \left(\frac{\sigma_1}{F_{1c}}\right)^2 \quad (2.7)$$

Matrix Mode:

Tensile Matrix Mode: if $\sigma_2 \geq 0$

$$I_{Fmt}^2 = \left(\frac{\sigma_2}{F_{2t}}\right)^2 + \left(\frac{\sigma_6}{F_6}\right)^2 \quad (2.8)$$

Compressive Matrix Mode $\sigma_{22} < 0$

$$I_{Fmc}^2 = \left(\frac{\sigma_2}{2F_4}\right)^2 + \left[\left(\frac{F_{2c}}{2F_4}\right)^2 - 1\right] \frac{\sigma_2}{F_{2c}} + \left(\frac{\sigma_6}{F_6}\right)^2 \quad (2.9)$$

Where

F1t is the Longitudinal tensile strength of the composite material

F2t is the Transverse tensile strength of the material

F3t is the Transverse-thickness tensile strength of the material

F1c is the Longitudinal compressive strength

F2c is the Transverse compressive strength of the material

F3c is the Transverse-thickness compressive strength of the material

F4, F5 and F6 are the in-plane shear strength

There are other failure criteria, the Tsai-Hill, Azzi-Tsai-Hill, and Tsai-Wu, but the Hashin failure criteria were selected because, compared to the other criteria, it does not overemphasize the interaction between the fibre (σ_1) and transverse matrix (σ_2) damage modes according to Barbero et al.[64]. Also, it is one of the few criteria that makes a clear distinction between the fibre tensile and compressive failure and the matrix tensile and compressive failure.

ANSYS is a very powerful tool that allows researchers the ability to evaluate the responses of composite material to the applied load. In ANSYS, the stresses in each lamina can be analyzed by

combining the 3D Virtual closure techniques and the Hashin criteria to investigate the response of the end notch flexural specimen to loading. The mode II interlaminar fracture toughness of the hybrid of flax fibre and glass fibre in the epoxy thermoset matrix is investigated which is one of the goals of this research. The next section presents an overview of the laminate properties in ANSYS simulation software.

2.7 Laminate properties in ANSYS simulation software

In ANSYS, a stack-up is applied as a single-ply, and in the analysis, the individual plies that make up the stack-up are evaluated. For each ply in the stack up, the fabric material and fibre orientation must be inputted.

The laminate properties can be obtained in ANSYS. This is based on the Classical Laminate Theory (CLT) Analysis. It is implemented based on the shell mesh layup. The laminate stiffness, compliance matrices, the normalized laminate stiffness, compliance matrices and the laminate engineering constants can be obtained.

An outline of the ABD matrix and the illustration of the different plies is shown in Figure 2-5. The laminate stiffness matrix comprises A, the in-plane stiffness matrix, B, the coupling matrix and D is the flexural stiffness matrix. Furthermore, the shear matrix C is also evaluated thus producing an 8 x 8 matrix in the analysis result. A 6 x 6 ABD matrix and a 2 x 2 C shear matrix [10].

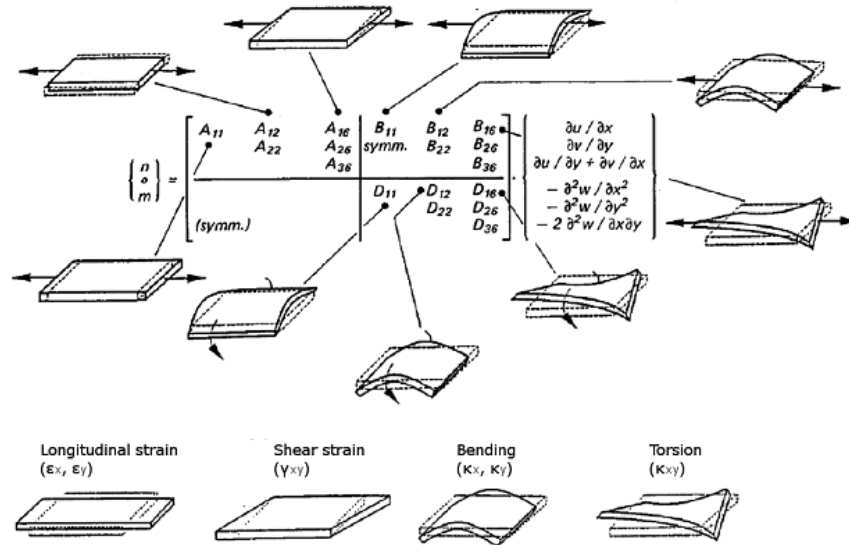


Figure 2-5: ABD matrix and the coupling between laminate forces and deformations [10]

The normalized laminate stiffness and compliance matrices are based on the laminate thickness h .

Thus, the A B D normalized stiffness is obtained using the equations below [10]:

In-plane stiffness matrix:

$$A^* = \frac{A}{h}$$

Coupling Matrix:

$$B^* = \frac{2 \cdot B}{h^2}$$

Flexural stiffness Matrix:

$$D^* = \frac{12 \cdot D}{h^3}$$

Out of Plane shear Matrix:

$$Q^* = \frac{Q}{h}$$

The normalized compliance matrix $a^* b^* d^*$ is obtained from the equations stated below [10]:

In-plane compliance matrix:

$$a^* = a \cdot h$$

Coupling Matrix:

$$b^* = \frac{h^2 \cdot b}{2}$$

Flexural Compliance matrix:

$$d^* = \frac{h^3 \cdot d}{12}$$

Out-of-plane shear matrix:

$$q^* = q \cdot h$$

2.7.1 Laminate Engineering Constants

The laminate engineering constant is obtained from the normalized compliance matrix [11]. Thus,

Laminate longitudinal stiffness:

$$E_1 = \frac{1}{E_L}$$

Laminate transverse stiffness:

$$E_2 = \frac{1}{E_T}$$

Laminate shear stiffness:

$$G_{12} = \frac{1}{S_{66}}$$

The flexural - constants are derived from the normalized flexural compliance matrix [10]. Thus,

Flexural laminate stiffness:

$$E_1^f = \frac{1}{d_{11}^*}$$

Flexural laminate stiffness:

$$E_2^f = \frac{1}{d_{22}^*}$$

Flexural laminate shear stiffness:

$$G_{12}^f = \frac{1}{d_{66}^*}$$

2.8 Representative Volume Element (RVE)

The representative volume element (RVE) is a sufficiently large volume of a composite material's microstructure that can ensure the statistical representation of the material and can effectively be applied to estimate the orthotropic properties of the material. The Representative Volume Element (RVE) is applied with a view of predicting the mechanical properties of a composite material. The RVE technique has developed to become an efficient tool to provide researchers with significant insight into the microstructure of different engineering materials [66].

In a review of literature on representative volume element by Gitman et al. [67], they revealed that an effective RVE must possess specific criteria. These criteria are listed as follows.

- The RVE must contain adequate information on the microstructure it is representing.
- The RVE should be suitably larger than the microstructural grain size and should be suitably smaller than the macroscopic structural sizes of the material.
- The RVE should comprise an adequate number of macro-heterogeneities (the fibre, matrix material, inclusions, voids, etc.)
- The RVE response to loading must be independent of the type of boundary condition
- The RVE should be statistically homogenous to be adequately representative of the macro responses.

Furthermore, finite element analysis of representative volume elements has been widely employed as a reliable method to obtain the material properties of unidirectional composite materials [68]. Maragoni et al. [68] highlighted in their research that a significant number of studies carried out to assess the validity of RVEs of composite materials. They compared the RVE results to the actual engineering material and a number of those research were successfully validated.

Experimental techniques can be used to understand the properties of composite materials, especially hybrid composite materials; the mechanical properties, the effect of volume fractions, fibre orientation and other properties. However, to suitably perform the required experiments, fabrication and preparation of the composite material sample are required and this is a time-consuming and cost-prohibitive process. With the growth in computational infrastructure and the advancement of micromechanics software, Finite Element Analysis can be employed to analyze the RVE of composite materials effectively and predict their mechanical properties [69].

Several researchers have successfully applied and investigated the properties of different engineering materials using the Representative Volume Element technique [66-73]. Pelissou et al. [66] successfully applied the RVE technique to accurately estimate the fracture energy and stiffness of a quasi-brittle composite zircaloy and randomly distributed zircaloy hydrides. Maragoni et al. [68] applied the RVE technique to investigate the mechanical properties of glass epoxy unidirectional laminates; they found the results from the RVEs model were in good agreement with the manufactured glass/epoxy laminates.

Sayan et al. [69] used a commercially available finite element analysis software ABAQUS to investigate the mechanical properties of hybrid composite with a polypropylene matrix reinforced with glass and carbon fibre. The RVE computation model developed was able to accurately predict the longitudinal modulus, the longitudinal Poisson's ratios and the longitudinal shear modulus. Also, the transverse moduli, transverse Poisson's ratio and transverse shear moduli were predicted with reasonable accuracy.

The different studies outlined in this review show that the Representative Volume Element (RVE) technique can be a useful tool to predict the longitudinal and transverse mechanical properties of isotropic and orthotropic materials. This technique can also be used to predict the

mechanical properties of both unidirectional and randomly distributed fibre reinforcement in composite materials.

In this research, the RVE technique is employed to predict the longitudinal and transverse properties of the glass/epoxy ply in the different hybrids of flax and glass studied. The FEA model will be implemented in ANSYS simulation software, a commercially available software.

ANSYS simulation software has an application called Material Designer (MD) that enables researchers to model and investigate microstructures and obtain the mechanical properties of different materials [10, 74]. In ANSYS MD, there are seven Representative Volume Element type; Lattice, UD composite, Random UD composite, chopped fibre composite, Woven composite, Particle and Random Particles. Figure 2-6 shows the shape of the seven RVE in ANSYS material designer [10].



Figure 2-6: Shape of Representative Volume Element in ANSYS [10]

In a White paper released by ANSYS, Inc, titled “The Use of Material Designer for Analysis of UD composite materials” [74], they compared the mechanical properties of a composite material reinforced with unidirectional carbon fibre and glass fibre in an epoxy matrix. Also, the properties predicted from ANSYS MD obtained were compared to the Altair Multiscale Designer tool (another RVE modelling tool) and properties obtained from using the rule of mixture and the Halpin – Tsai method. The results showed that ANSYS Material designer could accurately predict longitudinal and transverse properties of composite materials, but it was noted that using the right material property for fibre and matrix is essential as applying the wrong property can impact the accuracy of the results.

3 Mode II Interlaminar Fracture Toughness

3.1 An overview of Mode II interlaminar fracture toughness

The standard test method for determining the mode II interlaminar fracture toughness G_{IIc} of composite material is the shear loading of an end notch flexural specimen, usually referred to as the end-notch flexure (ENF) test ASTM Standard [17].

The end notch flexural specimen has a uniform thickness, rectangular cross section and contains a delamination initiator just like the double cantilever beam. A three point loading fixture is used to apply load to the specimen. The end-notch specimen and the loading fixture are shown in Figure 3-1.

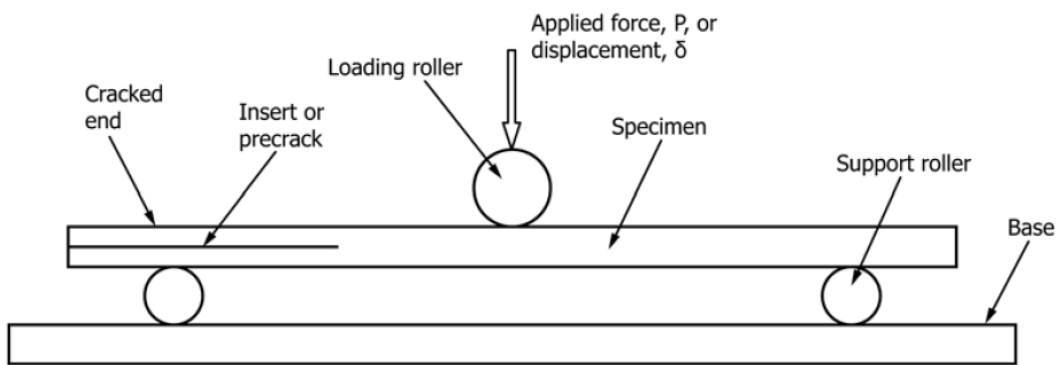


Figure 3-1: The ENF specimen and ENF fixtures [13]

As outlined in the ASTM Standard [13], the growth of the interlaminar crack is very unstable in the ENF test. Thus, the method described in the standard is given, so the interlaminar fracture toughness G_{IIc} at crack initiation can be obtained.

There are two techniques outlined in the ASTM standard D7905 [13] for obtaining the mode II interlaminar fracture toughness of composite material. The Non pre-cracked (NPC) method and the pre-cracked (PC) method, each of this method produces a fracture toughness referred to as the

non pre-cracked toughness and pre-cracked toughness, respectively. The major difference between both methods is that the crack created in the NPC test is used for the PC test [13].

In this research, the non-precracked test method is applied to obtain the mode II interlaminar fracture toughness of the material being investigated.

In the ENF test, the load is applied by the centre roller on the specimen. Each specimen is loaded in three locations. The force applied by the centre roller on each location is plotted against the displacement of the roller. A linear least square linear regression analysis is used to obtain the compliance from each test. The following paragraphs and sections outline how the mode II fracture toughness G_{IIc} is obtained.

In the ASTM Standard [13] the position and label of the ENF testing fixture geometry and the labels the dimension labels are shown in Figure 3-2. The bottom rollers r_2 spans a length of 100 mm ($2L$) and have a nominal half-length of 50 mm (L), and the radius of the loading roller r_1 should have a range between 4.7 to 9.6 mm and the radii of the bottom rollers r_2 should have a range between 3.0 to 6.4 mm. The loading roller should be centred between the bottom rollers. The rollers can either be fixed, rotatable or have a rolling arrangement as shown in Figure 3-2 [13].

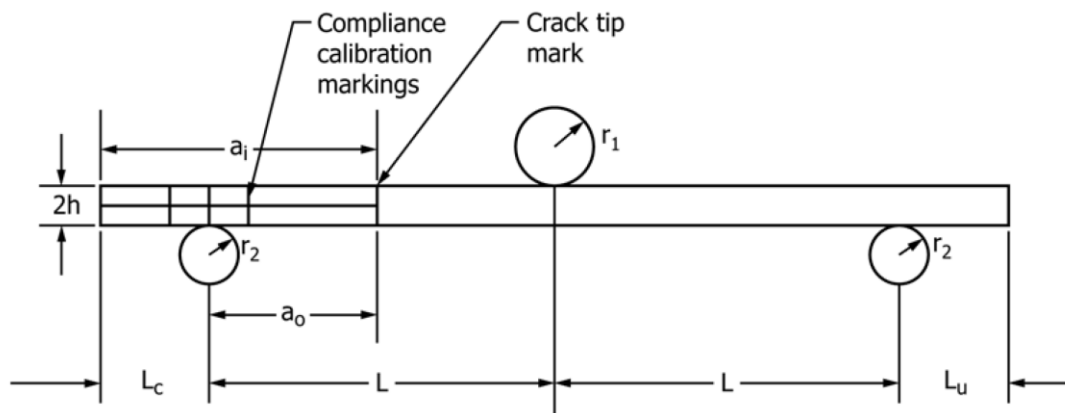


Figure 3-2: The ENF specimen and roller arrangement [13]

The ENF specimen should have a crack length of at least 45 mm, a thickness that ranges between 3.4 – 4.7mm, a length of at least 160 mm with a non-crack length of 115mm and a width ranging between 19-26 mm [8, 17].

The force applied at the 20 mm and 40 mm crack length is obtained from equation 3.1 [13].

$$P_j = \frac{2B}{3a_j} \sqrt{G_{IIc} E_{1f} h^3} \quad (3.1)$$

where P_j is the peak value of the applied force used during the compliance calibration experiment, and a_j is at 20 mm or 40 mm from the crack tip. B is the width of the specimen, h is half the height of the specimen, G_{IIc} is estimated fracture toughness of the material and E_{1f} is the flexural modulus of the specimen.

3.2 Data Reduction

The compliance calibration (CC) method is the data reduction method that is applied to obtain the candidate mode II interlaminar fracture toughness. Three compliances are obtained at 3 points from the crack tip on an ENF specimen. These points are at $a = 20$ mm, 40 mm, and during the fracture test at $a = 30$ mm. At each of these compliance calibration points, a linear least square regression analysis is performed to obtain the compliance which is the inverse of the slope of the linear regression analysis plot of the applied force (P) vs displacement (δ), this is illustrated in Figure 3-3, the broken line is the linear regression analysis plot and $1/C_0$ is the slope.

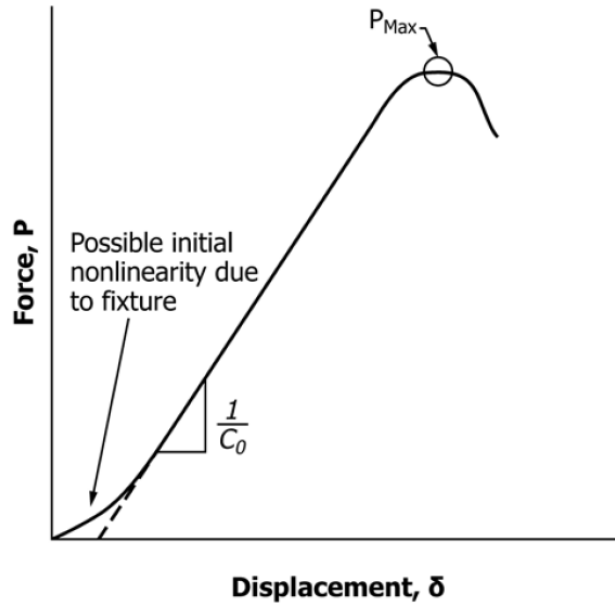


Figure 3-3: Plot of force vs displacement and the highlighted maximum load [13].

In accordance with the ASTM D7905 Standard [13], the linear regression analysis should only include data for which the force is equal to or greater than 90 N for the compliance calibration analysis.

For the linear regression analysis of the data from the fracture test, it should include all data with forces equal to or greater than 90 N and forces less than or equal to 50% of the maximum force observed during the fracture test. These forces are chosen so the curve-fit excludes any non-linear data [13].

Three compliances are obtained per sample, at crack length $a=20$ mm and $a=40$ mm and during fracture at $a=30$ mm. The three compliances are then plotted against the crack length cubed (a^3). Applying the least square linear regression analysis to the plot of compliance vs crack length data in the form shown in equation 3.2 is obtained:

$$c = A + ma^3 \tag{3.2}$$

where A is the intercept (mm/N) and m is the slope ($1/(\text{Nmm}^2)$) obtained from the linear regression analysis. Additionally, A and m are the compliance calibration coefficients required to obtain the fracture toughness and flexural modulus [13]. The application of these coefficients is outlined in the next section.

3.3 Candidate fracture toughness

An important parameter in this calculation is the maximum applied load during the fracture test. This is obtained from the plot of force vs displacement of the loading roller in the fracture test. Figure 3-3 shows a force vs displacement plot and highlight the position of the maximum load in the plot.

After obtaining the maximum force, the candidate interlaminar mode II fracture toughness is obtained by equation 3.3 [17]:

$$G_Q = \frac{3mP_{Max}^2 a_0^2}{2B} \quad (3.3)$$

where:

m = the Calibration Compliance coefficient ($1/(\text{Nmm}^2)$)

P_{Max} = the maximum force from the fracture tests (N)

a_0 = the crack length used in the fracture test (30mm)

B = the width of the ENF specimen (mm)

The candidate fracture toughness G_Q becomes the mode II interlaminar fracture toughness i.e. $G_{IIc} = G_Q$, If the percentage of the candidate fracture toughness ($\%G_{Q,J}$) achieved during the compliance calibration tests satisfies the limit $15 \leq \%G_{Q,J} \leq 35$.

The percentage of the candidate fracture toughness ($\%G_{Q,J}$) is obtained at $a = 20\text{mm}$ and 40mm , respectively achieved. The $\%G_{Q,J}$ is determined using equation 3.4:

$$\%G_{Q,j} = \left[\frac{100(P_j a_j)^2}{(P_{max} a_o)^2} \right]; j = 1,2 \quad (3.4)$$

where, $\%G_{Q,j}$ are the two values related to the two-compliance calibration test at 20 mm and 40 mm.

P_{max} is the maximum load observed during the fracture test

P_j is the peak value of load observed during the compliance calibration test at 20 mm and at 40 mm

3.4 Flexural modulus

In the ASTM standard D7095 with the data obtained, the flexural modulus of the composite material can be found using the equation 3.5 [13].

$$E_{1f} = \frac{L^3}{4ABh^3} \quad (3.5)$$

where L is the nominal half-length.

A is the compliance calibration coefficient (mm/N).

B is the width of the specimen (mm)

h is half the thickness of the specimen (mm)

4.1 Composite Specimen Manufacturing.

The material to be manufactured is first made by the hand lay-up procedure and then placed in a compression moulding machine that cures the material. The compression moulding machine available is the Carver Auto Series Press, with two hydraulically controlled 15 by 15 inch heated plates which are automatic and can produce up to 60 000 lbs of force. Figure 4.1 shows the compression moulding machine used to manufacture the composite material used in this research. This chapter details the steps necessary for the manufacture of the test specimens used in this research.



Figure 4-1: A Carver compression moulding machine.

The first step in this manufacturing process is the preparation of the fibre material used for the layup of the respective material used in this research. As have been previously stated, flax epoxy with lay-up sequence $[0_G/0_F]_8$, $[0_{4G}/0_{4F}]_S$ and $[0_{4G}/(90/0)_{2F}]_S$, specimens will be manufactured for this research.

A 12 by 12-inch square is marked out on the large roll of flax fibre and then a pair of scissors with a specially serrated edge is used to cut out the desired fibre size carefully. Twenty-four (24) layers of flax fibre and glass fibre are required to manufacture the three (3) laminates needed. After cutting all the required plies, the plies are cleaned by carefully sliding a hand along the direction of the fibre from the middle to the edge to remove debris from the plies; this helps to eliminate inclusions in the final hand lay-up process.

Two mould plates are used for the compression moulding. The plates are made of aluminum and have dimensions 15 by 15 inch similar to the dimensions of the heating plates on the compression moulding machine. These plates are necessary because the layup of the fibres is done on the plates to ensure easy transportation of the completed hand layup laminates to the machine for curing and easy removal after the curing process is completed.

Each plate is covered with a high-temperature plastic membrane and sealed on each edge using a plastic sealing machine. A 12 by 12 square is marked on one mould plate, and two layers of a silicon sealant tape are placed on the outer boundary of the marked out square. This 12 by 12 boundary created on one of the moulding plates will serve as the area the fibre lay-up assembly will be located. The silicon tape serves two purposes: (i) To prevent the flow of the epoxy resin during the hand layup and compression process (ii) To prevent slippage of the laminate during the compression process.

As stated in the previous chapter, the matrix used for the specimen manufacture is the high-temperature epoxy, which consists of Araldite®LY 1564 and Aradur®22962. The mixing ratio recommended by the manufacturer is 100-part Araldite to 30-part Aradur. Two 325 grams of epoxy which contained 250 g of Araldite and 75 g of Aradur, each is prepared in two separate containers. Each 250 g Araldite and 75 g Aradur are poured separately into a container and a stirrer is used to

slowly stir the mixture till the contents of the container become a clear mixture. A total of 650 grams of epoxy is used for the manufacturing of each laminate.

To enable easy release of the cured laminate from the mould, a peel ply 12 by 12inch is placed in the moulding area on the first mould plate. The peel ply is a tightly woven nylon-based fabric that allows for the flow of air and excess resin in order to reduce the air pockets that may be present in the laminate during the compression process.

After the peel ply is placed on the mould, a small percentage of the matrix mixture is poured into the mould and spread out with the aid of a paintbrush around the entire face of the ply. A serrated roller is used to push out air pockets that may be present between the ply and mould.

The next step is to place the plies according to the desired stacking sequence and orientation successively until all the plies needed for the laminate to be manufactured is complete. After the application of each ply, a portion of the epoxy should be poured, spread out with a paintbrush and the serrated roller applied to push out any trapped air pockets till the layer is completely soaked with the epoxy resin.

To create the crack site where delamination is initiated, a non-adhesive 12.7 μm (0.0005 inches) thick material about 330 by 112 mm is placed in the mid-plane after laying up the first eight plies of the laminate. Following the placement of the non-adhesive thin film, the lay-up of composite layers continues until completion.

When the hand stack up process of the plies is complete, a final peel ply is placed on the wet laminate. The second mould plate is placed on the mould. This assembly of the two-mould plate and wet laminate is then placed in a bag made of the high-temperature plastic and completely sealed with a plastic sealing machine. This bag is used because it traps excess resin flowing out of the mould in the compression process. A tiny hole is placed in the bag and to suck out the excess air.

The assembly is then placed in the compression moulding machine. Care should be taken to ensure that the mould plates are properly centred in the machine platen to ensure even distribution of temperature and loading pressure on the mould assembly.

This is the final process of the laminate manufacturing process. After the mould assembly is placed in the compression moulding machine, the machine's platens are closed, and the compression process and heating process start simultaneously. To complete the curing process of the composite, there are three stages: (i) initial stage (ii) the intermediate stage (iii) the final stage. The temperature and pressure in these three stages are important in order to ensure the volume fraction of the composite material is approximately 50%.

The stages in the curing process are stated in the paragraphs below.

In this stage, the temperature and the pressure are raised steadily for thirty minutes. The temperature is raised from room temperature 23°C to the curing temperature of 150°C. The pressure is steadily increased to 5 bars.

4.1.1.1 The intermediate stage:

This is a crucial process in the curing process as this is the stage where curing is accelerated and completed. This proceeds immediately after the first stage. In this stage, the temperature and pressure from the initial stage are held for two hours and thirty minutes.

4.1.1.2 The final stage:

In the final stage, the temperature and pressure are steadily reduced until room temperature and the platens of the machine are completely opened. This stage is completed in thirty minutes.

These three important stages for the curing of the composite material is programmed as recipes into the compression moulding machine. Thus, after the compression moulding process is

initiated, no input is required from the manufacturer as the rest of the process is automated. As stated earlier, the three curing stages are required to ensure a volume fraction of fibre is approximately 50%. This curing process is based on research done by Mahboob et al. [23] to determine the pressure that would produce a 50:50 fibre to matrix ratio with a laminate thickness of approximately 4 mm.

4.2 ENF Specimen Dimension

The samples for hybrid one, hybrid two and hybrid three are cut from three sample plates with the respective layup sequence investigated. The length of each specimen is 165 mm, the width of each specimen was measured in three locations, these locations correspond to the position of the loading roller and support rollers on the specimen during the first compliance calibration tests. The thickness of the specimen is measured from six locations, the left and right position of the location in which the width was measured. The specimen layout is shown in Figure 4-2. Tables 4-2, 4-3 and 4-4 show the specimen ID, the average width and the average thickness of the six specimens tested from each hybrid laminate to be tested. “H” represents the hybrid material, “SP” represents the sample of hybrid tested. The detailed data for the dimensions including the measurements for each location and the standard deviation is shown in Appendix 1.

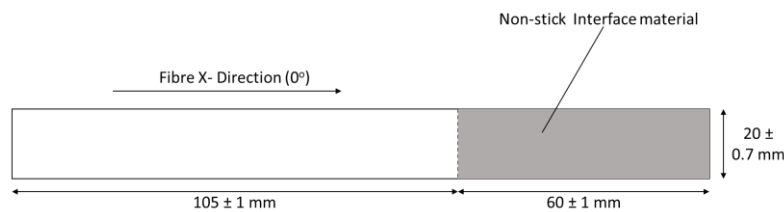


Figure 4-2: Specimen Layout

Table 4-2: Dimensions of samples of Hybrid 1 ([0G/0F] 8S) tested

Specimen ID	Width, B (mm)	Thickness, 2h (mm)
H1SP01	20.38	3.53
H1SP02	20.71	3.54
H1SP03	20.14	3.53
H1SP04	20.66	3.54
H1SP05	20.60	3.53
H1SP06	20.20	3.51

Table 4-3: Dimensions of samples of Hybrid 2 [04G/04F] S tested.

Specimen ID	Width, B (mm)	Thickness, 2h (mm)
H2SP01	20.38	3.61
H2SP02	20.71	3.61
H2SP03	20.14	3.61
H2SP04	20.66	3.54
H2SP05	20.60	3.55
H2SP06	20.20	3.59

Table 4-4: Dimensions of samples of Hybrid 3 [04G/ (90/0)2F] S tested.

Specimen ID	Width, B (mm)	Thickness, 2h (mm)
H2SP01	20.38	3.53
H2SP02	20.71	3.54
H2SP03	20.14	3.53
H2SP04	20.66	3.54
H2SP05	20.60	3.53
H2SP06	20.20	3.51

4.3 Experimental End Notch Flexural Test Procedure.

In the experiment, a tensile tester STM series test machine by United Calibration Corp with a 50kN load cell with an accuracy of $\pm 1\%$. The tests are performed in accordance with the ASTM D7905/D7905M [13] which describes the standard test procedure for evaluating a composite materials mode II interlaminar fracture toughness G_{II} .

Six specimens were tested per hybrid material. Three tests are performed on each specimen, the first two tests are used to determine the compliance calibration coefficients at 20 mm and 40 mm from the crack tip and the final test, the fracture test is performed to determine the maximum load at fracture. The fracture test is performed at 30 mm from the crack tip.

The testing machine was operated in displacement control mode with a constant displacement of 0.5 mm/min during the loading cycle, and an unload cycle rate of 0.8 mm/min. The machine recorded the load vs displacement at a sampling rate of 5 Hz. The loading rollers are fixed and have a radius of 6.35 mm (r_1, r_2 and $r_3 = 6.35$ mm).

Each sample was loaded based on the ASTM D7905/D7905M [13], as shown in Figure 4-3. The span lengths are $2L = 100$ mm and a nominal half-span length $L = 50$ mm. The ENF mode II test setup is shown in Figure 4-4.

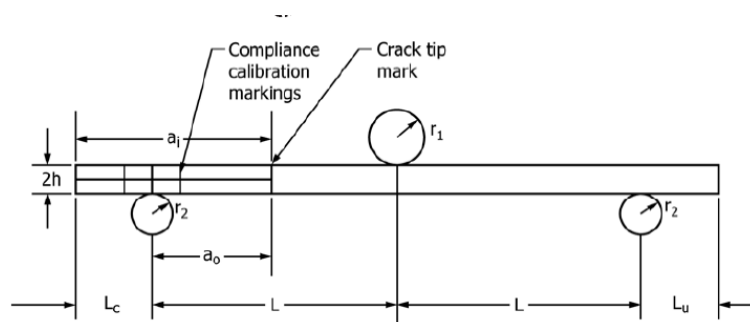


Figure 4-3: ENF specimen, Fixture and Dimensions [13]

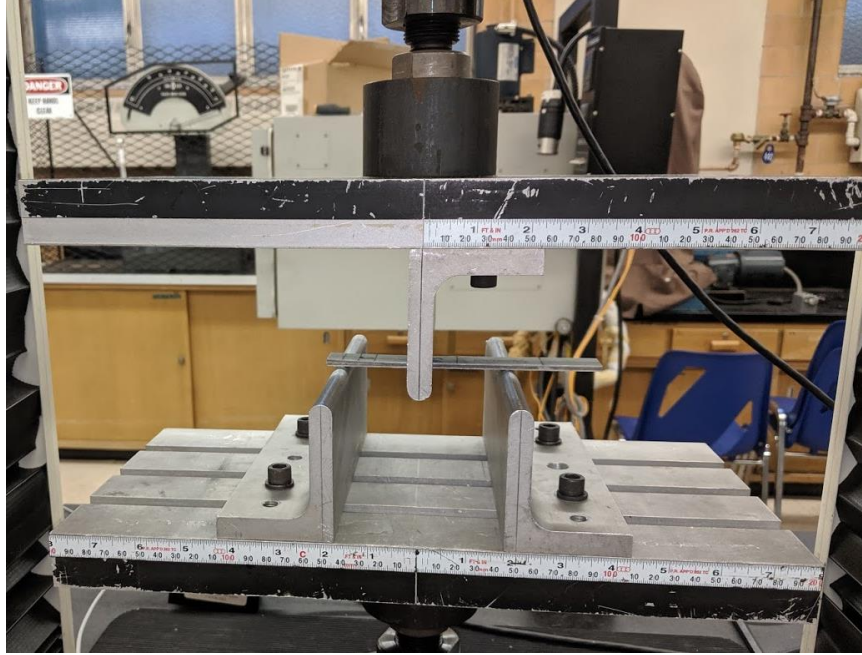


Figure 4-4: The ENF mode II test set-up

As stated in the literature review, the peak forces to be applied are obtained from equation 3.1.

$$P_j = \frac{2B}{3a_j} \sqrt{G_{IIc} E_{1f} h^3} \quad (3.1)$$

where P_j is the peak value of the applied force used during the compliance calibration experiment, a_j is the crack length at 20 mm or 40 mm. An initial estimate of G_{IIc} for each sample was estimated as that of glass epoxy stated in the ASTM D7905 standard – 1170 J/m² (1.17 N/mm).

The flexural modulus E_{1f} was estimated using ANSYS by applying the Representative Volume Element (RVE) technique and the Classical Laminate Theory (CLT). This is further explored in the next section.

4.4 Procedure for obtaining the Flexural Properties applying ANSYS simulation software.

As stated in the literature review section, the Representative Volume Element (RVE) is used to predict the mechanical properties of composite materials and applying this technique reduces the time and cost of manufacturing and testing the flax and glass hybrids to determine their initial flexural modulus for the exploratory study. It was also stated that this will be used to predict the longitudinal, and transverse properties of the glass/epoxy plies and the different hybrids of flax and glass used in this study.

This section presents how the initial flexural properties of the three laminates tested Hybrid one (H1) with layup sequence $[0_G/0_F]_{8S}$, Hybrid two (H2) with layup sequence $[0_{4G}/0_{4F}]_S$, and Hybrid three (H3) with layup sequence $[0_{4G}/(90/0)_{2F}]_S$ were obtained using the RVE technique and the ANSYS Composite PrepPost (ACP pre) tools in ANSYS Simulation Software 2019 R3.

The RVE technique was first applied to obtain the mechanical properties of glass epoxy composite material. Two material properties are required in order to apply the RVE technique effectively. The properties of glass fibre are shown in Tables 4-5.

Table 4-5: Material Properties of E glass [74]

Material property	Value	Unit
Density	2600	Kg/m ³
Young's Modulus	73	GPa
Poisson's Ratio	0.22	

The epoxy matrix isotropic properties used in the experiment are shown in Table 4-6. The properties shown in Tables 4-5 and 4-6 are applied in the ANSYS Mechanical Designer tool to obtain the mechanical properties of glass epoxy composite material.

Table 4-6: Material Properties of Epoxy [22]

Material property	Value	Unit
Density	1160	Kg/m ³
Young's Modulus	3	GPa
Poisson's Ratio	0.35	
Tensile Yield Strength	70	MPa

After the input of the constituent materials, the next step is to select the geometry of the RVE model. The geometry type selected for this simulation is the diamond geometry type. This geometry type was selected because it takes into account the interaction between a reinforcement fibre, four other surrounding fibre and the epoxy matrix. Figure 4-5 shows the diamond representative volume element used in this simulation.

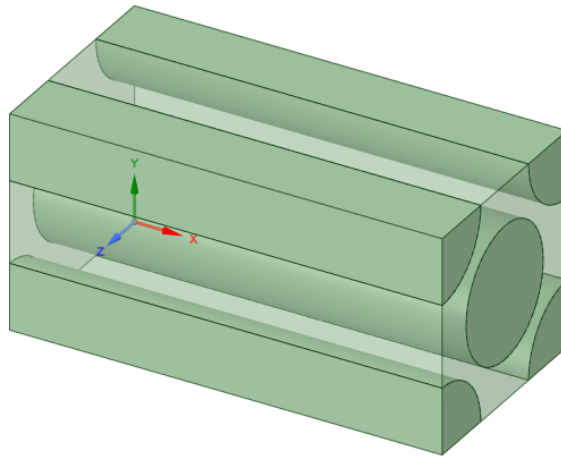


Figure 4-5: Diamond Representative Volume Element [74]

Two assumptions were made, the fibre volume fraction and the diameter of the epoxy reinforcement fibre. The fibre volume fraction used was 50%, and the fibre diameter was 5 μm . The length of the RVE is 17.72 μm , the width and depth are 8.86 μm respectively.[75] These dimensions

are automatically generated by the material designer tools in ANSYS simulation software, based on the selected fibre volume fraction and the diameter of the reinforcement fibre.

After the simulation is completed, the generated mechanical properties of the glass epoxy composite material are shown in Table 4-7. These properties obtained will be used to compute the mechanical properties of the hybrid composite of flax and glass in the respective hybrid configuration.

Table 4-7: RVE generated material property of glass epoxy composite using ANSYS MD.

Material Property	Value	Unit
Density	1705.51	Kg/m ³
Longitudinal Modulus (E_1)	38012	MPa
Transverse Modulus (E_2)	7071.3	MPa
Shear Modulus (G_{12})	3097.7	MPa
Shear Modulus (G_{23})	3736.5	MPa
Poisson's ratio (μ_{12})	0.2766	
Poisson's ratio (μ_{13})	0.2766	
Poisson's ratio (μ_{23})	0.5185	

4.5 Laminate Flexural Modulus

The flexural modulus of the hybrid composite was estimated by applying ANSYS simulation software in order to limit the amount of testing that had to be done. The values of the initial value of the flexural modulus E_{1f} applied is shown in Table 4-8.

Table 4-8: Material and their approximated flexural modulus.

Hybrid Material	Flexural Modulus
Material	E_{1f} (Mpa)
H1 [$0_G/0_F$] _{8S}	38762.72
H2 [$0_{G4}/0_{F4}$] _S	37317.80
H3 [$0_{G4}/(90/0)_{F2}$] _S	35945.50

where G represents glass fibre and F represents flax fibres. H1, H2 and H3 are the hybrid one, two and three, respectively.

5 Experimental Results and Discussion.

This section presents the results of the mode II interlaminar fracture experiment of three hybrids of flax fibre, glass fibre in an epoxy matrix. The tests were performed per the ASTM D7905/D7905M [13] which describes the standard test procedure for evaluating a composite materials Mode II interlaminar fracture toughness G_{II} . The three laminates tested are hybrid one (H1) with layup sequence $[0_G/0_F]_{8s}$, hybrid two (H2) with layup sequence $[0_{4G}/0_{4F}]_s$, and hybrid three (H3) with layup sequence $[0_{4G}/(90/0)_{2F}]_s$. Where G represents glass fibre and F represents glass fibre.

Three tests are performed on each specimen, the first two tests provide data to determine the compliances at 20 mm and 40 mm from the crack tip and the final test, the fracture test, is performed to determine the maximum load and the compliance at fracture. The fracture test is performed at 30 mm from the crack tip. The following subsection shows the results obtained from the different hybrids.

In this research, exploratory experiments are carried out to determine the appropriate load to obtain the two-compliances at 20 mm, 40 mm from the crack for the three composite material tested. This study is important because the accuracy of the forces applied to obtain the calibration compliance determines if the candidate fracture toughness G_Q is accepted or not, as stated in the annex A1.1 of the D7905 ASTM standard [13]. Furthermore, the ASTM standard D7905 recommends exploratory tests if new materials are tested. The candidate fracture toughness obtained is used to refine the approximation of G_{IIC} . The exploratory study also provides a better estimation of the flexural modulus E_{1f} .

The forces applied to obtain the compliance calibration at 20 mm and 40 mm from the crack tips obtained from equation 3.1:

$$P_j = \frac{2B}{3a_j} \sqrt{G_{IIc} E_{1f} h^3} \quad (3.1)$$

From the exploratory study, the initially applied forces applied where F_1 is the load at 20 mm, F_2 is the load at 40 mm from the crack tip. Table 5-1 shows the initial load applied to the hybrid specimens in the exploratory study. The respective values were obtained using the equation (9.1):

$$P_c = \frac{4B}{3a_o} \sqrt{G_{IIc} E_{1f} h^3} \quad (9.1)$$

Table 5-1: Applied forces F_1 and F_2 for the exploratory study.

Hybrid Material	F1 (N)	F2 (N)
Hybrid 1	310.09	115.05
Hybrid 2	332.36	166.18
Hybrid 3	321.50	160.75

After the forces have been obtained, the forces of the different hybrid are then applied to the hybrid sample via roller one. Force F_1 is applied at $a = 20$ mm and F_2 is applied at $a = 40$ mm from the crack front. The final loading of the specimen is at crack length $a = 30$ mm, and the sample is continuously loaded until there is a drop in the recorded force. Details on the experimental procedure are outlined in chapter 4 section 4.3.

After obtaining the results from the exploratory study, as previously stated, the data acquired is used to refine the load F_1 and F_2 in order to obtain the correct values of the mode II fracture toughness of hybrid one, hybrid two and hybrid three. The following section presents the results of the mode II interlaminar fracture tests of hybrid one, hybrid two and hybrid three.

5.1 Mode II interlaminar fracture toughness of hybrid one

As previously stated, the Non-Precracked Method (NPC) is the method applied to obtain the fracture toughness of the respective hybrids in this thesis research. During the test, the displacement vs load data is recorded during the loading at crack length $a = 20\text{mm}$, 40 mm and the fracture test at $a = 30\text{ mm}$ as specified in the ASTM D7509 standard [17].

Three compliances C are obtained from the linear least square regression analysis of the load vs displacement plot obtained from the two compliance calibration tests at crack length 20 mm and 40 mm and the fracture compliance test at 30 mm . Details of the procedure for the data reduction process are outlined in chapter 3, section 3.2.

To obtain the compliances at $a = 20\text{ mm}$ and 40 mm only the data equal to and greater than 90 N are considered. Also, to obtain the compliance at fracture, only data equal to and greater than 90 N and below 50% of the maximum load at fracture is considered for the linear least square regression analysis. These forces are chosen so the curve-fit excludes any non-linear data in accordance with the standard.

In this thesis research, MATLAB software is applied to perform the data reduction linear regression analysis described previously in section 3.2 for the respective hybrid data obtained from the respective compliance calibration tests on hybrid one, two and three materials.

The force $F1$ vs displacement of the exploratory study of hybrid one is shown in Figure 5-1. The red data points are excluded from the analysis. The compliance $C1$ is obtained from the plot shown in Figure 5-1.

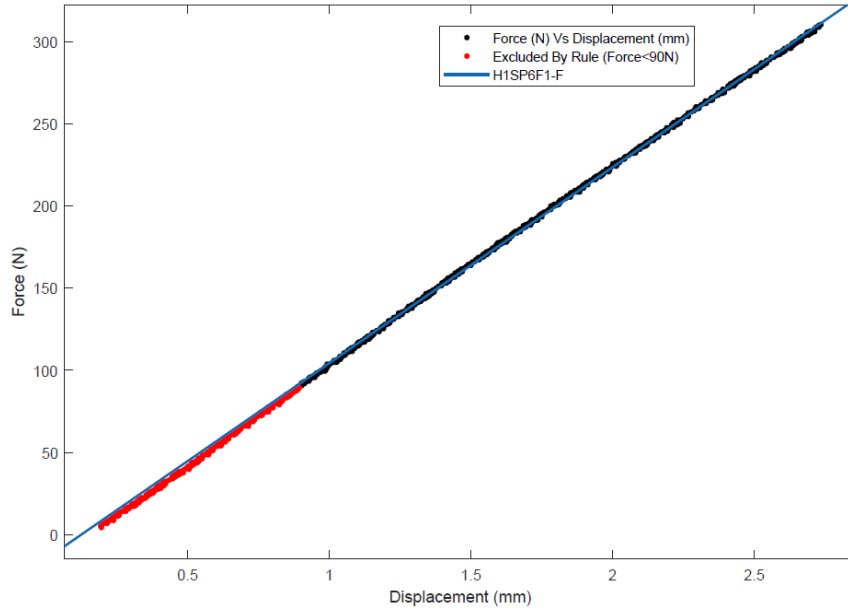


Figure 5-1: The plot of displacement vs force (F1) of Hybrid 1 exploratory study. (The red data points are excluded from the analysis)

The plot of force (F2) vs displacement of hybrid 1 exploratory study is shown in Figure 5-2. The compliance C2 is obtained from this plot. The data points highlighted in red are excluded from the linear regression analysis because the forces at these points are less than 90 Newtons.

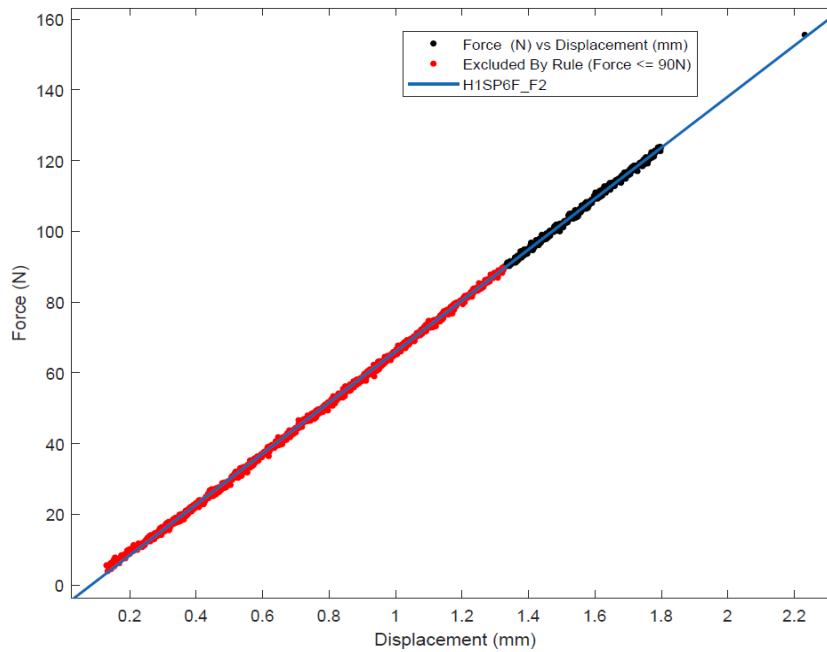


Figure 5-2: The plot of displacement vs force (F2) Hybrid 1 exploratory study (The red data points are excluded from the analysis).

The plot of force vs displacement during the fracture tests is shown in Figure 5-3. The compliance at fracture is obtained from this plot. The maximum force recorded for the hybrid one exploratory test is 409.45 Newtons. As previously stated, any forces greater than or equal to 90 Newtons and forces greater than 50% of the maximum force recorded during the fracture test are excluded from the curve-fit linear regression analysis. Thus, all data points highlighted in red are excluded from the data reduction analysis.

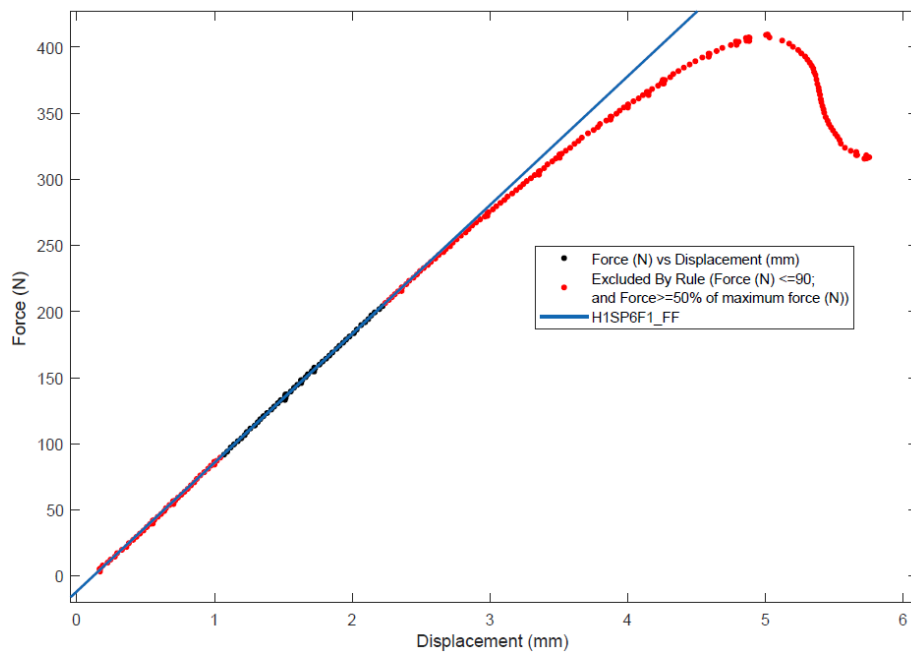


Figure 5-3: The plot of force (after fracture) vs displacement of Hybrid 1 exploratory study. (The red data points are excluded from the analysis; excluded data was according to the rule in ASTM D7905 [13])

The compliances of hybrid one at crack length $a = 20$ mm, $a = 40$ mm and at fracture $a = 30$ mm are the inverse of the slope of the blue diagonal line in Figures 5-1, 5-2 and 5-3. The compliances for the respective crack lengths are shown in Table 5-2.

Table 5-2: The compliances of the exploratory study of the hybrid one

Compliance	Unit (mm/N)
C1 ($a=20\text{mm}$)	0.00839
C2 ($a=40\text{mm}$)	0.01382
CF ($a=30\text{mm}$)	0.01026

The final step in the data reduction procedure is to obtain the compliance calibration coefficients A and m these coefficients are required in computing the flexural modulus and fracture toughness of the composite material. To obtain these coefficients, the compliances are plotted against the crack length cubed (a^3). Figure 5-4 shows the plot of the crack coefficient vs the crack length cubed. From the plot the compliance coefficient m was obtained as $9.68 \times 10^{-8} \text{ N}^{-1}\text{mm}^{-2}$ and the compliance coefficient A was obtained as 0.007629 mm/N .

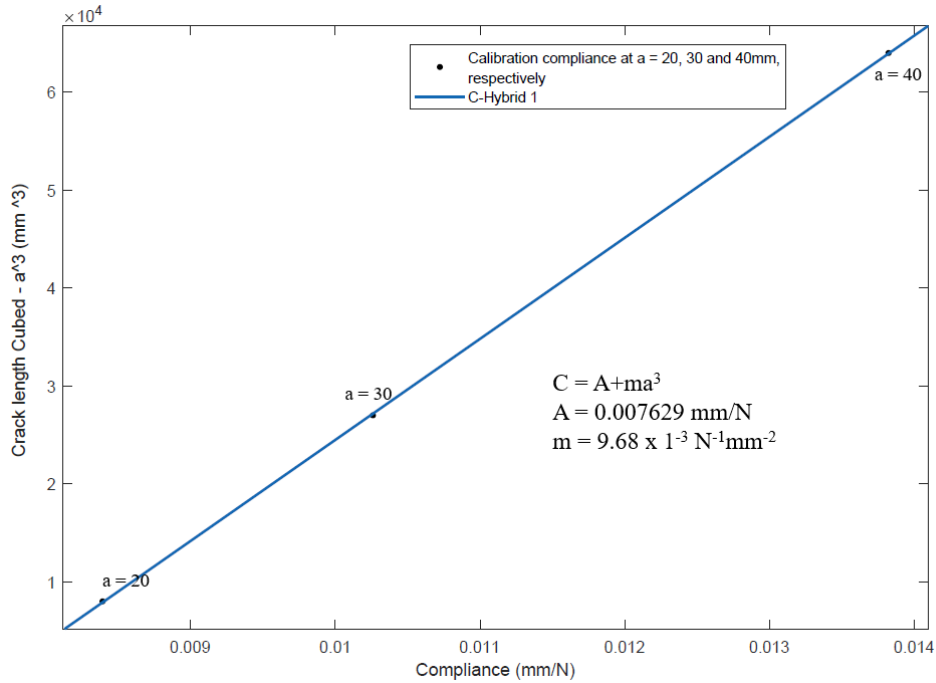


Figure 5-4: Crack length cubed (a^3) vs Compliance (C)

The candidate mode II fracture toughness (G_{IIQ}) and the flexural modulus (E_{1f}) of the exploratory study of hybrid one was obtained using the equations $G_Q = \frac{3mP_{Max}^2 a_0^2}{2B}$ and $E_{1f} = \frac{L^3}{4ABh^3}$ respectively. Thus, fracture toughness is 1.116 kJ/m^2 and the flexural modulus 38.76 GPa .

The goal of the exploratory study is to obtain better values of the fracture toughness, and the flexural modulus to better estimate the load required to obtain the compliance at 20 mm and 40 mm of the crack length.

Applying equation 3.1, the new forces to obtain the compliances at a =20 mm and a = 40 mm are obtained. Thus, the force F1 is obtained as 315.81 Newtons and the force F2 is obtained as 157.90 Newtons.

$$P_j = \frac{2B}{3a_j} \sqrt{G_{IIC} E_{1f} h^3} \quad (3.1)$$

Five samples are further tested using the new forces F1=315.81 N and F2=157.90 N. The procedure to obtain the compliances is the same as the exploratory study. Table 5-3 shows the compliances obtained from the data reduction of sample 1 to sample 5 of hybrid one material. Where H represents the hybrid number and SP represents the sample number.

Table 5-3: Compliances of tested samples of the hybrid one material

Compliance	H1SP01 (mm/N)	H1SP02 (mm/N)	H1SP03 (mm/N)	H1SP04 (mm/N)	H1SP05 (mm/N)
C1 (a=20mm)	0.0080	0.00775	0.00772	0.00765	0.00818
C2 (a=40mm)	0.0133	0.01229	0.01284	0.01267	0.01402
CF (a=30mm)	0.0096	0.00922	0.00819	0.00910	0.00990

The calibration compliances m and A of the respective sample material tested are obtained by performing a linear regression analysis of the compliances. The same procedure highlighted in the exploratory study of hybrid one material.

After obtaining the calibration compliance coefficients m and A, the final step is to compute the candidate fracture toughness and the flexural modulus using the equation 3.3

$$G_Q = \frac{3mP_{Max}^2 a_0^2}{2B} \quad (3.3)$$

Table 5-4 shows the computed values of the candidate fracture toughness of the respective samples of hybrid one tested. The respective values of the coefficients required to obtain the fracture toughness are shown in Table 5-4.

Table 5-4: Candidate fracture toughness of hybrid one material $[0_G/0_F]_{8S}$

Specimen ID	Compliance Coefficient m (1/Nmm ²)	Maximum recorded P _{max} (N)	P ² _{max} (N ²)	Crack Length a _o (mm)	a _o ² (mm ²)	Width B (mm)	Candidate Fracture toughness G _Q (kJ/m ²)
H1SP01	9.43E-08	497.40	247406.76	30	900	19.51	1.615
H1SP02	8.13E-08	517.88	268202.80	30	900	19.22	1.532
H1SP03	9.62E-08	480.80	231164.79	30	900	20.25	1.482
H1SP04	9.06E-08	490.32	240413.70	30	900	20.37	1.444
H1SP05	1.05E-07	437.12	191075.64	30	900	20.11	1.347

Additionally, the computed values for the flexural modulus E_{1f} of the respective hybrid one samples are shown in Table 5-5. The flexural modulus is computed using equation 3.5.

$$E_{1f} = \frac{L^3}{4ABh^3} \quad (3.5)$$

The respective values of the coefficients required to obtain the flexural modulus are also shown in Table 5-5.

Table 5-5: Flexural modulus of hybrid one material $[0_G/0_F]_{8S}$

Specimen ID	Nominal half length L (mm ²)	L ³ (mm ³)	Compliance Coefficient A (mm/N)	Width B (mm)	Thickness 2h (mm)	h ³ (mm ³)	Flexural Modulus E _{1f} (MPa)
H1SP01	50	125000	0.007179	19.51	3.55	5.58	40009.00
H1SP02	50	125000	0.007070	19.22	3.58	5.74	40090.62
H1SP03	50	125000	0.006407	20.25	3.55	5.57	43245.41
H1SP04	50	125000	0.006814	20.37	3.55	5.60	40208.82
H1SP05	50	125000	0.007224	20.11	3.52	5.43	39618.88

The mode II interlaminar fracture toughness for each sample tested is determined if the value of the percentages of the candidate fracture toughness ($\%G_{Q,J}$) achieved during the compliance calibration testing satisfies the limit $15 \leq \%G_{Q,J} \leq 35$. If the $\%G_{Q,J}$ are within this limit, the candidate fracture toughness becomes the mode II fracture toughness, i.e., $G_{IIc} = G_Q$. The value of the $\%G_{Q,J}$ for the respective samples of the hybrid one material is determined using the equation 3.4

$$\%G_{Q,j} = \left[\frac{100(P_j a_j)^2}{(P_{max} a_0)^2} \right]; j = 1,2 \quad (3.4)$$

Table 5-6 shows the value of the percentage of fracture $\%G_{Q,20}$ and $\%G_{Q,40}$ for hybrid one samples tested in the experiment. The percentage of candidate fracture toughness $\%G_Q$ is dimensionless.

Table 5-6: Percentage of candidate fracture toughness for Hybrid 1 [0G/0F]8S

Specimen ID	$\%G_{Q,20}$	$\%G_{Q,40}$
H1SP01	17.92	17.92
H1SP02	16.53	16.53
H1SP03	19.18	19.18
H1SP04	18.44	18.44
H1SP05	23.20	23.20

Based on evaluating the percentages of the candidate fracture toughness ($\%G_{Q,j}$) achieved during the compliance calibration testing of hybrid one, sample 1 to 5 satisfies the limit $15 \leq \%G_{Q,j} \leq 35$.

Thus, the mode II fracture toughness of hybrid one composite material is the average of the fracture toughness of H1SP01 to H1SP05. Furthermore, the flexural modulus of hybrid one material is taken as the average of the flexural modulus of samples 1 to 5. This is shown in Table 5-7. Thus, the mode II fracture toughness G_{IIc} and flexural modulus E_{1F} of Hybrid one material with lay up code $[0_G/0_F]_{8S}$ are 1.484 ± 0.089 kJ/m² and 40.63 ± 1.32 GPa respectively.

Table 5-7: Mode II fracture toughness and flexural modulus of hybrid One

Specimen ID	Mode II Fracture toughness G_{IIc} (kJ/m ²)	Flexural Modulus E_{1f} (Mpa)
H1SP01	1.615	40009.00
H1SP02	1.532	40090.62
H1SP03	1.482	43245.41
H1SP04	1.444	40208.82
H1SP05	1.347	39618.88
Mean	1.484	40634.55
SD	0.089	1320.35

5.2 Mode II interlaminar fracture toughness of hybrid two

Six samples of hybrid two material with layup code $[0_{4G}/0_{4F}]_S$ is tested in this research. Two exploratory studies to improve the estimation of forces F1 and F2 to obtain the compliances at $a = 20$ mm and $a = 40$ mm is performed. From the exploratory studies, the forces F1 and F2 applied for the testing of the other four samples are 251.50 N and 125.70 N.

The compliances obtained for the six samples of the hybrid two material at crack length $a = 20$ mm, $a = 40$ mm and fracture $a = 40$ mm are shown in Table 5-8. The procedure applied to obtain the compliance calibration is the same applied in the previous section and is further outlined in chapter 3.

Table 5-8: Compliances of tested samples of the hybrid two material

Compliance	H2SP01 (mm/N)	H2SP02 (mm/N)	H2SP03 (mm/N)	H2SP04 (mm/N)	H2SP05 (mm/N)	H2SP06 (mm/N)
C1 (a=20mm)	0.007960	0.008026	0.008153	0.008619	0.008672	0.008600
C2 (a=40mm)	0.019690	0.018090	0.019250	0.019620	0.019590	0.018830
CF (a=30mm)	0.011230	0.011420	0.011400	0.012030	0.012050	0.012100

Furthermore, linear regression analysis is applied to the compliances obtained for the respective sample in order to obtain the compliance calibration coefficients m and A . With these coefficients, the candidate fracture toughness can be computed.

Table 5-9 shows the compliance coefficient m for the respective hybrid two (H2) samples and the value of the candidate fracture toughness of sample 1 to sample 6. The procedure for obtaining the candidate fracture toughness is described in chapter 4 and outlined in the previous section.

Table 5-9: Candidate fracture toughness of hybrid two material $[0_{4G}/0_{4F}]_S$

Specimen ID	Compliance Coefficient m (1/Nmm ²)	Maximum recorded P_{max} (N)	P_{max}^2 (N ²)	Crack Length a_o (mm)	a_o^2 (mm ²)	Width B (mm)	Candidate Fracture toughness G_Q (kJ/m ²)
H2SP01	2.12E-07	330.00	108900.00	30	900	19.17	1.626
H2SP02	1.80E-07	307.40	94494.76	30	900	19.33	1.187
H2SP03	2.00E-07	321.45	103328.82	30	900	19.38	1.441
H2SP04	1.98E-07	330.78	109417.39	30	900	19.52	1.496
H2SP05	1.96E-07	300.28	90168.08	30	900	19.33	1.235
H2SP06	1.83E-07	304.87	92943.28	30	900	19.88	1.152

Also, the mode II flexural modulus of the hybrid two material was also obtained. Table 5-10 shows the calibration compliance A and the flexural moduli E_{1f} of the respective samples of the hybrid two tested.

Table 5-10: Flexural modulus of hybrid two material $[0_{4G}/0_{4F}]_S$

Specimen ID	Nominal half length L (mm ²)	L^3 (mm ³)	Compliance Coefficient A (mm/N)	Width B (mm)	Thickness 2h (mm)	h^3 (mm ³)	Flexural Modulus E_{1f} (MPa)
H2SP01	50	125000	0.005961	19.17	3.610	5.88	46494.51
H2SP02	50	125000	0.006579	19.33	3.608	5.87	41836.32
H2SP03	50	125000	0.006332	19.38	3.613	5.90	43191.27
H2SP04	50	125000	0.006901	19.52	3.543	5.56	41724.04
H2SP05	50	125000	0.006964	19.33	3.548	5.58	41562.46
H2SP06	50	125000	0.007152	19.88	3.585	5.76	38155.38

Finally, mode II fracture toughness is evaluated. Thus $G_Q = G_{IIc}$ if the percentages of the candidate fracture toughness ($\%G_{Q,J}$) achieved during the compliance calibration testing of hybrid two, satisfies the limit $15 \leq \%G_{Q,J} \leq 35$. The percentage of candidate fracture toughness $\%G_Q$ is dimensionless. The Table 5-11 shows the value of $\%G_{Q,20}$ and $\%G_{Q,40}$. From Table 5-11 only sample H2SP02 to H2SP05 satisfies the required limit.

Table 5-11: Percentage of candidate fracture toughness for Hybrid 2 [04G/04F] S

Specimen ID	$\%G_{Q,20}$	$\%G_{Q,40}$
H2SP01	43.11	43.11
H2SP02	29.75	29.73
H2SP03	27.08	27.08
H2SP04	25.58	25.58
H2SP05	31.04	31.04

For hybrid two, sample 2 to 5 satisfies the limit $15 \leq \%G_{Q,J} \leq 35$. Thus, the mode II fracture toughness is the average of the fracture toughness of H2SP02 to H2SP05. Furthermore, the flexural modulus of hybrid two material is taken as the average of the flexural modulus of sample 2 to 5, as shown in Table 5-12. Thus, the mode II fracture toughness G_{IIc} and flexural modulus E_{1f} of Hybrid two material with lay up code $[0_{4G}/0_{4F}]_S$ are $1.339 \pm 0.13 \text{ kJ/m}^2$ and $42.087 \pm 0.65 \text{ GPa}$ respectively.

Table 5-12: Mode II fracture toughness and flexural modulus of hybrid two

Specimen ID	Mode II Fracture toughness G_{IIc} (kJ/m ²)	Flexural Modulus E_{1f} (Mpa)
H2SP02	1.187	41836.32
H2SP03	1.441	43191.27
H2SP04	1.496	41724.04
H2SP05	1.235	41562.46
Mean	1.339	42078.52
S D	0.13	649.78

5.3 Mode II interlaminar fracture toughness of hybrid three

To evaluate the fracture toughness of hybrid three (H3) composite material, six samples of the material were tested. Two exploratory studies to improve the estimation of forces F1 and F2 to obtain the compliances at $a = 20$ mm and $a = 40$ mm was performed. Due to time constraints and the similarity in the layup sequence between the hybrid two and hybrid three materials the forces, F1 and F2 applied for the testing of the other four samples was selected as 251.50 N and 120 N.

Table 5-13 shows the compliances obtained for the six samples of the hybrid three material at crack length $a = 20$ mm, $a = 40$ mm and at fracture $a = 40$ mm. The procedure applied to obtain the compliance calibration is the same applied in the previous section and is further outlined in chapter 3.

Table 5-13: Compliances of tested samples of the hybrid three material

Compliance	H3SP01 (mm/N)	H3SP02 (mm/N)	H3SP03 (mm/N)	H3SP04 (mm/N)	H3SP05 (mm/N)	H3SP06 (mm/N)
C1 ($a=20$ mm)	0.008901	0.008454	0.008806	0.008780	0.008968	0.009122
C2 ($a=40$ mm)	0.022470	0.020560	0.022710	0.021410	0.022970	0.021980
CF ($a=30$ mm)	0.012580	0.012260	0.012890	0.012540	0.012500	0.013360

Also, the compliance calibration coefficients m and A are obtained by performing a linear regression analysis of the compliances obtained for the respective sample. With these coefficients, the candidate fracture toughness can be computed.

The compliance coefficient m for the respective hybrid three samples and the value of the candidate fracture toughness of sample 1 to sample 6 are shown in Table 5-14. The procedure for obtaining the candidate fracture toughness is described in chapter 4.

Table 5-14: Candidate fracture toughness of hybrid three material $[0_{4G}/(90/0)_{2F}]_S$

Specimen ID	Compliance Coefficient m (1/Nmm ²)	Maximum recorded P_{max} (N)	P_{max}^2 (N ²)	Crack Length a_o (mm)	a_o^2 (mm ²)	Width B (mm)	Candidate Fracture toughness G_Q (kJ/m ²)
H3SP01	2.46E-07	293.60	86200.96	30	900	20.38	1.403
H3SP02	2.17E-07	305.46	93305.8116	30	900	20.71	1.322
H3SP03	2.51E-07	285.30	81396.09	30	900	20.14	1.367
H3SP04	2.28E-07	289.92	84053.6064	30	900	20.66	1.249
H3SP05	2.55E-07	289.09	83574.18446	30	900	20.60	1.394
H3SP06	2.30E-07	275.70	76010.49	30	900	20.20	1.168

The mode II flexural modulus of the hybrid two material was also obtained. Table 5-15 shows the calibration compliance A and the flexural moduli E_{1f} of the respective samples of the hybrid two tested.

Table 5-15: Flexural modulus of hybrid three material $[0_{4G}/(90/0)_{2F}]_S$

Specimen ID	Nominal half length L (mm ²)	L^3 (mm ³)	Compliance Coefficient A (mm/N)	Width B (mm)	Thickness 2h (mm)	h^3 (mm ³)	Flexural Modulus E_{1f} (MPa)
H3SP01	50	125000	0.006541	20.380	3.530	5.50	42635.13
H3SP02	50	125000	0.006587	20.707	3.543	5.56	41200.85
H3SP03	50	125000	0.006531	20.140	3.530	5.50	43209.25
H3SP04	50	125000	0.006737	20.663	3.542	5.55	40425.00
H3SP05	50	125000	0.006413	20.600	3.530	5.50	43021.69
H3SP06	50	125000	0.007228	20.200	3.513	5.42	39483.21

Lastly, the mode II fracture toughness is assessed. Thus, if the percentages of the candidate fracture toughness ($\%G_{Q,J}$) achieved during the compliance calibration testing of hybrid three material satisfies the limit $15 \leq \%G_{Q,J} \leq 35$ then $G_Q = G_{IIC}$. Table 5-16 shows the value of $\%G_{Q,20}$

and $\%G_{Q.40}$ for hybrid three samples tested in the experiment. The percentage of candidate fracture toughness $\%G_Q$ is dimensionless.

Table 5-16: Percentage of candidate fracture toughness for Hybrid three $[04_G / (90/0)_{2F}]_s$

Specimen ID	$\%G_{Q.20}$	$\%G_{Q.40}$
H3SP01	49.91	49.91
H3SP02	29.61	27.09
H3SP03	27.08	27.08
H3SP04	25.58	23.40
H3SP05	31.04	28.39

For hybrid three, sample 2 to 5 satisfies the limit $15 \leq \%G_{Q,J} \leq 35$. Thus, the mode II fracture toughness of hybrid three is the average of the fracture toughness of H3SP02 to H3SP05. Furthermore, the flexural modulus of hybrid three material is taken as the average of the flexural modulus of sample 2 to 5, as shown in Table 5-17. Thus, the mode II fracture toughness G_{IIc} and flexural modulus E_{1f} of Hybrid three material with lay up code $[04_G / (90/0)_{2F}]_s$ are 1.333 ± 0.055 kJ/m² and 41.96 ± 1.19 GPa respectively.

Table 5-17: Mode II fracture toughness and flexural modulus of hybrid three

Specimen ID	Mode II Fracture toughness G_{IIc} (kJ/m ²)	Flexural Modulus E_{1f} (Mpa)
H3SP02	1.322	41200.85
H3SP03	1.367	43209.25
H3SP04	1.249	40425.00
H3SP05	1.394	43021.69
Mean	1.333	41964.20
SD	0.055	1185.36

5.4 Damage observed in the hybrid specimens

After the experiment the respective hybrid materials was inspected under a plugable USB2.0 digital microscope. Figure 5-5 shows the delamination crack in hybrid one only propagates in the

crack interface where the 12.7µm PTFE insert was placed. No other damage was observed from all six samples of hybrid one.

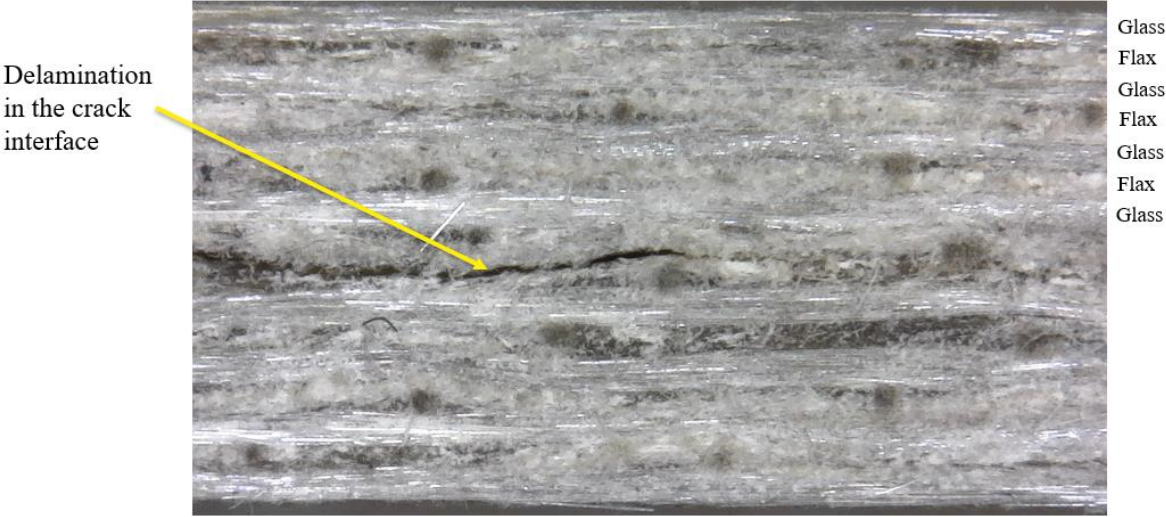


Figure 5-5: Delamination observed in hybrid one

Figure 5-6 shows the delamination and secondary delamination observed in the hybrid two material. Unlike the hybrid one material where delamination occurred only in the crack interface, secondary delamination is observed in the hybrid two material. The secondary delamination is observed between the glass and flax interface and also between the flax and flax interface of the hybrid material for all the sample inspected.

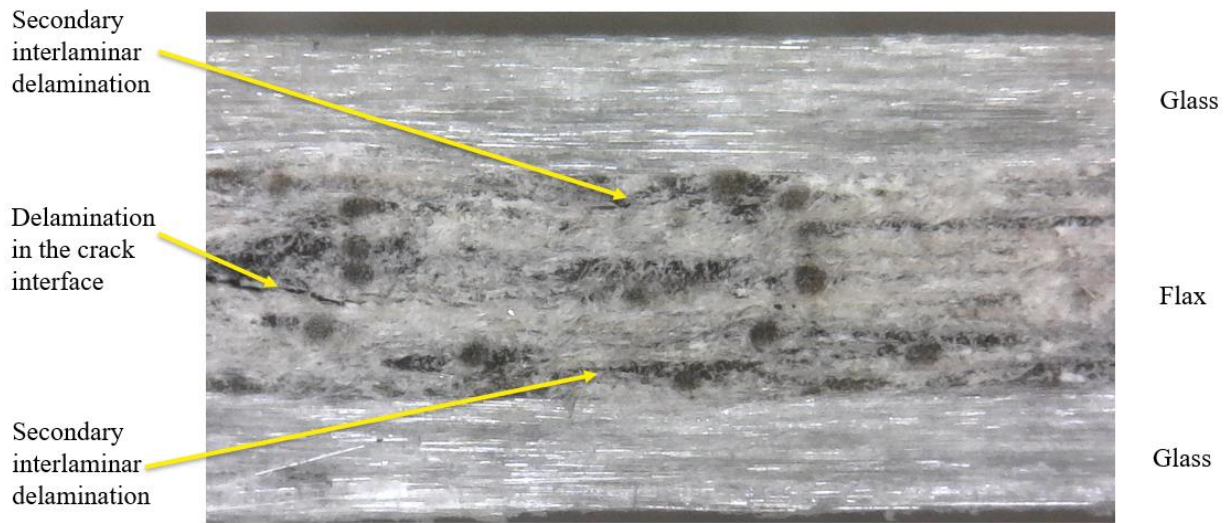


Figure 5-6: Delamination and secondary delamination in observed in the hybrid two material.

Figure 5-7 shows the delamination and secondary interbundle delamination in the hybrid three material. In the hybrid three material, delamination is observed in the crack interface where the PTFE material is location, additionally, secondary delamination is observed between 90 degree flax ply and 0 degree flax ply shown in Figure 5-7a and interbundle delamination is observed along the 90 degree ply shown in Figure 5-7b.

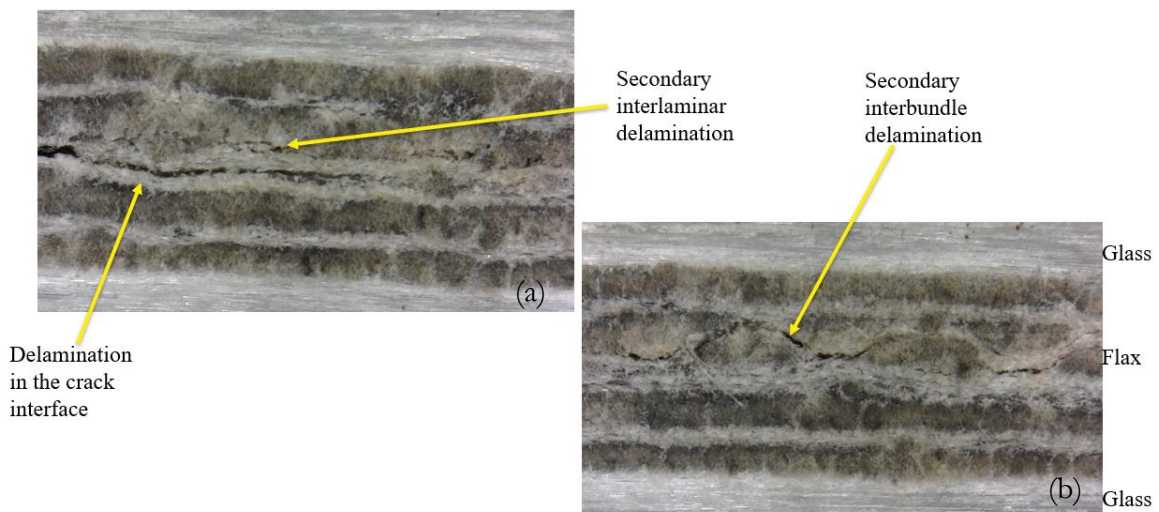


Figure 5-7: Delamination and secondary interbundle delamination in the hybrid three material.

5.5 Discussion

This study investigates the mode II interlaminar fracture toughness of three hybrids of flax and glass fibre. This study further investigates the impact of the lay-up sequence on the mode II fracture toughness of these hybrid materials. Examining the force vs displacement during the fracture calibration compliance tests for all three hybrids, the hybrid one has the highest strength compared to hybrid two and hybrid three, as represented in the plot of force vs displacement of hybrid one, two and three shown in Figure 5-5.

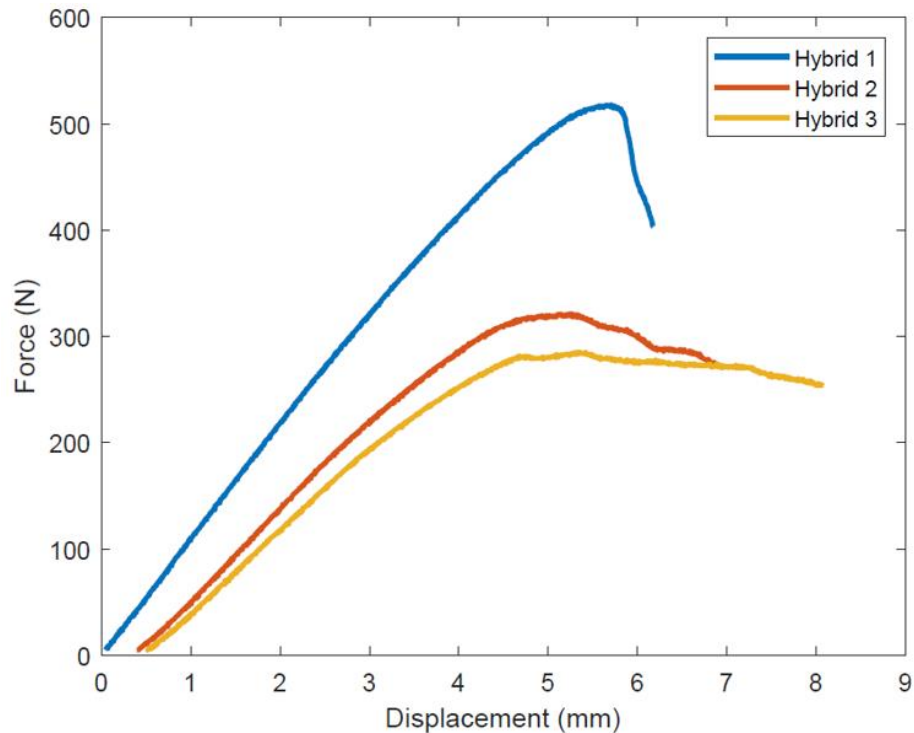


Figure 5-8: Force vs Displacement during compliance calibration test of Hybrid 1,2 and 3

The record forces required for mode II delamination to occur in hybrid one, two and three are $484.70 \pm 26.73\text{N}$, $314.98 \pm 11.89\text{ N}$ and $292.44 \pm 7.71\text{ N}$ respectively. The displacement at fracture where delamination occurs is recorded as 5.65 mm, 5.25 mm and 5.35 mm for hybrid one, hybrid two and hybrid three, respectively. Delamination occurred around 5 mm displacement for all three laminate.

Comparing the differences between the forces required to cause delamination, hybrid one has a 42.6% higher strength compared to hybrid two and 49.34% higher strength compared to hybrid three. This clearly illustrates how a change in the stacking sequence can impact a hybrid composite material mechanical property, in this case arranging the flax and glass ply in the stack-up sequence $[0_G/0_F]_{8S}$ of hybrid one results in the best bending mechanical property.

A study by Czél et al. [76] that examined the pseudo-ductility in high-performance hybrids of glass/epoxy and carbon prepreg showed how the failure mode in the hybrid composites changes based on the layup sequence of the composite material. In their work, they showed three hybrid material with different thickness of the glass and carbon plies shown in Figure 5-6. In Figure 5-6a, the thicker carbon plies cause a brittle failure of the laminate – fibre cracking of the carbon plies which propagated to the glass plies. In Figure 5-6b, after the carbon plies fail, it instantaneously results in unstable delamination at the layer-to-layer interface between the carbon and glass plies. Czél et al. [76] described this failure as the most common mode of failure in hybrid laminates. In Figure 5-6c, the carbon ply damage is a stable localized pull-out which is the desired behaviour of hybrid composites.

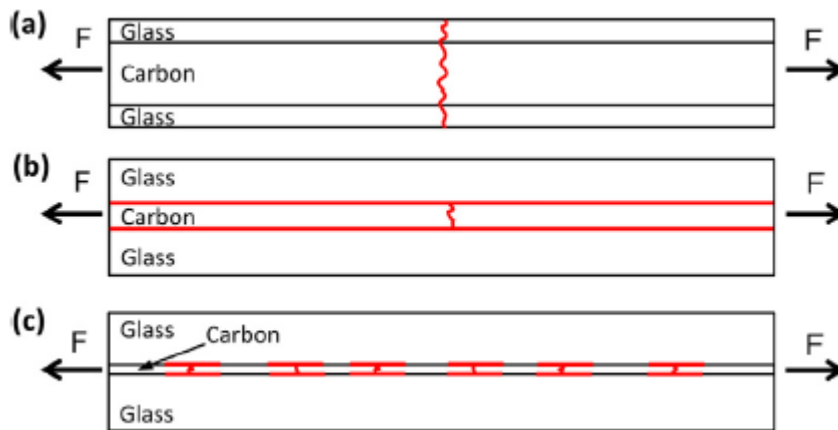


Figure 5-9: Failure modes in hybrids of glass and carbon laminates with different ply thickness. [75]

This thesis research evaluated the mode II fracture toughness of three hybrid laminates of glass and flax epoxy with configuration $[[0_G/0_F]_{8S}, 0_{4G}/0_{4F}]_S$, and $[0_{4G}/(90/0)_{2F}]_S$. From the results of

the tests and the plot shown in Figure 5-5, the laminate configuration with the higher strength is the hybrid one. Thus, from the damage observed in the hybrid two and three materials shown in the section 5.4 further validated by research done by Czél et al. [76], it can be stated that secondary delamination is present in the hybrid two and hybrid three materials. This secondary delamination present in hybrid two and three material resulted in the reduced strength of these materials.

The mode II fracture toughness property of the hybrid one, two and three is evaluated. The bar chart in Figure 5-7 shows a comparison of the mode II interlaminar fracture toughness of all three hybrids.

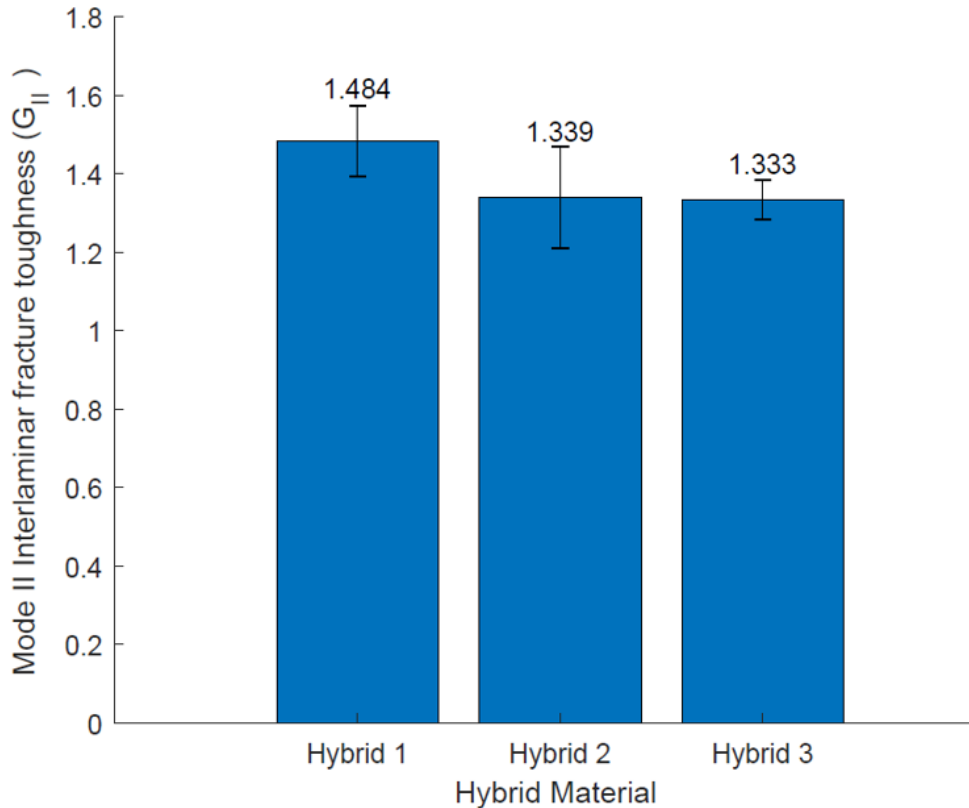


Figure 5-10: Mode II Interlaminar Fracture Toughness G_{IIc} of hybrid 1, 2 and 3.

The mode II fracture toughness of hybrid one, two and three have a fracture toughness of 1.484 ± 0.09 kJ/m², 1.339 ± 0.13 kJ/m² and 1.333 ± 0.05 kJ/m², respectively. Hybrid one's fracture toughness is 10.27 % higher than hybrid two and 10.72 % higher than hybrid three. The contribution

of the layup sequence to the mode II fracture toughness of the hybrid material is only about 10 %. One reason for this difference in the mode II strain energy release rate G_{IIc} is because of the unstable interface delamination present in the flax and glass ply to ply interface.

Furthermore, the result from the experiments validates the study by Bensadoun et al. [6] of the interlaminar fracture toughness of flax epoxy composites. In the research by Bensadoun et al. [6], it was stated that the initiation and evolution of delamination are directly linked to the interlaminar fracture toughness of the composite material. Also, the results of the study showed that the architecture of the interface plies that is, if the interface material is a low twist, a plain weave or quasi UD, impacts the fracture toughness of the laminate. Thus, the flax material with woven architecture had the highest mode II fracture toughness of 1.87 kJ/m^2 compared to the other materials. Figure 5-8 shows the mode II fracture toughness of materials with different interface flax epoxy ply architecture.

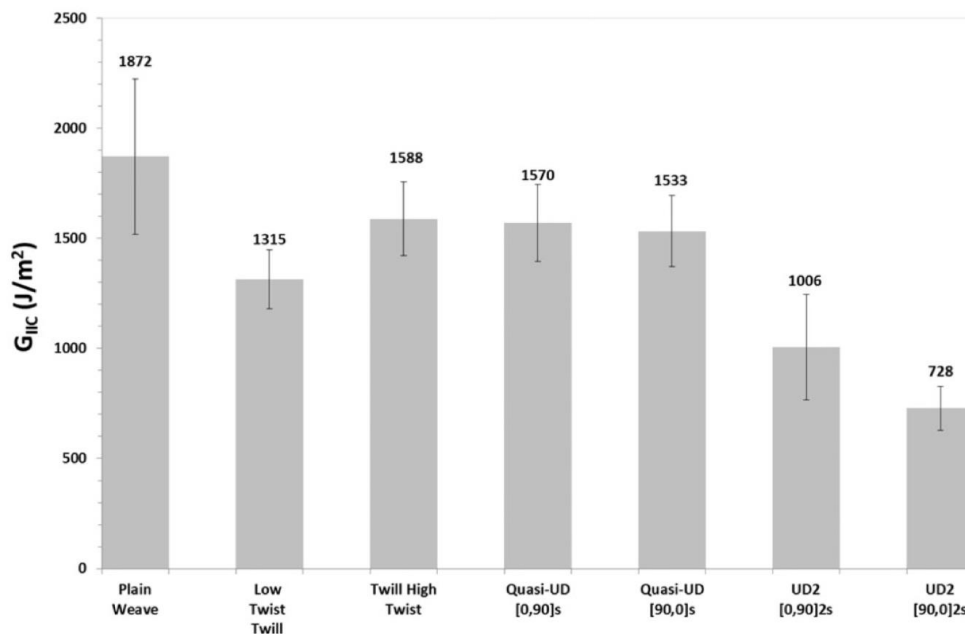


Figure 5-11: Mode II fractural toughness of different architecture of flax epoxy composite [6]

Bensadoun et al. [6] concluded in their research that the high mode II interlaminar fracture toughness G_{IIC} of plain weave flax epoxy composites is because of the irregular path the crack is forced to follow resulting in higher energy required for delamination.

Also, Saidaine et al. [24] made a similar observation in their research. They showed that the hybrid flax reinforced epoxy (HFRE) had a 50% higher mode I interlaminar fracture toughness during crack propagation compared to the glass epoxy laminate because the flax fibres causes deviations on the crack path impeding or slowing down the crack growth.

In the results presented about the mode II fracture toughness of the three hybrid materials shown in Figure 5-7, the results show a 10% difference between the fracture toughness of hybrid one compared to the other materials whereas, Hybrid II and III has a less than 1% difference between their fracture toughness. This result validates the conclusion by Bensadoun et al. [6] about the architecture of the interface material at the crack surfaces affecting the mode II fracture toughness. In this case, hybrids two and three have the same architecture at the interfaces where the crack lies and also similar failure mechanisms.

Furthermore, from the layup sequence of hybrid two with layup code $[0_{4G}/0_{4F}]_S$ and three with layup code $[0_{4G}/(90/0)_{2F}]_S$, the change in the angle of four plies to 90 degrees did not make a significant impact in its mode II fracture toughness.

Additionally, it can be concluded that the major factor that affects the mode II interlaminar fracture toughness of hybrid composite materials with flax fibre is firstly the architecture of the interface material, and finally the lay-up sequence, with the flax fibre arranged in an alternating position of the hybrid one material $[0_G/0_F]_{8S}$ having the superior mode II delamination property.

The flexural modulus of the three hybrid was compared. Table 5-17 shows the flexural modulus of hybrid one, two and three materials. From the results, the percentage difference between

all three hybrid material is less than 5%. Thus, it can be concluded that the the lay up sequence does not impact the flexural modulus of the hybrid material

Table 5-18: Flexural Modulus of hybrid one,two and three material

Hybrid Material	Flexural Modulus E_{lf} (GPa)
H1 $[0_G/0_F]_{8S}$	40.63±1.32
H2 $[0_{G4}/0_{F4}]_S$	42.08±0.65
H3 $[0_{G4}/(90/0)_{F2}]_S$	41.96±1.19

Finally, in the ASTM D7905 Standard [13] the reported mode II fracture toughness was 1.17 kJ/m². Comparing this to the fracture toughness to the three hybrid composite material tested, there is an improvement in the fracture toughness because of the hybridization of the glass epoxy composites with flax fibre. The hybrid one has a 23.66% higher fracture toughness compared to the non-hybrid glass-epoxy composite material and hybrid 2 and 3 have a mode II fracture toughness that is about 13% higher than the non-hybrid glass epoxy composite.

In Table 5-18, the mode II fracture toughness of the hybrid materials in this study was compared to flax epoxy and glass epoxy materials. It becomes evident from the result that the hybrid materials have a superior mode II fracture toughness compared to non hybridized flax epoxy and glass epoxy materials. Thus, hybridizing glass-epoxy composites with flax fibres can improve the mode II fracture toughness properties of both glass and flax epoxy composite material.

Table 5-19: Mode II fracture toughness of the hybrid, flax and glass epoxy composite material

Material	Mode II fracture toughness (kJ/m²)	Reference
Hybrid one [0 _G /0 _F] _{8S}	1.484	
Hybrid two [0 _{4G} /0 _{4F}] _S	1.339	
Hybrid three [0 _{4G} / (90/0) _{2F}] _S	1.333	
Flax Epoxy [0/90] _{2S}	1.000	[6]
Flax Epoxy [90,0] _{2S}	0.728	[6]
Glass Epoxy S2/5216 [ASTM]	1.170	[13]
Glass Epoxy	0.991	[77]

6 Finite Element Analysis

In this chapter, the procedure applied in this research to model the mode II interlaminar fracture toughness (G_{IIc}) of Hybrid one (H1) with layup code $[0_G/0_F]_{8S}$, Hybrid two (H2) with layup code $[0_{4G}/0_{4F}]_S$, and Hybrid three (H3) with layup code $[0_{4G}/(90/0)_{2F}]_S$ by applying FEA is described. This chapter will present the geometry, boundary conditions, tools and ANSYS schematic used for the simulations. Furthermore, this chapter will describe the ANSYS settings used for the structural analysis of the respective composite hybrid models.

The procedure applied can be broken down into geometry creation, composite laminate assembly, setting up the mechanical model, which is classified as preprocessing, numerical analysis, postprocessing and finally validation which is done by comparing the results obtained from the simulation to that of an experimental investigation of the mode II fracture toughness presented in the previous chapter.

6.1 Geometry

The dimensions of the End Notch Flexural specimen used for the analysis are approximated based on the dimensions of the experimental samples. Two planes are created in SolidWorks, then exported to ANSYS ACP-pre where the laminate assembly is performed. Figure 6-1 shows the dimensions of the planes created in SolidWorks (all dimensions are in mm). It should be noted that the width of the geometry used for the FEA analysis is the average width of the experimental samples for each hybrid, as shown in Appendix 1.

The overall length of the geometry used for the simulation has a length of 100 mm which is the overall span of the supporting rollers. This dimension is selected because it is the domain of interest and the section that represents the physical structure where the mode II delamination is observed. Furthermore, modelling only this physical section reduces the number of elements,

boundary conditions, complexities and computation time for the simulation. The geometry of the ply used in this research is shown in Figure 6-1.

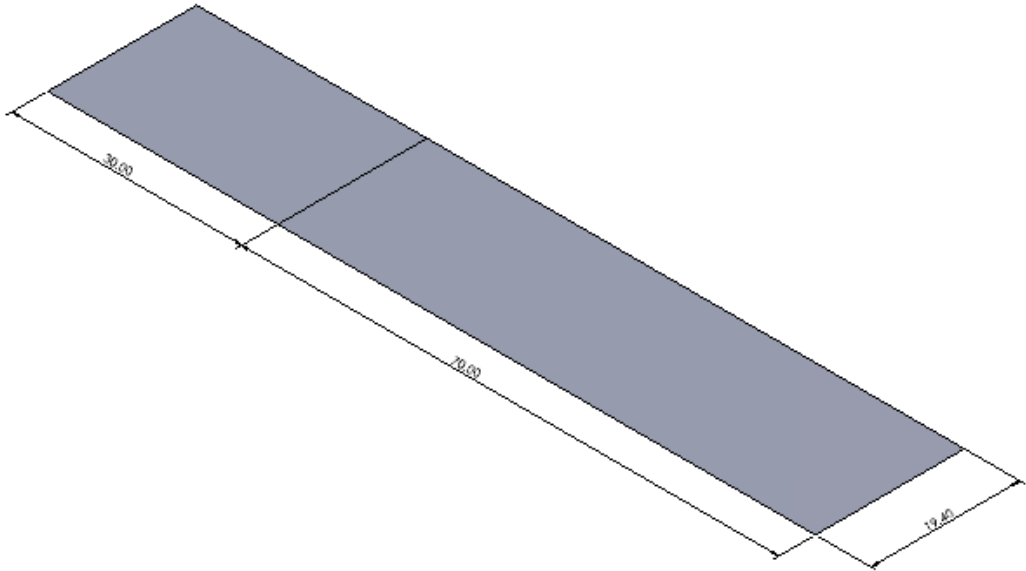


Figure 6-1: Geometry of laminate for the FEA analysis.

A second geometry is required. This represents the loading roller where a displacement boundary condition to simulate the loading of the laminate is applied. The geometry is of the loading pin used in the simulation and is shown in Figure 6-2. (All stated dimensions are in mm).

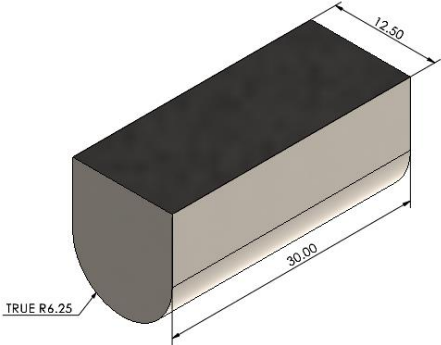


Figure 6-2: Geometry of loading rollers used in the simulation.

6.2 End Notch flexural sample modelling (Preprocessing)

The End-Notch flexural model was created in ANSYS ACP. This section describes the process of modelling the specimen in ANSYS ACP. ANSYS ACP is a robust tool in ANSYS Workbench that enables the creation of composite laminates with plies of different material, stack up sequence and ply orientation. Three types of hybrids of flax and glass were investigated in this research, Hybrid one (H1) with layup sequence $[0_G/0_F]_{8S}$, Hybrid two (H2) with layup sequence $[0_{4G}/0_{4F}]_S$, and Hybrid three (H3) with layup sequence $[0_{4G}/(90/0)_{2F}]_S$.

The First step for the creation of the ENF model is to enter the material property into the engineering data form in ANSYS. The material properties of glass epoxy are obtained from the Representative Volume Element technique, an overview of the technique is presented in section 2.8. The property of flax epoxy used in this research was obtained from research done by Mahboob et al. [23] titled the tensile and compressive damage response in fibre reinforced composites. The material properties of flax epoxy laminate applied in the ANSYS simulation are shown in Appendix 2 and 3 respectively.

Two fabric was created by selecting the Flax epoxy and glass epoxy composite material already created in the Engineering toolbox, the thickness of a single flax epoxy lamina is set to 0.2 mm while that of the glass epoxy lamina was set to 0.24375 mm, these dimensions were selected to ensure the dimensions of the assembled plies is the same as the thickness obtained from the manufacturing of the glass and flax epoxy unidirectional plate with 16 plies. Thus, the overall thickness of the model of hybrid one, two and three used in the FEA simulation is 3.55 mm.

To model a ply in ANSYS, you must create a rosette and an orientation set. The rosette defines the longitudinal, and transverse direction of the composite lamina and the orientation set defines the layup direction of the composite material.

In this project, the rosette created sets the longitudinal property of the flax epoxy lamina to the X direction and the Y and Z direction as the transverse directions.

Two orientation sets were created, this is to enable the easy modelling of the crack in the composite material: a top orientation set and a bottom orientation set. Eight plies were created with top orientation set to stack up the plies from the middle plane in the positive Y direction, and the bottom orientation set was applied to 8 plies stacked up from the middle plane in the negative Y direction.

In ANSYS ACP two modelling ply groups were created, a top modelling ply group with eight plies and a bottom modelling ply group with eight plies. The stack-up sequence of the plies for the respective hybrid tested is the same as the experimental samples. Table 4-1 shows the sequence of the ENF laminate model used in the simulation. A crack opening was applied to the middle plane in the top modelling ply. This crack element is what is evaluated by ANSYS, applying the 3D VCCT. A solid model is then created with a crack interface, a bonded interface between the laminate group and the bottom laminate group with a total ply stack up of 16 plies. Figure 6-3 shows the simulation setup of the model of the mode II end-notch flexural simulation in ANSYS simulation software.

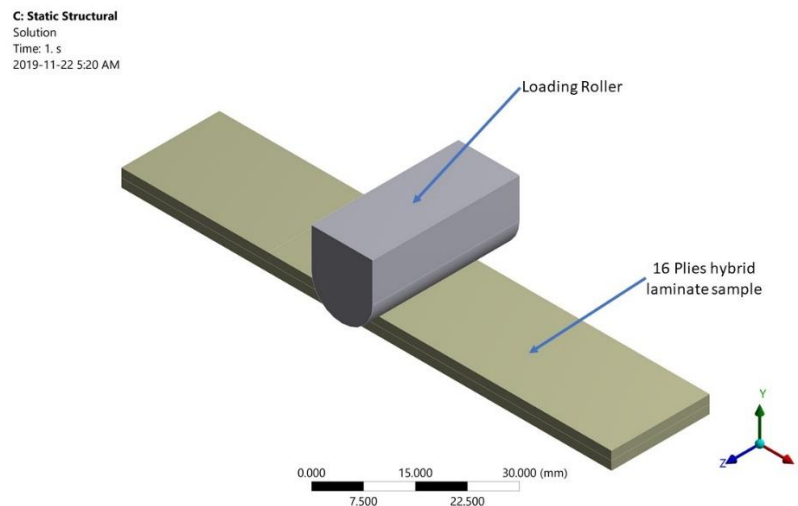


Figure 6-3: Model setup of the mode II ENF simulation.

6.3 ENF Simulation Boundary Conditions and simulation setup.

6.3.1 Boundary Conditions

In the simulation, there are three important boundary conditions necessary for the ENF simulation investigation. The fixed support, the displacement, and the remote displacement. These locations where these are applied are shown in Figure 6-4 .

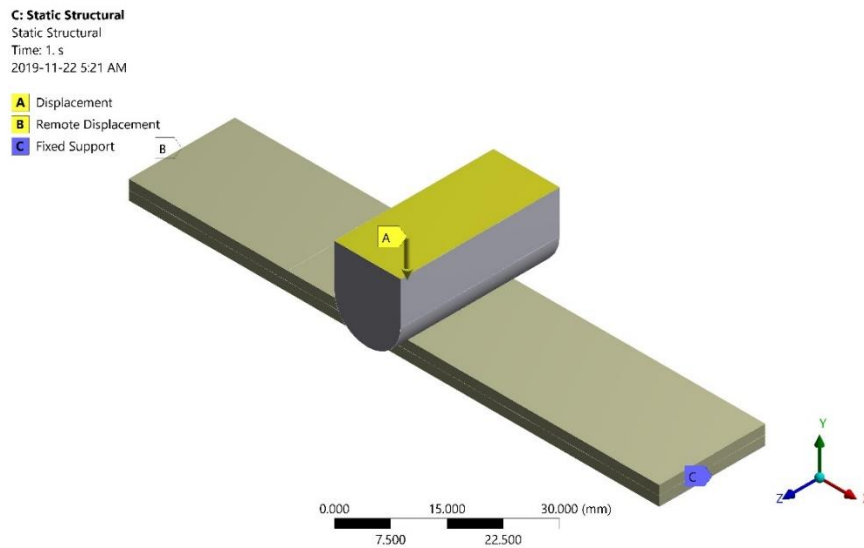


Figure 6-4: ENF geometry with boundary conditions

The displacement boundary condition was applied to the loading roller this is to ensure similarity in the loading between the simulation and the experiment. Fixed support is applied to the right bottom edge of the sample; this is necessary to ensure that the end of the sample rotates about that edge during loading. Finally, a remote displacement was applied to the left face of the sample as shown in Figure 6-4. A remote displacement is applied to ensure the face simultaneously slides and rotates about the edge during the loading of the sample. The remote displacement settings are shown in Table 6-1.

Finally, the displacement is set to a maximum of 6 mm for the three hybrids being investigated. This boundary condition represents the loading condition in the experiments.

Table 6-1: Remote Displacement settings

Details of "Remote Displacement"	
Scope	
Scoping Method	Named Selection
Named Selection	SOLIDMODEL.1_REMOTE ZERO DISPLAC...
Coordinate System	Global Coordinate System
X Coordinate	-30. mm
Y Coordinate	0. mm
Z Coordinate	0. mm
Location	Click to Change
Definition	
Type	Remote Displacement
X Component	Free
Y Component	0. mm (ramped)
Z Component	Free
Rotation X	Free
Rotation Y	Free
Rotation Z	Free
Suppressed	No
Behavior	Deformable
Advanced	
Pinball Region	All

6.3.2 Simulation setup in ANSYS

A schematic of the ANSYS analysis setup is shown in Figure 6-5. This section summarizes the different analysis systems and component systems required to investigate the mode II delamination in ANSYS. As seen in the schematic in Figure 6-5, the simulation setup comprises of two-component systems and two-analysis system systems.

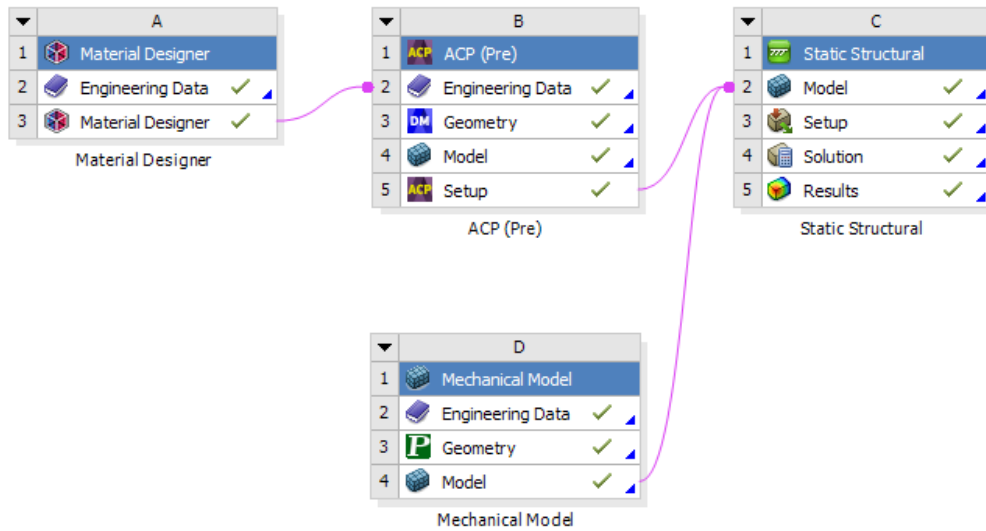


Figure 6-5: Project Schematic of the ANSYS ENF simulation.

Component systems are stand-alone editors that represent a subset of functions of a complete analysis that can be used to build a project. They do not consist of all the cells and steps required to complete an analysis system. The material designer and the mechanical model labelled A and D,

respectively, are both component systems as shown in the project schematic of the ANSYS ENF simulation.

In the material designer component system, the Representative Volume Element technique was performed in this module, the properties of glass fibre and epoxy resin was applied in the engineering data component. After obtaining the properties of the glass epoxy lamina, which is shown in Appendix 3, the data is transferred to the engineering data cell in the ACP (Pre) analysis system.

Analysis systems include all the necessary components, modules, steps required and defined, ready to be populated. For example, a static structural analysis system includes all the cells needed for the analysis, engineering data through results[10].

6.4 Mesh Convergence Analysis

The types of mesh elements used in the ENF simulation are the solid element 185, surface contact element type 22 and the CZM element CPATH26. The different element types are automatically generated and applied by the ANSYS simulation software.

To reduce the error in the Finite Element Analysis results, a mesh convergence analysis is essential. A reduced error will ensure a solution similar to the experimental results. Mesh convergence is achieved through the refinement of the mesh applied in the simulation. There are different types of mesh refinements technique used in FEA, by applying any of these methods, convergences of the FEA solution can be achieved. These include [78, 79]:

- I. h – refinement: In the FE analysis, the same type of element is used, but refinement is obtained by reducing the size of the element (also referred to as element subdivision), where “ h ” is described as the size of the element, by reducing the size of the element, the number

of mesh elements increases. This method is widely used in FEA and well implemented in commercially available FEA software.

- II. P – refinement: In this refinement method, the same size of element is used, and refinement of the element is achieved by increasing the order of the polynomial used in the element definition in the FEA model, from linear to quadratic and so on, here, “p” is the highest order of the polynomial used.
- III. R – refinement: This method involved the rearrangement of the nodes in the mesh; this is also dependent on the type of element used in the analysis.
- IV. Hp- refinement: As implied in the name, the h and p refinement method are combined to obtain a better FEA solution.

In this research, the h-refinement method is applied in the mesh convergence study. This mesh refinement method was selected because only one input requirement is needed by the software and the rest of the process is automated, thus no other setting adjustment is required from the user. The hybrid one laminate was used for the mesh convergence study. The mesh size was refined from 3.95mm to 0.65 mm with an interval of 0.6mm (3.95 is the default size automatically generated by ANSYS). The number of mesh elements was plotted against the force reaction obtained in the simulation result to observe the mesh convergence. The number of mesh elements generated was between 0.24×10^4 to 7.32×10^4 . Figure 6-6 shows the plot of the number of mesh elements against force reaction (N). The force reaction is the amount of force that is generated as the displacement load is applied to the specimen. For the mesh convergence study, a 3 mm displacement was applied to the hybrid one laminate. Thus, the force reaction is the maximum force obtained when a displacement load of 3 mm is applied. From the mesh convergence plot in Figure 6-6, it is clear that mesh convergence occurs between 3×10^4 to 7×10^4 number of elements.

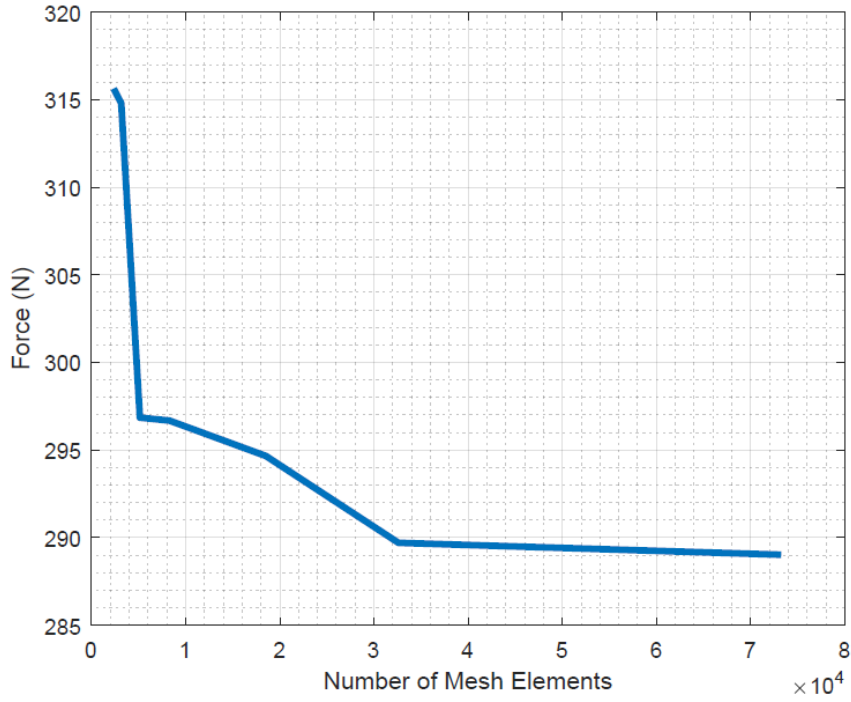


Figure 6-6: Number of mesh element vs Force reaction

Furthermore, a research by Daricik et al. [80] on the mesh sensitivity analysis for the interlaminar fracture of composite materials using the VCCT, showed that the optimal mesh size to acquire the strain energy release rate during mode II delamination is obtained if the ratio of the laminae thickness t and the element length Δa is between 0.125 mm/mm to 1.25 mm/mm that is

$$0.125 \leq \frac{t}{\Delta a} \leq 1.25$$

A mesh length of 0.9882 mm was selected in the ENF simulation and the flax laminae thickness is 0.2 mm. A ratio of $\frac{t}{\Delta a} = 0.20$ mm/mm which satisfies the limit proposed by Daricik et al.

Also, Krueger et al. [81] proposed a similar ratio of laminae thickness and element length. The ratio is also satisfied by the selected mesh element length used in this research. Thus, validating the mesh convergence study which satisfies the limit stated below.

$$0.05 \leq \frac{t}{\Delta a} \leq 1$$

6.5 Results and Discussion of Finite Element Simulation Result

This section presents the results of the End Notch Flexural specimen simulation. The force vs displacement plot of the results from the FEA is compared to that of the experiments hybrid one (H1) with layup code $[0_G/0_F]_{8S}$, hybrid two (H2) with layup code $[0_{4G}/0_{4F}]_S$, and hybrid three (H3) with layup code $[0_{4G}/(90/0)_{2F}]_S$. The failure distribution plot on each of the flax epoxy ply in the hybrid laminate is analyzed. The results are presented in the following section.

Each simulation required at least 20 minutes to complete and was done on a workstation, with an AMD threadripper processor model 2920X with 12 cores, 64 Gb of Ram and an Nvidia P4000 graphics card. All simulation was completed using ANSYS Simulation Software version 2019 R3

To validate the results of the FEA simulation, the FEA result of the force vs displacement are compared with the experimental result. Also, the mode II fracture toughness obtained from the FEA are compared to the experimental results for all three hybrids tested.

The goal of this section is to apply the Hashin Criteria in a finite element simulation, to examine failure in the flax epoxy plies of the respective hybrid materials investigated in this research. In the failure analysis, the strength ratio is applied to determine if failure has occurred, it is defined by the equation 2.5

$$R = \frac{1}{I_F} = \frac{\text{strength}}{\text{stress}} \quad (2.5)$$

The strength of the material is obtained from the material property data inputted into ANSYS. Failure is said to have occurred when $R \leq 1$. This strength ratio is also referred to as the safety factor in the simulation results presented in the following section. Thus, in this research, safety factor ≤ 1 is considered a failure.

6.5.1 Hybrid one

The force vs displacement plot comparing the experimental result and FEA result of hybrid one is shown in Figure 6-7. The percentage difference between the peak force of the FEA and experiment when delamination occurs is 3.69%, and the percentage difference of the displacement when delamination occurs between the experimental and FEA analysis is 0.60% at the peak of the plot for hybrid one material with a lay up code $[0_G/0_F]_{8s}$.

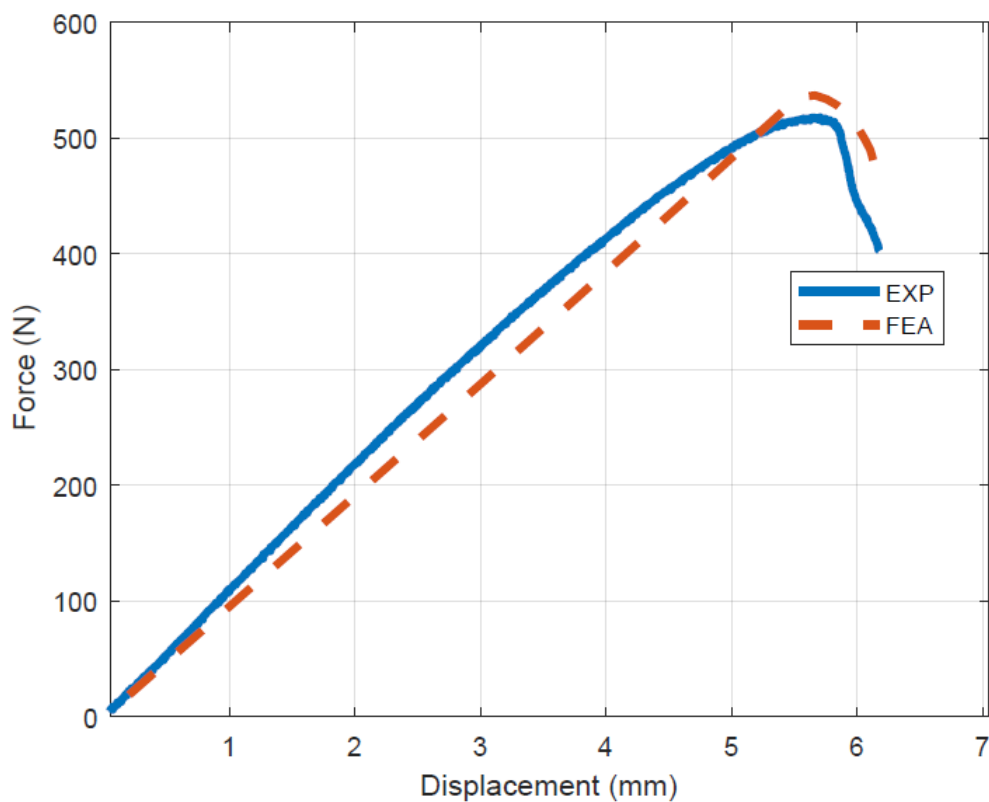


Figure 6-7: Plot of Displacement (mm) vs Force (N) of the experimental and FEA results after fracture test of the hybrid one material.

Also, the average of the mode II fracture toughness across the width of the hybrid one specimen is equal to the experimental result 1.484 kJ/m^2 . It should be noted that this value was applied as part of the input parameter, but when delamination occurs, the average of fracture toughness must be equal to the inputted value for the simulation to be considered an accurate representation of the experiment. Figure 6-8 shows the mode II fracture toughness distribution across the crack front in

the FEA simulation after delamination has occurred. The fracture toughness distribution is plotted against the width of the laminate. The fracture toughness at different points in the crack front is shown in Figure 6-9. The edges have the the lowest fracture toughness compared to the centre of the specimen which has the highest fracture toughness distributed over one third of the crack front.

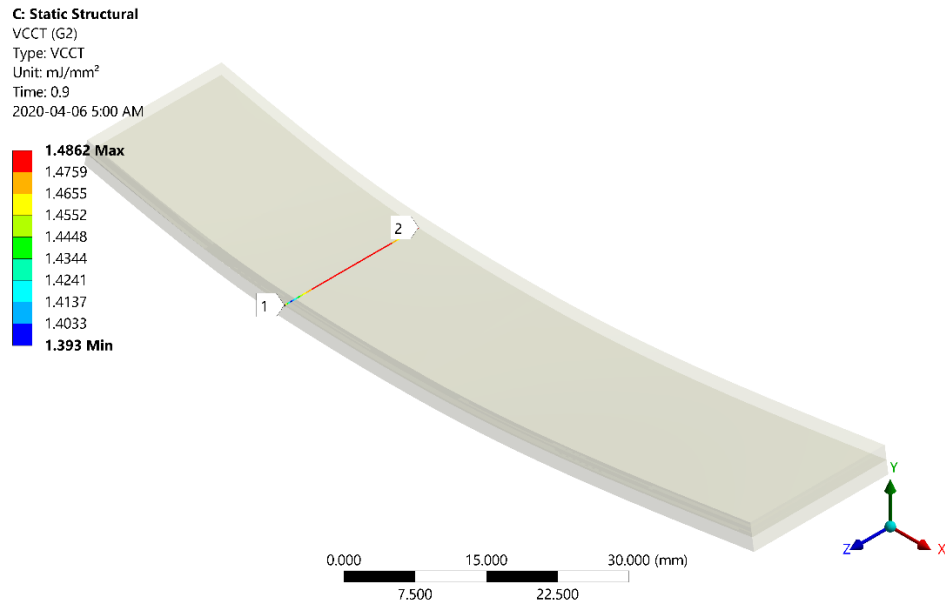


Figure 6-8: Mode II fracture toughness distribution at the crack front.

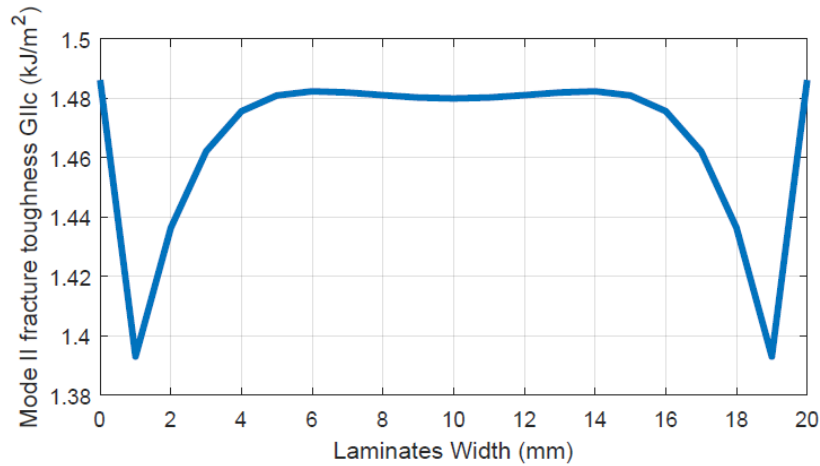


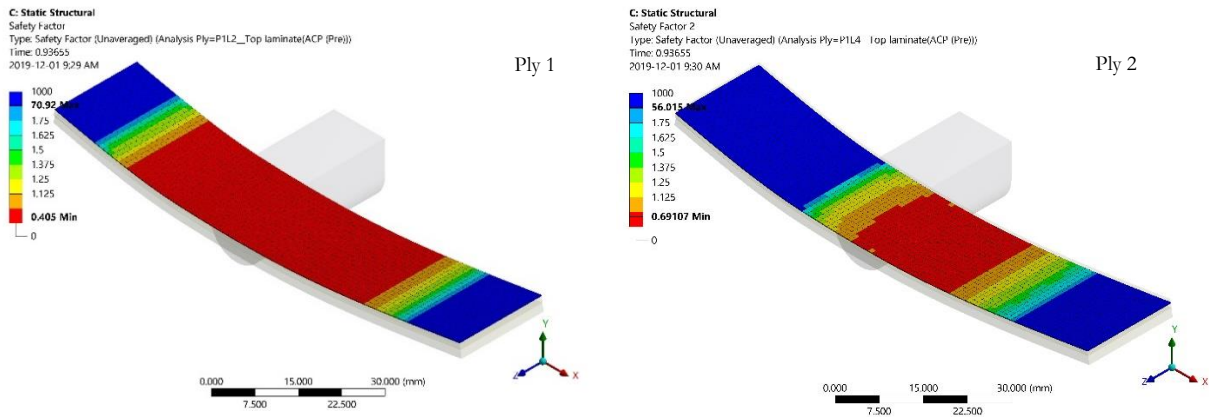
Figure 6-9: Mode II fracture toughness across the width of the hybrid one specimen.

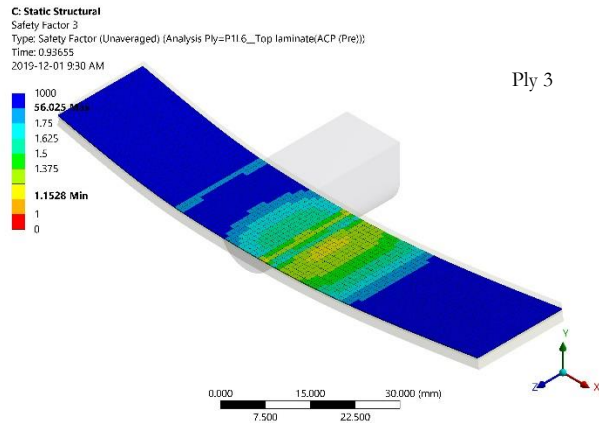
Further examining the plot in Figure 6-9, delamination starts at the sides with the lowest fracture toughness at 1mm and 19mm along the width of the specimen.

Additionally, as stated in the introductory chapter, the goal of the FEA simulation is to analyze the failure of the flax plies in the respective hybrid materials. Table 6-2 and Table 6-3 shows the longitudinal failure and transverse failure analysis of the flax epoxy plies in hybrid one, respectively. The failure analysis was performed by applying the Hashin criteria and the strength ratio also referred to as the safety factor.

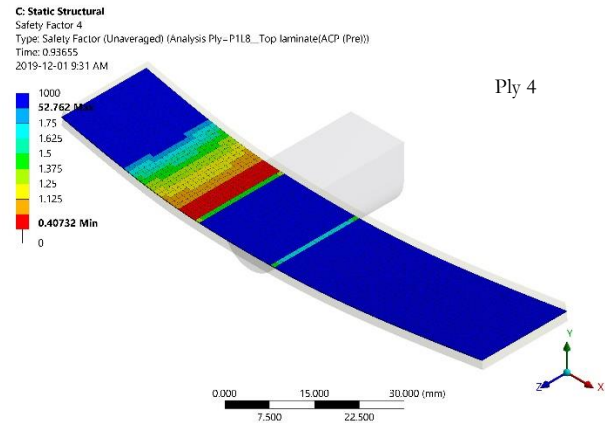
Examining the FEA failure analysis results shown in Table 6-2, three of the eight plies did not fail in the longitudinal direction, ply 3, ply 7 and ply 8, and their lowest recorded strength ratio is greater than one – 1.15, 1.36 and 1.10, respectively. Further examination of the plies that failed showed that flax ply was critical to carrying the load applied at delamination, as seen in the ply 1 with the distribution of failure in the lamina. Failure is observed after the crack front in ply 2 whereas, in the plies where the crack is located ply 4 and 5, failure is observed before the crack as seen in ply 4, ply 5 and ply 6.

Table 6-2: Longitudinal failure analysis of the flax epoxy plies in Hybrid one

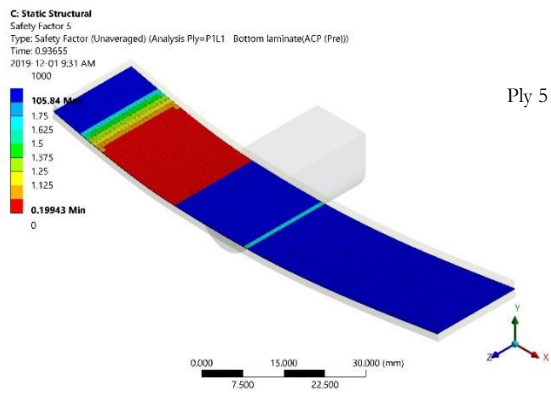




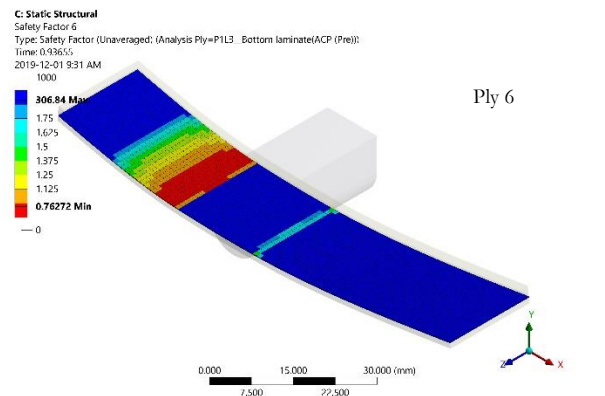
Ply 3



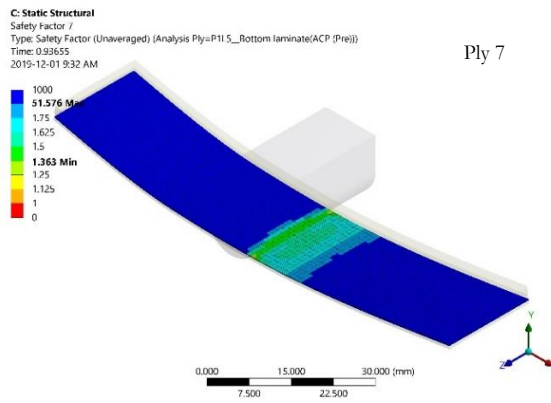
Ply 4



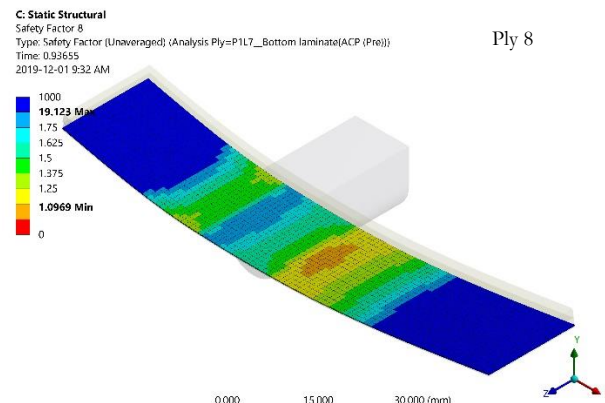
Ply 5



Ply 6



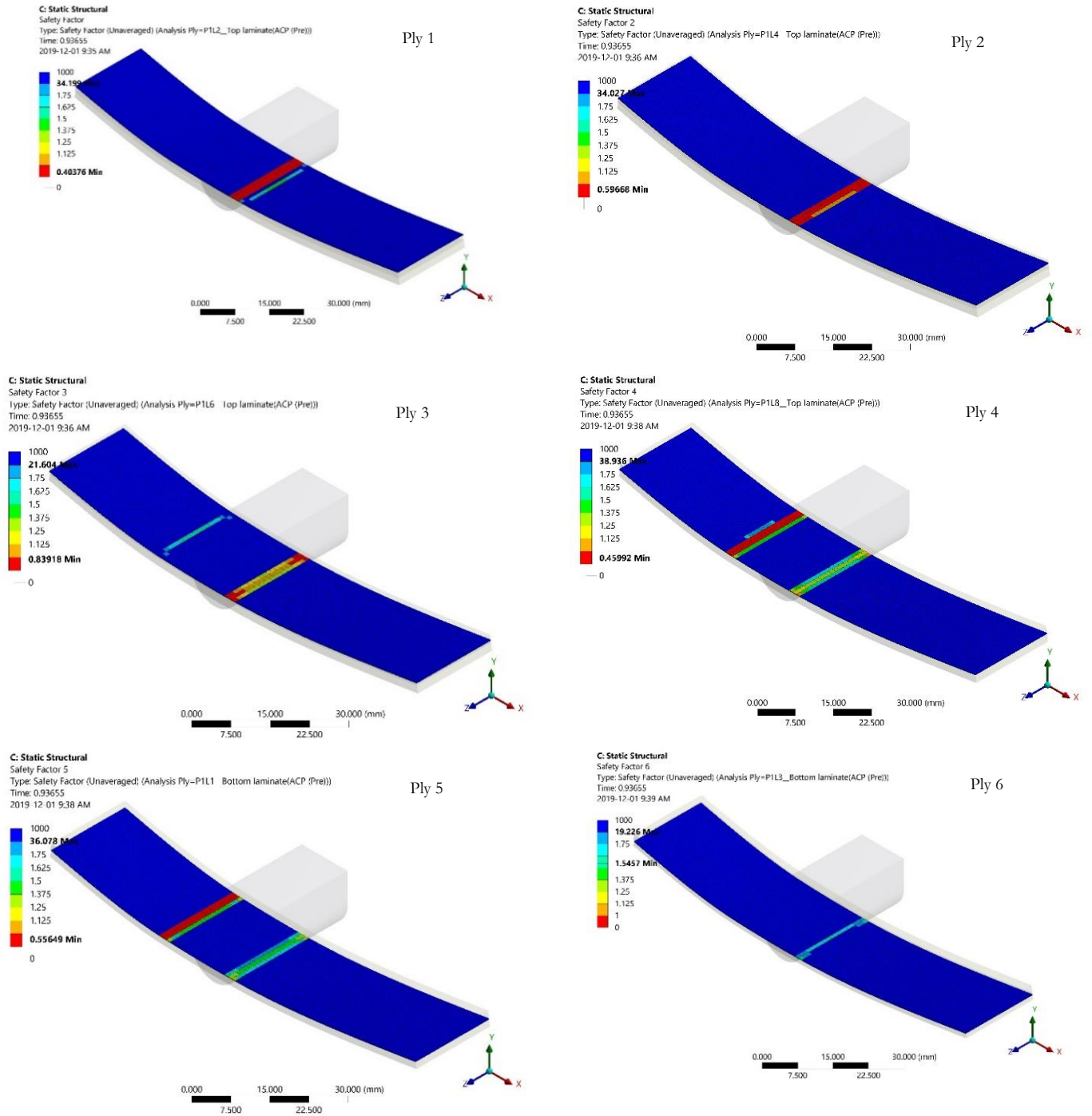
Ply 7

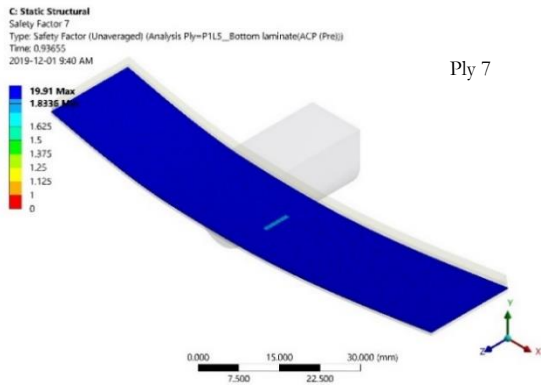


Ply 8

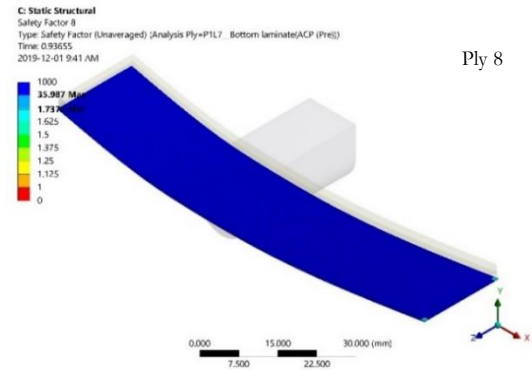
Examining the transverse failure on the hybrid one material shown in Table 6-3 plies 1 to 3 fail were the load is applied. Additionally, failure at the crack location between ply 4 and 5 is observed, no transverse failure is observed in ply 6, ply 7 and ply 8. Finally, from the FEA failure analysis of the various flax epoxy plies, it is clear, the dominant direction of failure is in the longitudinal direction (the X direction).

Table 6-3: Transverse failure analysis of the flax epoxy plies in hybrid one





Ply 7



Ply 8

6.5.2 Hybrid two

Like the hybrid one material, the force vs displacement plot comparing the experimental and FEA results is shown in Figure 6-10. The force and the displacement percentage difference between the experimental and FEA at delamination are 43.38% and 3.64%, respectively. The high percentage difference between the forces required to cause the mode II interlaminar fracture signifies that there are other failure mechanisms that occurred during the experiment that is not captured by the FEA simulation. In this case, one of the failure mechanisms is the secondary delamination that is observed in the hybrid two material with layup code $[0_{4G}/0_{4F}]_S$. This failure mode is outlined in section 5.4. Thus, if there were no other failure modes in the laminate material, the results of the FEA results will be similar to the experimental results are observed in the hybrid one material.

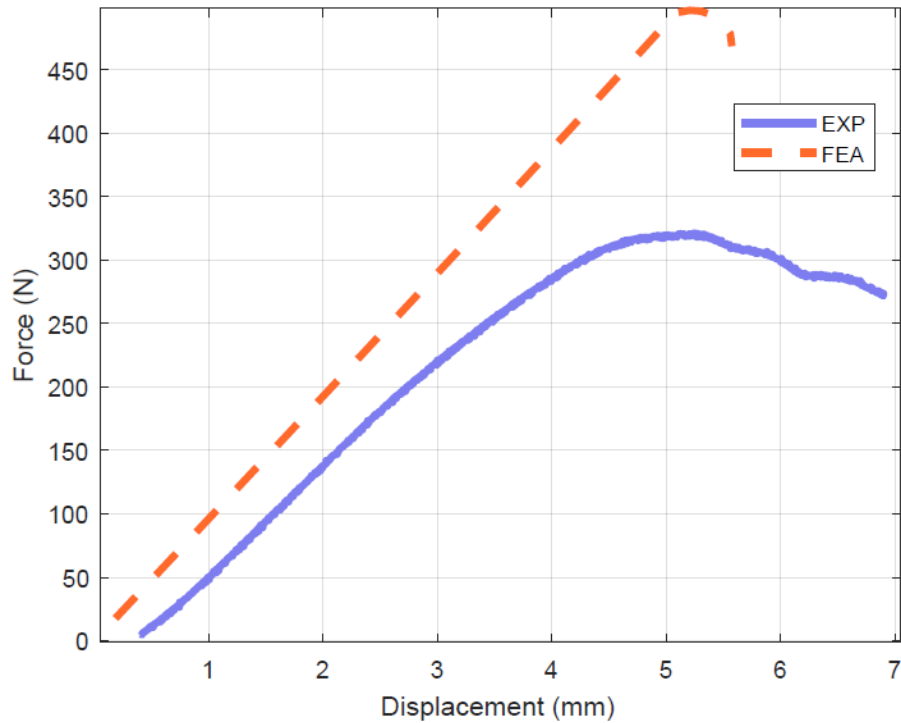


Figure 6-10: Plot of Displacement (mm) vs Force (N) of the experimental and FEA results after fracture of hybrid two

Furthermore, examining the mode II fracture toughness plot across the width of the FEA model of hybrid two, the sum of fracture toughness across the crack is equal to the 1.399 kJ/m². Figure 6-11 shows the mode II fracture distribution across the crack length in the FEA simulation after mode II fracture has occurred.

It should be noted of the three parameters required for validation of the FEA simulation; only two were satisfied for the hybrid two configuration. – the sum of fracture toughness across the width of the specimen and the displacement at delamination. Thus, this might introduce errors to the results of the simulation, and the failure analysis of the hybrid two material might overestimate the failure coefficients for each ply that fails, but the result of the analysis can still serve as a good indicator of the plies which are most likely to fail.

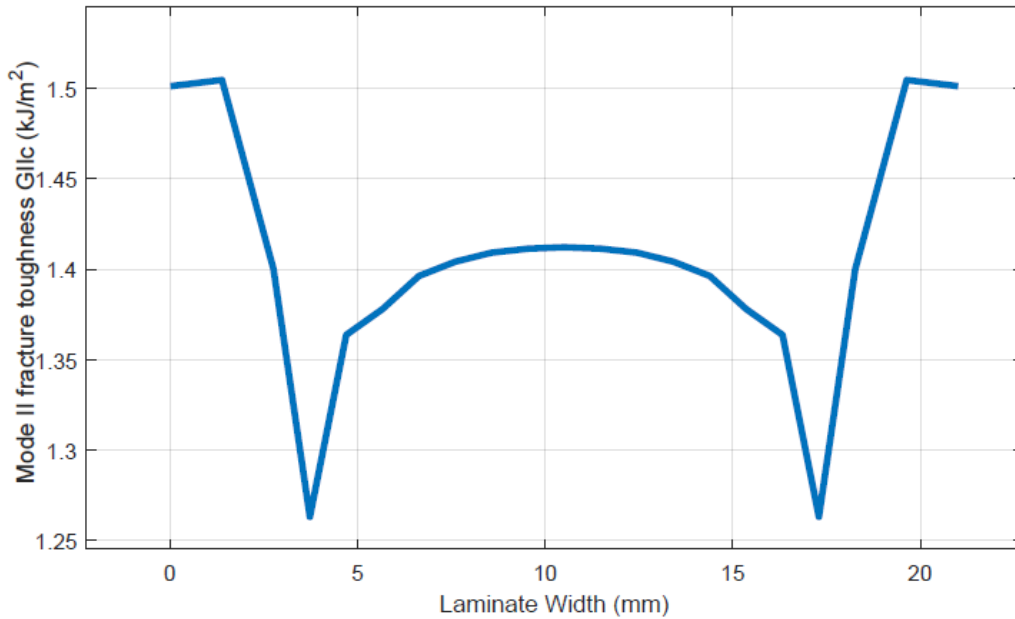
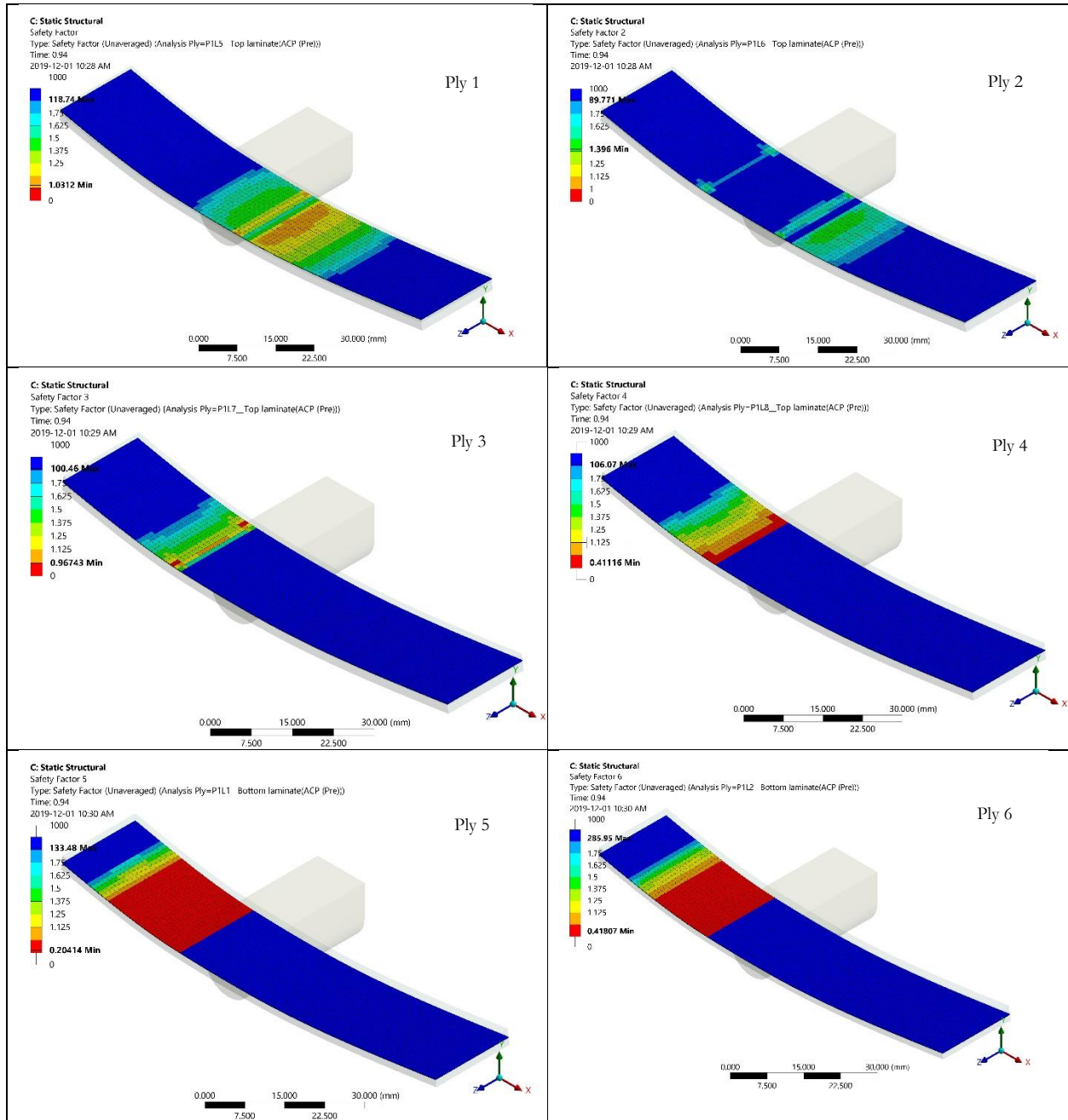
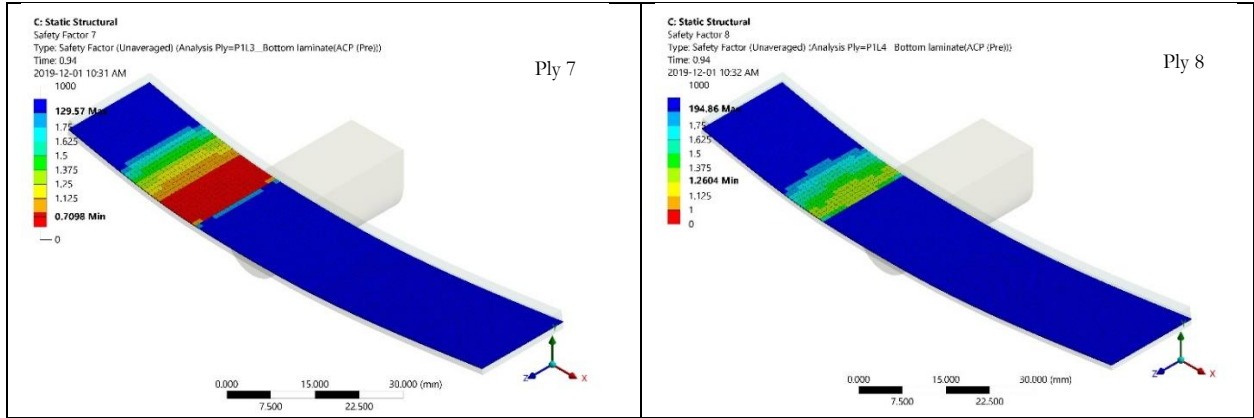


Figure 6-11: Mode II fracture toughness across the width of the hybrid two specimen

Table 6-4 shows the longitudinal failure analysis of the flax epoxy plies in hybrid two. The failure analysis of hybrid two overestimates the failure coefficient of the different flaxy plies because, the model overestimates the strength of the material, and the observed secondary delamination is not accounted for in the simulation. Examining the respective plies, it is seen that no failure is observed in the longitudinal direction in ply 1, ply 2 and ply 8 whereas failure is observed in ply 3,4,5,6, and ply 7. Also, all the failure of the flax epoxy plies occurred before the crack, no failure was observed after the crack.

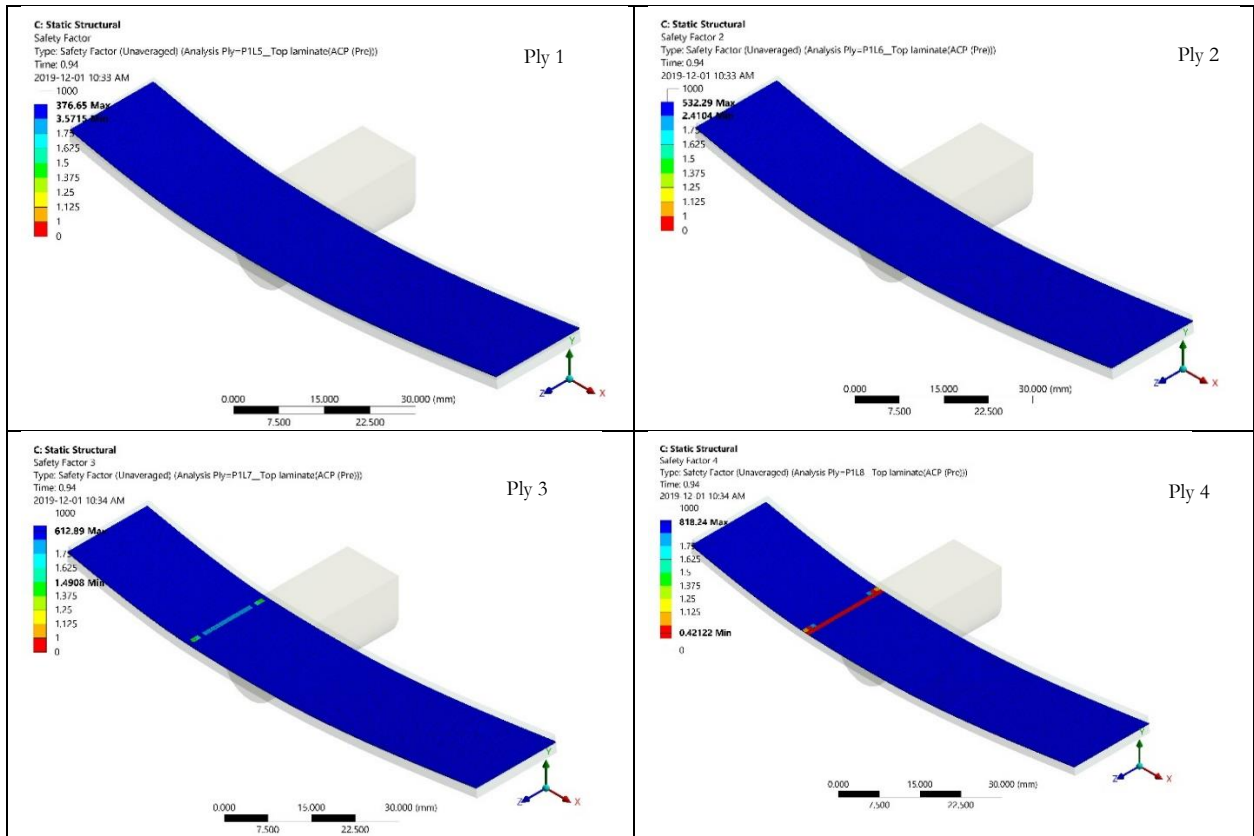
Table 6-4: Longitudinal failure analysis of the flax epoxy plies in Hybrid two

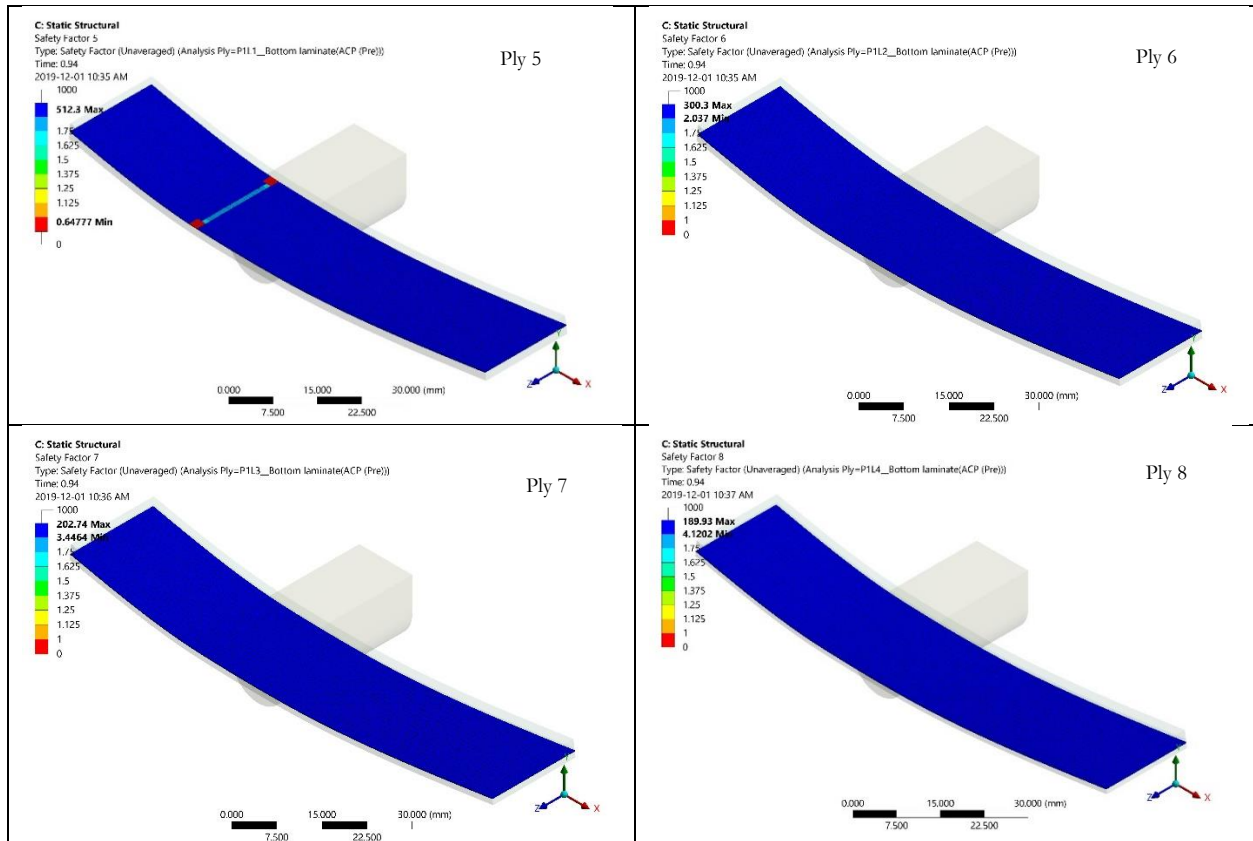




The plot of the transverse failure result analysis is shown in Table 6-5. Failure is only observed in the plies at the crack interface that is ply 4 and 5. The other plies did not exhibit any indication of failure.

Table 6-5: Transverse failure analyses of the flax epoxy plies in Hybrid two





6.5.3 Hybrid three

The force vs displacement plot of the experimental and FEA results of hybrid three is shown in Figure 6-12. Like hybrid one and two the percentage difference between the two results are compared. The percentage difference of the force at delamination between the experimental and FEA results is about 57.69%, while that of the displacement is about 0.084%. This is similar to hybrid two, with a high force percentage difference and an almost identical displacement at delamination initiation. The high percentage difference shows that there are other mechanisms of failure that occur in the hybrid laminate that reduces its strength and this mechanism is not accounted for in the FEA simulation of the $[0_{4G}/(90/0)_{2F}]_S$ hybrid. One of the failure modes is the unstable delamination of the flax and glass interface layer of the laminates outlined in the previous section.

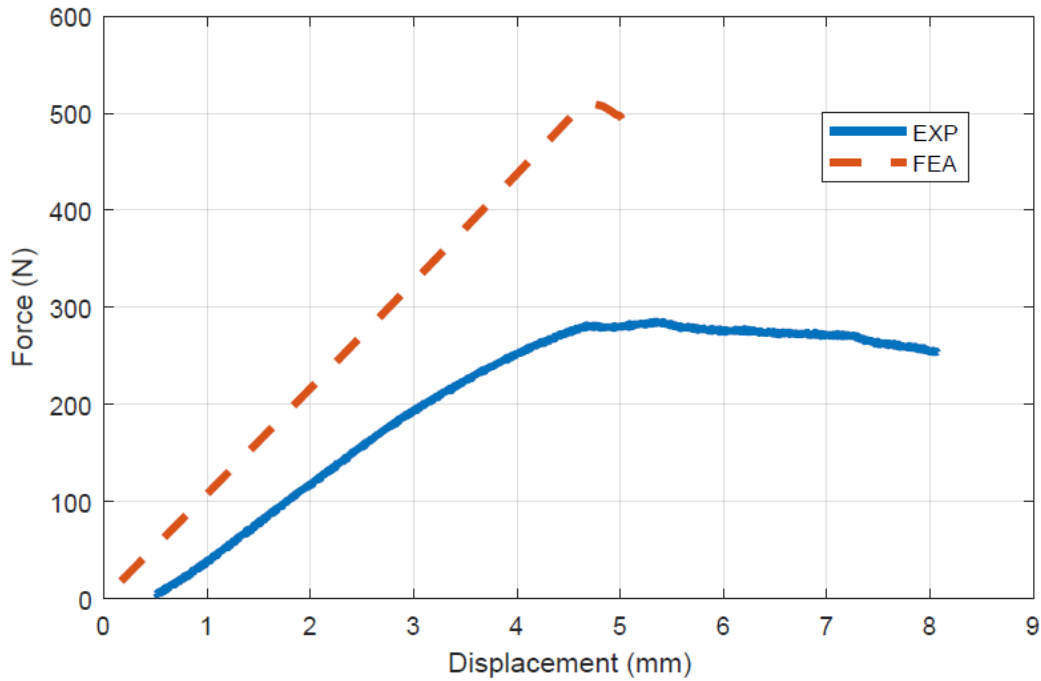


Figure 6-12: Plot of Displacement (mm) vs Force (N) of the experimental and FEA results after fracture of hybrid three

To validate the FEA simulation results, the force, displacement and fracture toughness of the FEA are compared to the experimental results. Like the hybrid two material, only the displacements are identical. Comparing the mode II fracture toughness across the crack width as shown in Figure 6-13, the average of the fracture toughness is 1.33 kJ/m^2 at the mode II fracture delamination which is an input parameter for the simulation. As stated earlier while examining hybrid two, the damage mechanism not accounted for in the FEA simulation might introduce errors to the results of the simulation and also overestimate the failure coefficients for the ply analysis. Although the result of the ply failure analysis might not be exact but will serve as a good indicator of the failure that might occur.

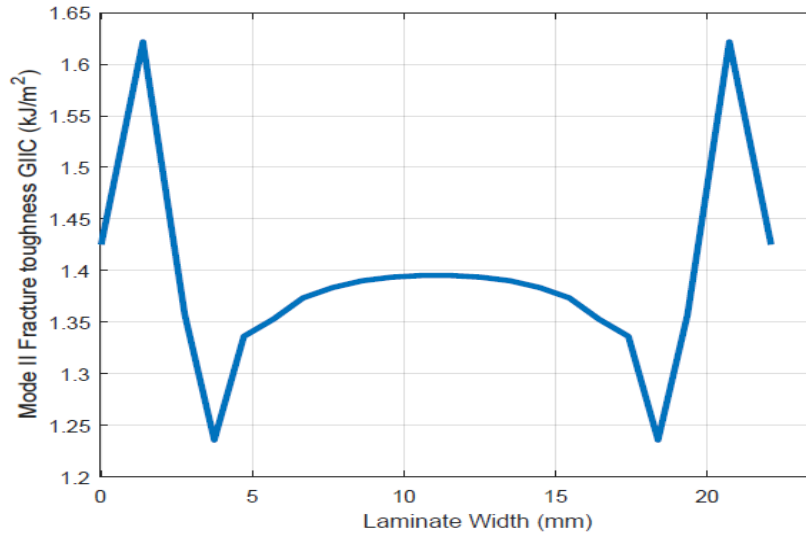
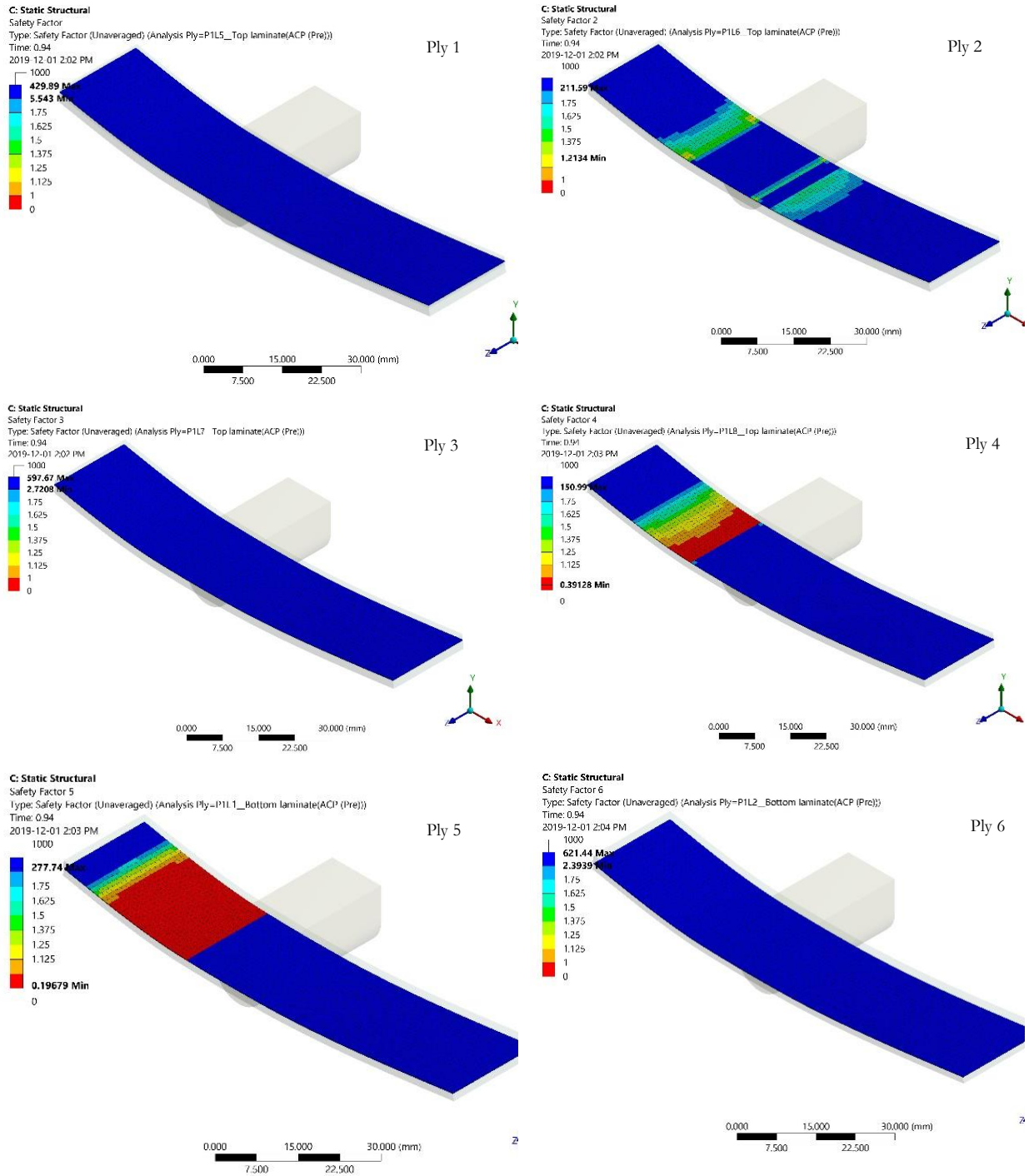
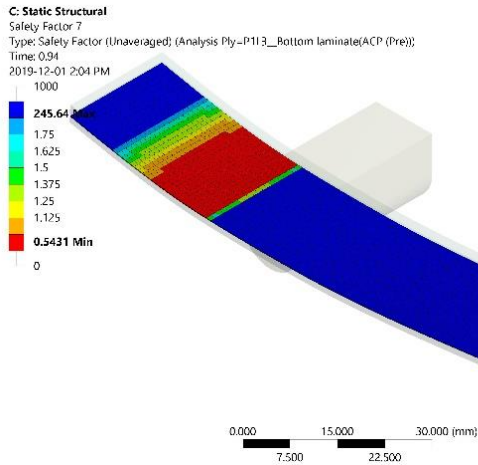


Figure 6-13: Mode II fracture toughness across the width of the hybrid three specimen.

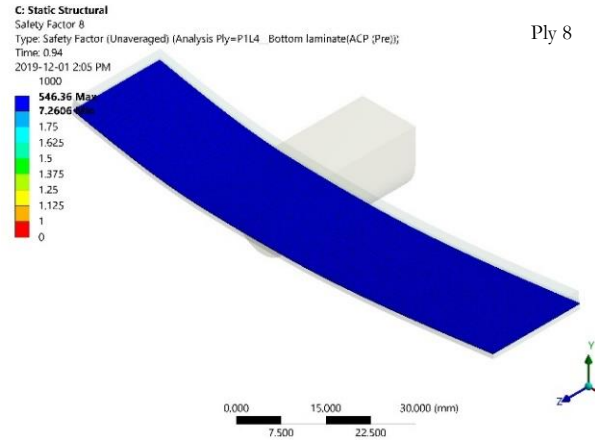
The result of the failure analysis of each ply in the hybrid three $[0_{4G}/(90/0)_{2F}]_S$ is shown in Table 6-6 and Table 6-7. Table 6-6 shows failure that occurs in the longitudinal direction while Table 6-7 shows the failure analysis of the plies in the transverse direction. From Table 6-6, it is seen that failure only occurs in ply 4,5 and 7 and the failures in these three plies occurred before the crack.

Table 6-6: Longitudinal failure analyses of the flax epoxy plies in Hybrid three





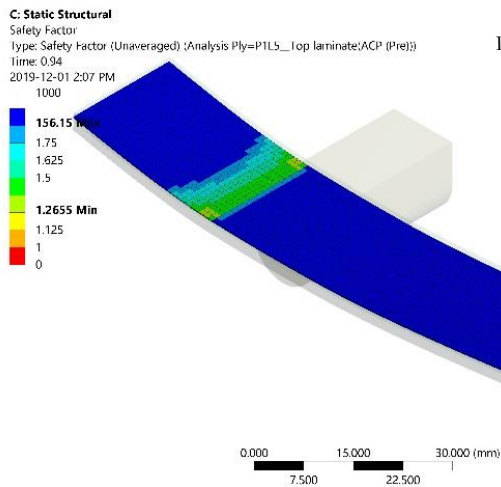
Ply 7



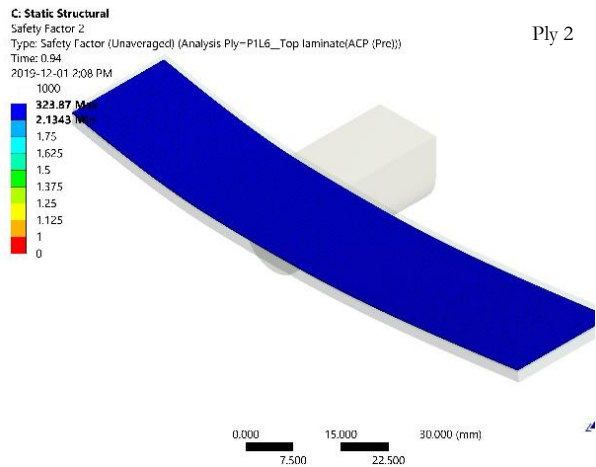
Ply 8

Examining the transverse failure of the hybrid three laminate shown in Table 6-7, failure is observed in ply 3, 4 and 5. The failure in the ply 4 is observed on the crack front location and in ply 5 the failure is observed at the edge of the crack. Comparing the failure results of hybrid two and hybrid three, although they have similar fracture toughness, the differences in the respective ply orientation had a significant impact on their failure profile.

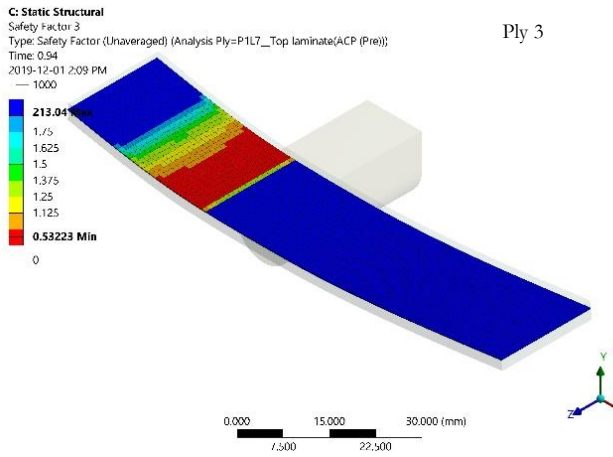
Table 6-7: Transverse failure analyses of the flax epoxy plies in Hybrid three



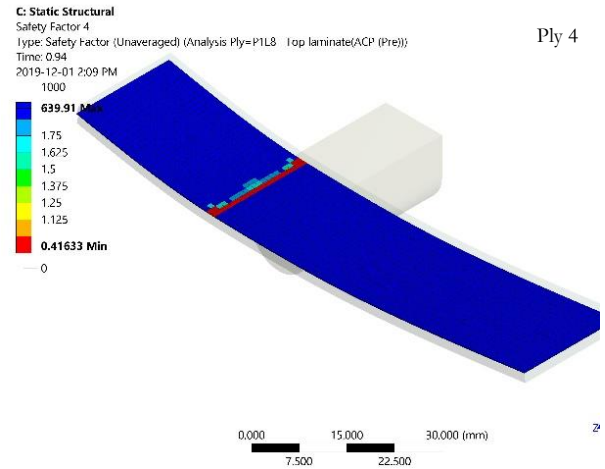
Ply 1



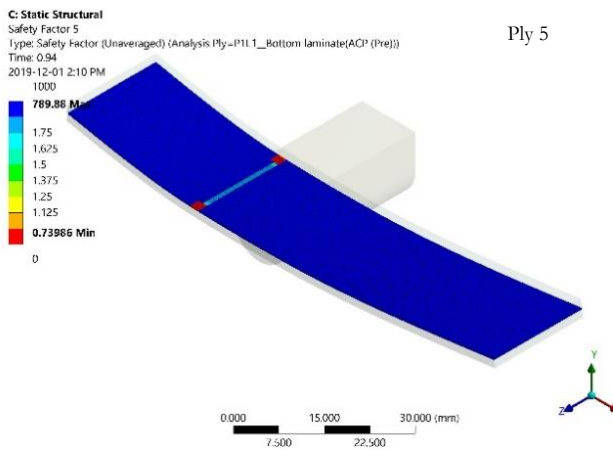
Ply 2



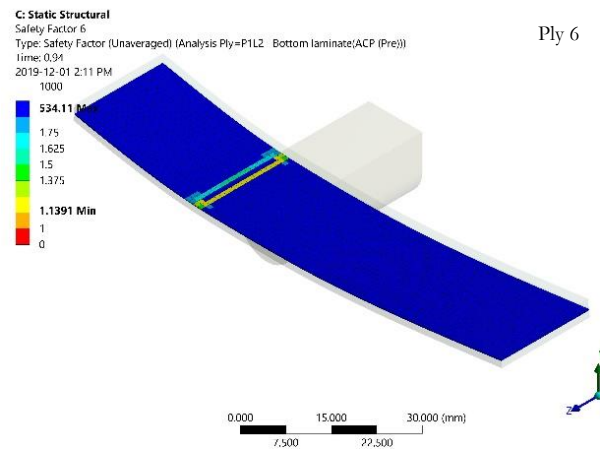
Ply 3



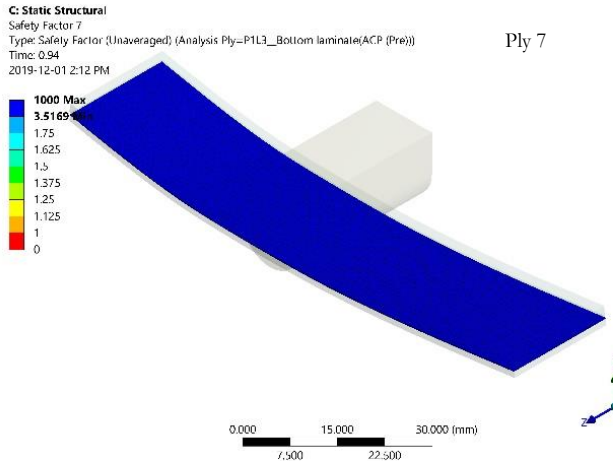
Ply 4



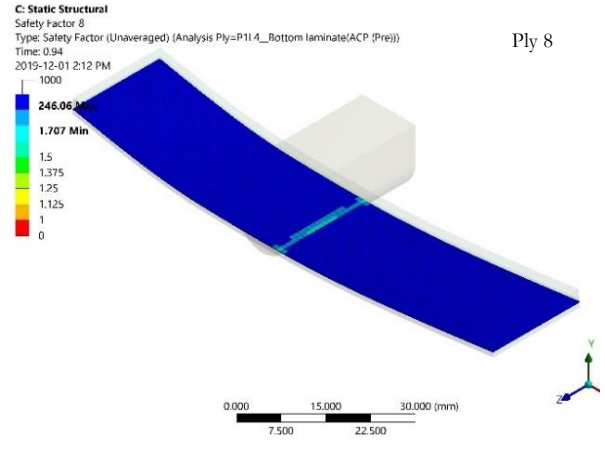
Ply 5



Ply 6



Ply 7



Ply 8

Finally, the failure results of the hybrid one, hybrid two and hybrid three showed that the layup sequence and ply orientation impact the material responses to failure. With the three hybrids exhibiting different failure modes and the plies responding differently to loading. Also, hybrid two and three had similar failure mechanism that was not accounted for in the simulation. The failure mechanism is the unstable interface delamination of the flax and glass interface. To account for this failure mode in the future, incorporating a robust damage model into the mode II simulation that could analyze delamination between individual plies in a composite material could produce a better FEA representation of the experimental model. There have been significant developments in different damage models that can adequately predict the damage evolution in composite materials.

Research by Chen et al. [82] studied the progressive failure analysis of AS4/PEEK composite materials and aluminum/carbon fibre reinforced polymer fibre metal composite laminates respectively. They combined a continuum damage mechanic model with a cohesive zone model to evaluate the progressive failure of the composite material to tensile loading and low-velocity impact load. These researchers showed that an FE model could be developed that incorporates a damage model and a delamination model for simulating the different failure mechanisms. This model could account for the interaction of the different failure mechanisms and this is a more accurate model that predicts the failure of the composite material.

Other research by Liu et al.[83] and Morais et al. [84] developed delamination models that account for the transverse cracking, stress distribution, and delamination of composite materials also concluded that the combination of a damage model and a delamination model provides an advance numerically robust model.

7 Conclusion and Future Work

The goal of this thesis research was to investigate the effects of the layup sequence of on the mode II interlaminar fracture toughness of hybrids of glass fibre and flax fibre in an epoxy matrix, examine if hybridization can improve the fracture toughness of a glass epoxy laminate and determine if Finite Element Analysis (FEA) tools like ANSYS can be applied to assess the response of plies in a composite material to failure during delamination. The research consisted of a series of End Notch Flexural (ENF) experiments and FEA simulation conducted on hybrid one $[0_G/0_F]_8$, hybrid two $[0_{4G}/0_{4F}]_8$ and hybrid three $[0_{4G}/(90/0)_{2F}]_8$ glass and flax epoxy composite materials. The following paragraphs will provide the conclusions drawn from the experiments and FEA simulation also provide recommendations for future work.

The mode II interlaminar fracture toughness of hybrid one, hybrid two and hybrid three was successfully characterized in this research. The layup sequence of the respective hybrid materials does affect the mode II fracture toughness, also, to a greater degree the architecture of the interface material at the interface where the crack is located have a higher effect compared to the layup sequence. Additionally, hybridization of glass epoxy laminate with flax fibre improves the mode I and mode II fracture toughness compared to non hybridized glass epoxy laminate thus, it can be concluded that the effects of delamination in a synthetic composite material containing glass fibre can be reduced by hybridization with flax fibres which will increase its fracture toughness improving the overall mechanical performance of the material in service.

The flexural modulus of the respective hybrid composite materials was evaluated and compared. Hybrid one, hybrid two and hybrid three have a flexural modulus of 40.63 ± 1.32 GPa, 42.087 ± 0.65 GPa and 41.96 ± 1.19 GPa respectively. The percentage difference between the three

flexural modulus is under 3.5 % thus it can be concluded that the lay up sequence does not affect the flexural modulus of the composite material.

As stated earlier, another goal of the thesis research was to evaluate the application of FEA as a damage assessment tool during delamination. It can be concluded that engineering FEA simulation tools like ANSYS simulation software can be used to assess the damage in each ply during delamination. From the simulation results, applying the Hashin criteria and Virtual Crack Closure Technique only provide accurate results for hybrid one materials. The secondary interlaminar delamination and interbundle delamination observed in the laminates of hybrid two and three wasn't successfully captured. Thus, applying the Hashin Criteria and the VCCT to assess failure in laminate plies during delamination is limited because the accuracy of the results is depended on the layup sequence and the orientation of the laminates fibre.

With the growth of computer processing power and speed, and the growth in the capabilities of engineering simulation software, Finite Element Analysis simulation has the potential of being both a predictive tool and an analysis.

The importance of engineering simulation cannot be overstated in the current manufacturing industry, because the industry has become highly competitive, there is a constant push to produce more innovative products and product development time has reduced. Furthermore, products are increasingly more complex, versatile and there is a growing need for customization. To gain better insights of engineering systems and their performance, 3D modelling, simulation and analysis provide a very cost-effective opportunity to develop and test new design concept, examine vulnerabilities and provide information and knowledge before manufacturing which leads to more efficient manufacturing. With the growth and development of the functionality in these simulation tools in the last decade, the quality of data and information obtained from these tools have increased [85].

The glass – flax epoxy material composites with layup sequence of hybrid one is suitable for applications where delamination is the major mode of failure. Also, because this is a hybrid material, the excellent mechanical properties – excellent tensile strength, flexural strength, impact resistance, and other properties, of both glass fibres and flax fibres are present in the hybrid. Examples of such applications are in sporting equipment – bikes, skis, surfboards etc.

Finally, for future research, a numerically robust model that accounts for the stress distribution and interaction of the different failure mechanisms can be developed to assess the mode I and mode II fracture toughness properties of composite materials by combining a damage model and a delamination model.

As stated in chapter one, the introductory chapter, there are three basic modes of delamination mode I, mode II and mode III, these three modes of failure may occur at the same time as mixed modes in a material.

One limitation of this work in the characterization of the delamination properties of hybrids of glass and flax epoxy laminates is that only the mode II delamination mode was examined during static loading. To fully understand the improvements due to hybridization of glass fibre with flax natural fibres on the delamination properties of the laminate material, mode I, and the mixed modes of delamination also need to be characterized.

Furthermore, this research only investigated the mode II delamination properties during static loading.

Other future work relevant to this research that would improve the knowledge and provide more information the performance of composite materials includes:

- I. Perform Mode I, mode III and mixed-mode I/II interlaminar fracture toughness characterization of the hybrid one, two and three glass and flax epoxy composite material.
- II. Evaluate the mode I and mode II delamination properties during fatigue loading.
- III. Assess the impact of the hybrid manufacturing on the thickness of each ply.
- IV. Develop a robust model that can predict and assess delamination initiation for the respective delamination modes in the composite material.
- V. Develop a FE model that combines continuum damage mechanic with a cohesive zone model to evaluate the progressive failure of the composite material during delamination static and dynamic loading.

Appendix

Appendix 1: Complete Dimensions of Hybrid 1 ([0G/0F] 8S), Hybrid 2 [04G/04F] S and Hybrid 3 [04G/(90/0)2F] S

These are the dimensions obtained from the six samples tested for the respective hybrid material of glass and flax epoxy.

Specimen Geometry for Panel No: 1						Material: [0 _G /0 _F] _{8S} (H1)							
Date of Measurement: 23-July-2019						Operator: WS							
Specimen Width and Thickness Data						Thickness, 2h (mm)							
Specimen Number	Width, B (mm)					Location 1		Location 2		Location 3		Avg	Standard Deviation
	Loc1	Loc 2	Loc3	Avg	Standard Deviation	Left	Right	Left	Right	Left	Right		
H1SP01	19.24	19.49	19.80	19.51	0.23	3.65	3.60	3.50	3.50	3.52	3.51	3.55	0.06
H1SP02	19.20	19.45	19.02	19.22	0.18	3.65	3.57	3.55	3.55	3.58	3.58	3.58	0.03
H1SP03	19.85	20.45	20.46	20.25	0.29	3.70	3.56	3.50	3.51	3.50	3.50	3.55	0.07
H1SP04	20.05	20.49	20.56	20.37	0.23	3.68	3.55	3.49	3.51	3.54	3.54	3.55	0.06
H1SP05	19.58	20.22	20.54	20.11	0.40	3.70	3.55	3.49	3.45	3.45	3.45	3.52	0.09
H1SP06	19.57	19.66	19.67	19.63	0.04	3.68	3.54	3.46	3.46	3.45	3.44	3.51	0.08

Specimen Geometry for Panel No: 1						Material: [0G4/0F4] S (H2)							
Date of Measurement: 24-July-2019						Operator: WS							
Specimen Width and Thickness Data						Thickness, 2h (mm)							
Specimen Number	Width, B (mm)					Location 1		Location 2		Location 3		Avg	Standard deviation
	Loc1	Loc 2	Loc3	Avg	Standard deviation	Left	Right	Left	Right	Left	Right		
H2SP01	19.00	19.01	19.51	19.17	0.24	3.90	3.72	3.50	3.50	3.51	3.53	3.61	0.15
H2SP02	19.00	19.50	19.50	19.33	0.24	3.83	3.75	3.50	3.52	3.52	3.53	3.61	0.13
H2SP03	19.03	19.50	19.60	19.38	0.25	3.85	3.75	3.50	3.50	3.54	3.54	3.61	0.14
H2SP04	19.37	19.56	19.62	19.52	0.11	3.80	3.69	3.40	3.41	3.48	3.48	3.54	0.15
H2SP05	19.01	19.44	19.55	19.33	0.23	3.83	3.64	3.40	3.42	3.50	3.50	3.55	0.15
H2SP06	19.80	20.00	19.85	19.88	0.08	3.83	3.80	3.43	3.43	3.51	3.51	3.59	0.17

Specimen Geometry for Panel No: 1						Material: [0G4/(90/0) F2]S (H3)							
Date of Measurement: 26-July-2019						Operator: WS							
Specimen Width and Thickness Data						Thickness, 2h (mm)							
Specimen Number	Width, B (mm)					Location 1		Location 2		Location 3		Avg	Standard Deviation
	Loc1	Loc 2	Loc3	Avg	Standard deviation	Left	Right	Left	Right	Left	Right		
H3SP01	20.23	20.34	20.57	20.38	0.14	3.77	3.66	3.43	3.44	3.44	3.44	3.53	0.13
H3SP02	20.77	20.85	20.50	20.71	0.15	3.75	3.75	3.44	3.44	3.44	3.44	3.54	0.15
H3SP03	19.71	20.21	20.50	20.14	0.33	3.73	3.66	3.45	3.44	3.45	3.45	3.53	0.12
H3SP04	20.61	20.67	20.71	20.66	0.04	3.77	3.69	3.46	3.45	3.44	3.44	3.54	0.14
H3SP05	20.22	20.77	20.81	20.60	0.27	3.76	3.62	3.46	3.46	3.44	3.44	3.53	0.12
H3SP06	20.00	20.20	20.40	20.20	0.16	3.74	3.63	3.43	3.43	3.43	3.42	3.51	0.13

Appendix 2: Material property of flax epoxy composite [22]

This is the material properties of flax epoxy used in the finite element simulation in ANSYS.

Properties of Outline Row 4: Flax Epoxy Laminate					
	A	B	C	D	E
1	Property	Value	Unit		
2	Material Field Variables	Table			
3	Density	1310	kg m ⁻³		<input type="checkbox"/>
4	Orthotropic Elasticity			<input type="checkbox"/>	
5	Young's Modulus X direction	31420	MPa		<input type="checkbox"/>
6	Young's Modulus Y direction	5580	MPa		<input type="checkbox"/>
7	Young's Modulus Z direction	5580	MPa		<input type="checkbox"/>
8	Poisson's Ratio XY	0.352			<input type="checkbox"/>
9	Poisson's Ratio YZ	0.38			<input type="checkbox"/>
10	Poisson's Ratio XZ	0.353			<input type="checkbox"/>
11	Shear Modulus XY	2070	MPa		<input type="checkbox"/>
12	Shear Modulus YZ	2021.7	MPa		<input type="checkbox"/>
13	Shear Modulus XZ	2070	MPa		<input type="checkbox"/>
14	Orthotropic Stress Limits			<input type="checkbox"/>	
15	Tensile X direction	286.7	MPa		<input type="checkbox"/>
16	Tensile Y direction	33.86	MPa		<input type="checkbox"/>
17	Tensile Z direction	33.86	MPa		<input type="checkbox"/>
18	Compressive X direction	-127.11	MPa		<input type="checkbox"/>
19	Compressive Y direction	-79.94	MPa		<input type="checkbox"/>
20	Compressive Z direction	-79.94	MPa		<input type="checkbox"/>
21	Shear XY	37.35	MPa		<input type="checkbox"/>
22	Shear YZ	37.35	MPa		<input type="checkbox"/>
23	Shear XZ	37.35	MPa		<input type="checkbox"/>
24	Orthotropic Strain Limits			<input type="checkbox"/>	
25	Tensile X direction	0.0153			<input type="checkbox"/>
26	Tensile Y direction	0.0136			<input type="checkbox"/>
27	Tensile Z direction	0.0136			<input type="checkbox"/>
28	Compressive X direction	-0.016			<input type="checkbox"/>
29	Compressive Y direction	-0.0261			<input type="checkbox"/>
30	Compressive Z direction	-0.0261			<input type="checkbox"/>
31	Shear XY	0.1492			<input type="checkbox"/>
32	Shear YZ	0.2			<input type="checkbox"/>
33	Shear XZ	0.1492			<input type="checkbox"/>
34	Ply Type			<input type="checkbox"/>	
35	Type	Regular			

Appendix 3: Material property of glass epoxy composite (obtained from RVE analysis using ANSYS [74])

This is the material properties of glass epoxy used in the finite element simulation in ANSYS.

Properties of Outline Row 3: E-glass epoxy UD					
	A	B	C	D	E
1	Property	Value	Unit		
2	Density	1880	kg m ⁻³	<input type="checkbox"/>	<input type="checkbox"/>
3	Orthotropic Elasticity			<input type="checkbox"/>	
4	Young's Modulus X direction	38012	MPa	<input type="checkbox"/>	<input type="checkbox"/>
5	Young's Modulus Y direction	7071.3	MPa	<input type="checkbox"/>	<input type="checkbox"/>
6	Young's Modulus Z direction	7071.3	MPa	<input type="checkbox"/>	<input type="checkbox"/>
7	Poisson's Ratio XY	0.2766		<input type="checkbox"/>	<input type="checkbox"/>
8	Poisson's Ratio YZ	0.51852		<input type="checkbox"/>	<input type="checkbox"/>
9	Poisson's Ratio XZ	0.2766		<input type="checkbox"/>	<input type="checkbox"/>
10	Shear Modulus XY	3097.7	MPa	<input type="checkbox"/>	<input type="checkbox"/>
11	Shear Modulus YZ	3736.5	MPa	<input type="checkbox"/>	<input type="checkbox"/>
12	Shear Modulus XZ	3097.7	MPa	<input type="checkbox"/>	<input type="checkbox"/>
13	Ply Type			<input type="checkbox"/>	
14	Type	Regular			

References

1. Reis, P.N.B., et al., *Effect of Interlayer Delamination on Mechanical Behavior of Carbon/Epoxy Laminates*. Journal of Composite Materials, 2009. **43**(22): p. 2609-2621.
2. Amaro, A.M., P.N.B. Reis, and M.F.S.F. de Moura, *Delamination Effect on Bending Behaviour in Carbon-Epoxy Composites: Bending Behaviour in Carbon-Epoxy Composites*. Strain, 2011. **47**(2): p. 203-208.
3. Pereira, A.B., et al., *Mode II interlaminar fracture of carbon/epoxy multidirectional laminates*. Composites Science and Technology, 2004. **64**(10): p. 1653-1659.
4. Bonhomme, J., et al., *Influence of the Matrix Toughness in Carbon-Epoxy Composites Subjected to Delamination under Modes I, II, and Mixed I/II*. Mechanics of Advanced Materials and Structures, 2013. **20**(8): p. 679-686.
5. Mathews, M.J. and S.R. Swanson, *Characterization of the interlaminar fracture toughness of a laminated carbon/epoxy composite*. Composites Science and Technology, 2007. **67**(7): p. 1489-1498.
6. Bensadoun, F., I. Verpoest, and A.W. Van Vuure, *Interlaminar fracture toughness of flax-epoxy composites*. Journal of Reinforced Plastics and Composites, 2017. **36**(2): p. 121-136.
7. Madhukar, M.S. and L.T. Drzal, *Fiber-Matrix Adhesion and Its Effect on Composite Mechanical Properties: IV. Mode I and Mode II Fracture Toughness of Graphite/Epoxy Composites*. Journal of Composite Materials, 1992. **26**(7): p. 936-968.
8. Turon, A., et al., *An engineering solution for mesh size effects in the simulation of delamination using cohesive zone models*. Engineering Fracture Mechanics, 2007. **74**(10): p. 1665-1682.
9. Gay, D. and S.V. Hoa, *Composite materials: design and applications*. 2007: CRC press.
10. ANSYS, *ANSYS® Workbench 2020 R1, help system*, ANSYS, Inc. 2020.
11. Agarwal, B.D., L.J. Broutman, and K. Chandrashekhara, *Analysis and performance of fiber composites*. 3rd ed. 2006: John Wiley.
12. Dowling, N.E., *Mechanical behavior of materials: engineering methods for deformation, fracture and fatigue*. 5th ed. 2018: Pearson Prentice Hall.
13. Standard, A., *D7905/D7905M-14*. Standard Test Method for Determination of the Mode II Interlaminar Fracture Toughness of Unidirectional Fiber-Reinforced Polymer Matrix Composites, 2014.
14. Kim, B.W. and A.H. Mayer, *Influence of fiber direction and mixed-mode ratio on delamination fracture toughness of carbon/epoxy laminates*. Composites Science and Technology, 2003. **63**(5): p. 695-713.
15. Hodgkinson, J.M., *Mechanical testing of advanced fibre composites*. 2000: Elsevier.
16. Standard, A., *D5528-13, 2013, "Standard test method for mode I interlaminar fracture toughness of unidirectional fiber-reinforced matrix composites," ASTM International, West Conshohocken, PA, 2013*. 2013.
17. Standard, A., *Standard test method for determination of the mode II interlaminar fracture toughness of unidirectional fiber-reinforced polymer matrix composites*. ASTM D7905, 2014.
18. Standard, A., *D6671/D6671M (2006) Standard test method for mixed mode I-mode II interlaminar fracture toughness of unidirectional fiber reinforced polymer matrix composites*. ASTM International, West Conshohocken, PA. doi, 2006. **10**: p. D6671_D6671M.
19. Argüelles, A., et al., *Influence of temperature on the delamination process under mode I fracture and dynamic loading of two carbon-epoxy composites*. Composites Part B, 2015. **68**: p. 207-214.
20. Mortazavian, S. and A. Fatemi, *Fatigue behavior and modeling of short fiber reinforced polymer composites: A literature review*. International Journal of Fatigue, 2015. **70**: p. 297-321.

21. El Sawi, I., et al., *An investigation of the damage mechanisms and fatigue life diagrams of flax fiber-reinforced polymer laminates*. Journal of Materials Science, 2014. **49**(5): p. 2338-2346.
22. Manteghi, S., et al., *Investigation of the mechanical properties and failure modes of hybrid natural fiber composites for potential bone fracture fixation plates*. Journal of the Mechanical Behavior of Biomedical Materials, 2017. **65**: p. 306-316.
23. Mahboob, Z., et al., *Tensile and compressive damaged response in Flax fibre reinforced epoxy composites*. Composites Part A: Applied Science and Manufacturing, 2017. **92**: p. 118-133.
24. Saidane, E.H., et al., *Mode-I interlaminar fracture toughness of flax, glass and hybrid flax-glass fibre woven composites: Failure mechanism evaluation using acoustic emission analysis*. Polymer Testing, 2019. **75**: p. 246-253.
25. Hao, L.I.Y.W.D.M., *Improving interlaminar fracture toughness of flax fiber/epoxy composites with chopped flax yarn interleaving*. 2015. **58**(10): p. 1745-1752.
26. Ravandi, M., et al. *Mode I Interlaminar Fracture Toughness of Natural Fiber Stitched Flax/Epoxy Composite Laminates—Experimental and Numerical Analysis*. in *Proceedings of the American Society for Composites: Thirty-First Technical Conference*. 2016.
27. Rajendran, T.S., et al., *Mode I and Mode II Delamination of Flax/Epoxy Composite Laminate*. MATEC Web of Conferences, 2018. **202**: p. 1002.
28. Rajendran, T.S., et al., *Interlaminar fracture toughness of a plain weave flax/epoxy composite*. Plastics, Rubber and Composites, 2019. **48**(2): p. 74-81.
29. Dhakal, H.N., et al., *Development of flax/carbon fibre hybrid composites for enhanced properties*. Carbohydrate Polymers, 2013. **96**(1): p. 1-8.
30. Jawaid, M. and H.P.S. Abdul Khalil, *Cellulosic/synthetic fibre reinforced polymer hybrid composites: A review*. Carbohydrate Polymers, 2011. **86**(1): p. 1-18.
31. Nisini, E., C. Santulli, and A. Liverani, *Mechanical and impact characterization of hybrid composite laminates with carbon, basalt and flax fibres*. Composites Part B, 2017. **127**: p. 92-99.
32. Pandya, K.S., C. Veerajuu, and N.K. Naik, *Hybrid composites made of carbon and glass woven fabrics under quasi-static loading*. Materials and Design, 2011. **32**(7): p. 4094-4099.
33. Ramesh, M., K. Palanikumar, and K.H. Reddy, *Mechanical property evaluation of sisal–jute–glass fiber reinforced polyester composites*. Composites Part B, 2013. **48**: p. 1-9.
34. Sarasini, F., et al., *Damage tolerance of carbon/flax hybrid composites subjected to low velocity impact*. Composites Part B, 2016. **91**: p. 144-153.
35. Liang, S., P.-B. Gning, and L. Guillaumat, *A comparative study of fatigue behaviour of flax/epoxy and glass/epoxy composites*. Composites Science and Technology, 2012. **72**(5): p. 535-543.
36. Bensadoun, F., et al., *Fatigue behaviour assessment of flax–epoxy composites*. Composites Part A: Applied Science and Manufacturing, 2016. **82**: p. 253-266.
37. Yan, L. and N. Chouw, *Crashworthiness characteristics of flax fibre reinforced epoxy tubes for energy absorption application*. Materials and Design, 2013. **51**: p. 629-640.
38. Yan, L. and N. Chouw, *Experimental study of flax FRP tube encased coir fibre reinforced concrete composite column*. Construction and Building Materials, 2013. **40**: p. 1118-1127.
39. Shah, D.U., P.J. Schubel, and M.J. Clifford, *Can flax replace E-glass in structural composites? A small wind turbine blade case study*. Composites Part B, 2013. **52**: p. 172-181.
40. Moudood, A., et al., *Flax fiber and its composites: An overview of water and moisture absorption impact on their performance*. Journal of Reinforced Plastics and Composites, 2019. **38**(7): p. 323-339.
41. Pickering, K.L., M.G.A. Efendy, and T.M. Le, *A review of recent developments in natural fibre composites and their mechanical performance*. Composites Part A, 2016. **83**: p. 98-112.
42. Shah, D.U., *Developing plant fibre composites for structural applications by optimising composite parameters: a critical review*. Journal of Materials Science, 2013. **48**(18): p. 6083-6107.

43. El-Hafidi, A., et al., *Determination of dynamic properties of flax fibres reinforced laminate using vibration measurements*. Polymer Testing, 2017. **57**: p. 219-225.
44. Li, X., S. Panigrahi, and L. Tabil, *A study on flax fiber-reinforced polyethylene biocomposites*. Applied Engineering in Agriculture, 2009. **25**(4): p. 525-531.
45. Liang, S., P.B. Gning, and L. Guillaumat, *A comparative study of fatigue behaviour of flax/epoxy and glass/epoxy composites*. Composites Science and Technology, 2012. **72**(5): p. 535-543.
46. Baley, C., *Analysis of the flax fibres tensile behaviour and analysis of the tensile stiffness increase*. Composites Part A, 2002. **33**(7): p. 939-948.
47. Flynn, J., A. Amiri, and C. Ulven, *Hybridized carbon and flax fiber composites for tailored performance*. Materials & Design, 2016. **102**: p. 21-29.
48. Bos, H.L., v.d.M.J.A. Oever, and O.C.J.J. Peters, *Tensile and compressive properties of flax fibres for natural fibre reinforced composites*. Journal of Materials Science, 2002. **37**(8): p. 1683-1692.
49. Mallick, P.K., *Fiber-reinforced composites: materials, manufacturing, and design*. 3rd ed. 2007: Taylor & Francis.
50. Zhang, M. and J.P. Matinlinna, *E-Glass Fiber Reinforced Composites in Dental Applications*. Silicon, 2012. **4**(1): p. 73-78.
51. Thomason, J., P. Jenkins, and L. Yang, *Glass Fibre Strength—A Review with Relation to Composite Recycling*. Fibers, 2016. **4**(4): p. 18.
52. Wong, K.J., et al., *R-Curve Modelling of Mode I Delamination in Multidirectional Carbon/Epoxy Composite Laminates*. Applied Mechanics and Materials, 2014. **606**: p. 159-163.
53. Czabaj, M.W. and J.G. Ratcliffe, *Comparison of intralaminar and interlaminar mode I fracture toughnesses of a unidirectional IM7/8552 carbon/epoxy composite*. Composites Science and Technology, 2013. **89**: p. 15-23.
54. Krueger, R., *Virtual crack closure technique: History, approach, and applications*. Applied Mechanics Reviews, 2004. **57**(2): p. 109.
55. Rybicki, E.F. and M.F. Kanninen, *A finite element calculation of stress intensity factors by a modified crack closure integral*. Engineering Fracture Mechanics, 1977. **9**(4): p. 931-938.
56. Tan, P.W., K.N. Shivakumar, and J.C. Newman, Jr., *A virtual crack-closure technique for calculating stress intensity factors for cracked three dimensional bodies*. 1988.
57. Krueger, R., et al., *Comparison of 2D finite element modeling assumptions with results from 3D analysis for composite skin-stiffener debonding*. Composite Structures, 2002. **57**(1-4): p. 161-168.
58. Society of Automotive, E. and R. National Institute for Aviation, *Composite materials handbook. Volume 2, Polymer matrix composites, materials properties*. 2012: SAE International on behalf of CMH-17, a division of Wichita State University.
59. ANSYS, *ANSYS® Mechanical APDL, 19.2, help system, [book and chapter reference name/numbers]*, ANSYS, Inc, in 2.6. VCCT Energy-Release Rate Calculation. 2018. p. 2.6.1. Using VCCT for Energy-Release Rate Calculation
60. Khatir, S., et al., *Delamination detection in laminated composite using Virtual crack closure technique (VCCT) and modal flexibility based on dynamic analysis*. Journal of Physics: Conference Series, 2017. **842**: p. 12084.
61. Shokrieh, M.M., et al., *Simulation of mode I delamination propagation in multidirectional composites with R-curve effects using VCCT method*. Computational Materials Science, 2012. **65**: p. 66-73.

62. Xie, D. and S.B. Biggers, *Strain energy release rate calculation for a moving delamination front of arbitrary shape based on the virtual crack closure technique. Part I: Formulation and validation*. Engineering Fracture Mechanics, 2006. **73**(6): p. 771-785.
63. Xie, D. and S.B. Biggers, *Progressive crack growth analysis using interface element based on the virtual crack closure technique*. Finite Elements in Analysis & Design, 2006. **42**(11): p. 977-984.
64. Barbero, E.J., *Finite element analysis of composite materials using ANSYS*. Second ed. 2014: CRC Press, Taylor & Francis Group.
65. Hashin, Z., *Failure criteria for unidirectional fiber composites*. Journal of applied mechanics, 1980. **47**(2): p. 329-334.
66. Pelissou, C., et al., *Determination of the size of the representative volume element for random quasi-brittle composites*. International Journal of Solids and Structures, 2009. **46**(14): p. 2842-2855.
67. Gitman, I., H. Askes, and L. Sluys, *Representative volume: existence and size determination*. Engineering fracture mechanics, 2007. **74**(16): p. 2518-2534.
68. Maragoni, L., P. Carraro, and M. Quaresimin, *Development, validation and analysis of an efficient micro-scale representative volume element for unidirectional composites*. Composites Part A: Applied Science and Manufacturing, 2018. **110**: p. 268-283.
69. Banerjee, S. and B.V. Sankar, *Mechanical properties of hybrid composites using finite element method based micromechanics*. Composites Part B: Engineering, 2014. **58**: p. 318-327.
70. Harris, W.M. and W.K. Chiu, *Determining the representative volume element size for three-dimensional microstructural material characterization. Part 1: Predictive models*. Journal of Power Sources, 2015. **282**: p. 552-561.
71. Harris, W.M. and W.K. Chiu, *Determining the representative volume element size for three-dimensional microstructural material characterization. Part 2: Application to experimental data*. Journal of Power Sources, 2015. **282**: p. 622-629.
72. Cao, Y., *Representative Volume Element (RVE) Finite-Element Analysis (FEA) of Al Metal-matrix Composites*. 2016.
73. Ogierman, W. and G. Kokot, *Generation of the representative volume elements of composite materials with misaligned inclusions*. Composite Structures, 2018. **201**: p. 636-646.
74. ANSYS, I., *The Use of Material Designer for Analyses of UD Composite Materials*. 2018. p. 17.
75. ANSYS®, *ANSYS® WorkBench*. 2019, ANSYS Inc.
76. Czél, G. and M.R. Wisnom, *Demonstration of pseudo-ductility in high performance glass/epoxy composites by hybridisation with thin-ply carbon prepreg*. Composites Part A, 2013. **52**: p. 23-30.
77. Pereira, A.B. and A.B. de Morais, *Mode II interlaminar fracture of glass/epoxy multidirectional laminates*. Composites Part A, 2004. **35**(2): p. 265-272.
78. Chen, X. and Y. Liu, *Finite element modeling and simulation with ANSYS Workbench*. 2014: CRC Press.
79. Zienkiewicz, O.C., R.L. Taylor, and J.Z. Zhu, *The finite element method: its basis and fundamentals*. 6th ed. 2005: Elsevier Butterworth-Heinemann.
80. Daricik, F., *Mesh size sensitivity analysis for interlaminar fracture of the fiber-reinforced laminated composites*. Journal of Engineered Fibers and Fabrics, 2019. **14**: p. 155892501988346.
81. Krueger, R., *Virtual crack closure technique: History, approach, and applications*. Applied Mechanics Reviews, 2004. **57**(2): p. 109-143.
82. Chen, J.-F., E.V. Morozov, and K. Shankar, *Progressive failure analysis of perforated aluminium/CFRP fibre metal laminates using a combined elastoplastic damage model and including delamination effects*. Composite Structures, 2014. **114**: p. 64-79.
83. Liu, P.F. and M.M. Islam, *A nonlinear cohesive model for mixed-mode delamination of composite laminates*. Composite Structures, 2013. **106**: p. 47-56.

84. de Morais, A.B., et al., *Analysis of crack propagation in double cantilever beam tests of multidirectional laminates*. *Mechanics of Materials*, 2003. **35**(7): p. 641-652.
85. Mourtzis, D., M. Doukas, and D. Bernidaki, *Simulation in Manufacturing: Review and Challenges*. *Procedia CIRP*, 2014. **25**: p. 213-229.